

BULGARIAN CHEMICAL COMMUNICATIONS

2016 Volume 48 / Special Issue C

Selected papers presented on the 2nd International Conference on the New Trends in Chemistry, Zagreb, Croatia, April 19-22, 2016

*Journal of the Chemical Institutes
of the Bulgarian Academy of Sciences
and of the Union of Chemists in Bulgaria*

Preface

This special issue of the Bulgarian Chemical Communications is dedicated to new trends in chemistry and consists papers based on oral and posters presentations from the All in One Conferences, 2nd International Conference on New Trends in Chemistry organized in Zagreb, Croatia, 19-22 April 2016. The topics are Polymer Chemistry and Applications, Pharmaceutical Chemistry, Computational Chemistry, Environmental Chemistry, Bio Chemistry, Physical Chemistry, Analytical Chemistry, Inorganic Chemistry, Organic Chemistry, Material Chemistry and Inorganic Chemistry. In this issue, it is selected 11 manuscripts for publication.

This conference is provided a common platform for scientists and experts from various institutions to share knowledge, ideas, and achievements, to discuss impedance data analysis in a friendly environment. The symposium was dedicated to recent developments in chemistry field.

We would like to express our sincere gratitude to all the authors and reviewers of the manuscripts, and to the editorial team of the Bulgarian Chemical Communications, all of whom have critically evaluated and improved the content.

Guest Editors,

Prof. Dr.Frieder W. Scheller

Institute of Biochemistry and Biology,

University of Potsdam, Potsdam, Germany

Assoc. Prof. Dr. Dolunay SAKAR DASDAN (Chemistry Conference Chair)

Department of Chemistry, Yildiz Technical University

Istanbul, Turkey

Investigation of possible degradation reactions of amoxicillin molecule

T. Tekpetek, Y.Y. Gurkan*

Namik Kemal University, Department of Chemistry, Tekirdag / Turkey

Received June 26, 2016, Revised September 10, 2016

Amoxicillin is used to treat infections caused by bacteria, including infections of the ears, lungs, sinus, skin and urinary tract. Antibiotics those taken by living beings are disposed of from living metabolism as unchanged or little transformed. Antibiotic traces disposed of can not be treated in conventional wastewater treatment plants and enter directly to the receiving environment. In receiving environments, low concentrations of antibiotic traces can cause microorganism resistance increase and high concentrations of antibiotic traces can cause toxic effects. Therefore wastewaters those includes antibiotic traces have to be treated. In this study is discussed theoretically possible reaction pathways of amoxicillin, which has a high toxic effects and is able to dissolve in the water. For this purpose, possible reactions was examined numerically using Gaussian 09 package software. DFT method was used in theoretical study.

Keywords: Amoxicillin, DFT, OH radical, Antibiotic

INTRODUCTION

Antibiotics are currently regularly used in veterinary and human medicine, and these released into the aquatic environment pose a potential risk for aquatic and terrestrial organisms [1]. Recent studies have focused on the application of advanced oxidation processes (AOPs) to degrade pharmaceuticals in water, and this approach is based on highly reactive species such as hydroxyl radicals to destroy the target pollutant [2]. In industries, amoxicillin is presently produced through a chemical coupling process by using a β -lactam nucleus and appropriate acyl donors. Chemical coupling of amoxicillin involves the reaction of an amino β -lactam such as 6-aminopenicillanic acid (6-APA) usually having its carboxyl group protected with an activated side-chain derivative, where the protecting group is removed through hydrolysis [3]. Waste of pharmaceutical products is one of the most important basic risk factors that threaten human health and ecological balance [4].

In its reactions with organic molecules, OH behaves as an electrophile whereas O is a nucleophile. Thus, OH readily adds to unsaturated bonds while O does not. Both forms of the radical abstract H from C-H bonds and this can result in the formation of different products when the pH is raised to a range where O rather than OH is the reactant. For example, if an aromatic molecule

carries an aliphatic side chain, O attacks there by H abstraction whilst OH adds preferentially to the aromatic ring [5]. Hydroxyl radical which is the most reactive type known in biological systems reacts with every biomolecule it encounters including water. Potentially, every biomolecule is a hydroxyl radical scavenger at different speeds [6]. Aromatic compounds are good detectors since they hydroxylate. In addition, the position of attack to the ring depends on the electron withdrawal and repulsion of previously present substituents. The attack of any hydroxyl radical to an aromatic compound results in the formation of a hydroxylated product [7]. In recent years, the density functional theory (Density Functional Theory, DFT) based on the methods have become very popular. Best DFT methods, requires less power from conventional correlation techniques.

This study investigated theoretically possible reaction pathways of amoxicillin and a water-soluble high toxicity. Optimized geometries draw with Gaussian calculations were made in Gaussian09 View 5 software package [8]. DFT method is used in the program. First amoxicillin molecule is drawn through Gaussview5 program on the computer. Then, Gaussian 09 program were made geometric optimization of the lowest energy state. Geometric structures have been analyzed and the bond lengths and bond angles are calculated. In this way, thanks to this program, which will be analyzed in greater costs in terms of material and experimental as more power is intended to calculate the theoretical.

* To whom all correspondence should be sent:
E-mail: yyalcin@nku.edu.tr

COMPUTATIONAL SET-UP AND METHODOLOGY

Molecular modelling

- Cartesian coordinates of the atoms of a molecule, the bond lengths, bond angles, and dihedral angles (the atomic positions);
- Depending on the molecular surface of the position of the atoms and atomic radii;
- atomic distances, atom types and the energy derived from the link arrangement

The mathematical expression is called Molecular Modelling. So theoretically the method of calculating the properties of molecules and their behaviour on the computer and is not simulated. Advances in computer technology advances in quantum chemistry and molecular modelling have played a role in use. The first theoretical calculations were made in 1927 by Walter Heitler and Fritz London. Molecular Modelling; Physics, Chemistry, Biology and supporting experimental work in the pharmaceutical industry or the results to be obtained from experimental studies are used to predict.

Methodology

The reaction model used in the computational part of this study is the reaction between the amoxicillin molecule and the photo-generated $\bullet\text{OH}$ radicals [9]. Therefore, all the calculations were based on hydroxyl radical chemistry. Hydroxyl radicals can react with organic compounds by (i) hydrogen abstraction from single bonds, (ii) addition to double bonds, and (iii) one-electron oxidation, which is mostly loss of water from hydroxyl radical adducts. The reaction system under consideration consists of $\bullet\text{OH}$ radicals, in other words open-shell species. It is well known that open-shell molecules pose severe problems in quantum mechanical calculations. Hartree–Fock (HF) methods suffer from spin contamination, because they are wave function based. In contrast to the HF methods, density functional theory (DFT) methods use the exact electron density instead of the wave function to calculate molecular properties and energies. Electron correlation, whose absence is the main drawback to HF methods, is accounted for in DFT methods. They suffer from spin contamination less than HF methods and this feature makes them suitable for calculations involving open-shell systems. Therefore, geometry optimizations of the reactants were performed with the DFT method. The DFT calculations were carried out as implemented in GAUSSIAN 09 code [8], using the exchange-correlation functional

B3LYP, which combines HF and Becke exchange terms with the Lee–Yang–Parr correlation functional, in combination with the 6-31G* basis set. Vibrational frequencies were calculated for the determination of the structures as stationary points and true minima on the potential energy surfaces. All the possible stationary geometries located as minima were generated by free rotation around single bonds [10].

RESULTS AND DISCUSSION

Theoretical prediction of the degradation mechanism

In the search for a plausible mechanism for the photocatalytic degradation reaction of amoxicillin, DFT reactivity descriptors were employed to have information about the most susceptible sites for hydroxyl radical attack. The hydroxyl radical is a very active species and has a strong electrophilic character [11]. Once formed, it can readily attack the aminotoluene molecule and produce the reaction intermediates. Fig. 1 shows the optimized structure of amoxicillin molecule and the numbering system that is used throughout the calculations. The calculated local softness and Fukui functions are presented in Table 1.

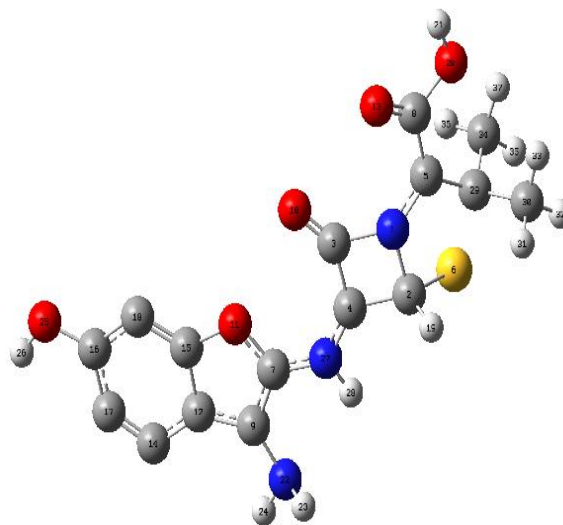


Fig. 1. Optimized structure of amoxicillin and the numbering system (gray, carbon; red, oxygen; blue, nitrogen; white, hydrogen; yellow, sulfur).

Three main competing reaction pathways shown in Fig. 2 were determined by selecting the specific sites of amoxicillin molecule, on the basis of their softness values being close to that of the $\bullet\text{OH}$ radical. The predicted mechanism was confirmed by comparison with the experimental results on simple structures reported in the literature, as explained below.

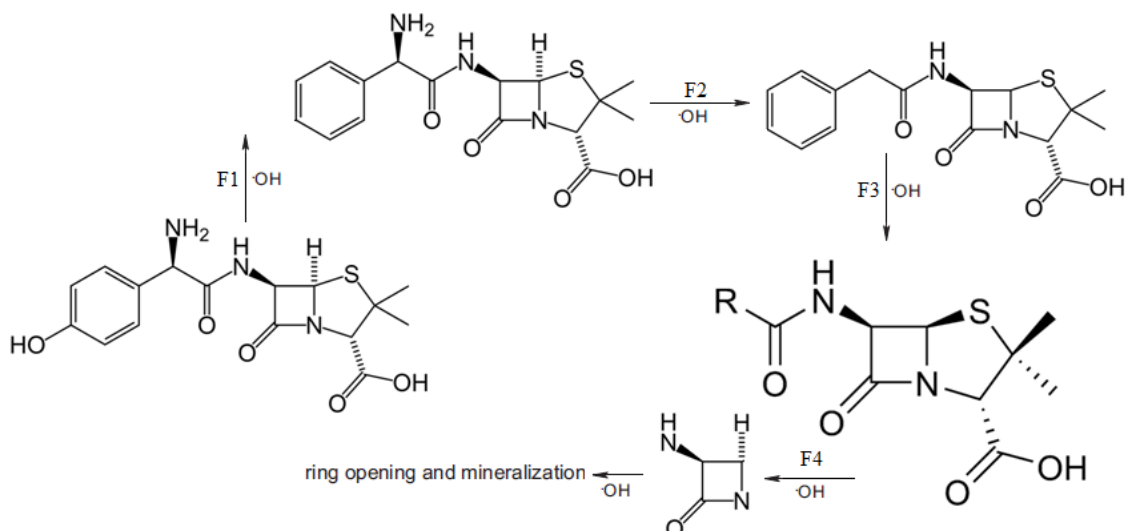


Fig. 2. Possible pathways for the photocatalytic degradation of amoxicillin.

Table 1. Chemical reactivity descriptors for amoxicillin and for the $\bullet\text{OH}$ radical.

	f°	s°	Δs°
S6	0.1489	1.17176	1.6103
C5	0.0457	0.5698	2.6879
N22	0.0311	0.3941	2.9845
N5	0.0269	0.3267	2.8896
N27	0.0265	0.2789	2.9547
C7	0.0274	0.5336	2.5478
C9	0.0368	0.4897	2.6489
H21	0.0258	0.3126	2.9478
H26	0.0121	0.1427	3.0643
H23	0.0048	0.0568	3.1507

OH radical fragmentation reaction is carried out with the N22 had attacked. OH bond breakage of the molecular fragments resulting ampicillin 1 (F1) has been called. Geometry optimization results obtained is shown in Fig. 3.

Electronegative group NH_2 group of breakage caused by penicillin G molecule fragment 2 (F2) has been called and shown in Fig. 4.

Due to the electronegativity of the oxygen bound to a benzene ring group of benzene ring was separated from the resulting penicillin molecule

fragment 3 (F3) has been called. Geometry optimization results obtained is shown in Fig.5.

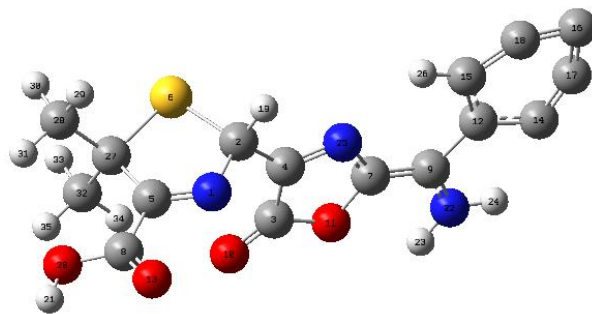


Fig. 3. Optimized structure of ampiciline.

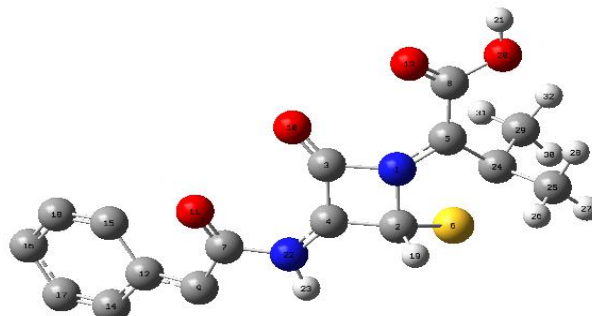


Fig. 4. Optimized structure of penicillin G.

Sulfur and oxygen electronegativity due to the degradation reactions was realized. The smallest fragment and into the water, which is harmless substances β -lactam antibiotics has become. Molecular fragment, 4 (F4) has been called. Geometry optimization results obtained is shown in Fig.6.

Degradation of amoxicillin was predicted to occur through intramolecular β -lactam, ring cleavages followed by subsequent reactions with $\bullet\text{OH}$ radicals transforming the fragments into smaller species such as SO_4^{2-} , NO_3^- and NH_4^+ .

Energies are shown in the Table 2 of possible reaction pathways.

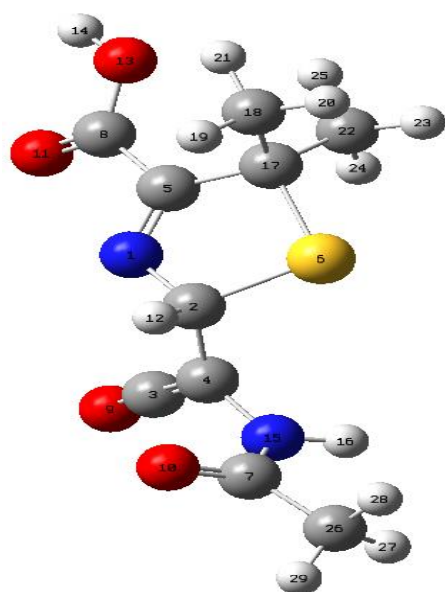


Fig. 5. Optimized structure of penicillin.

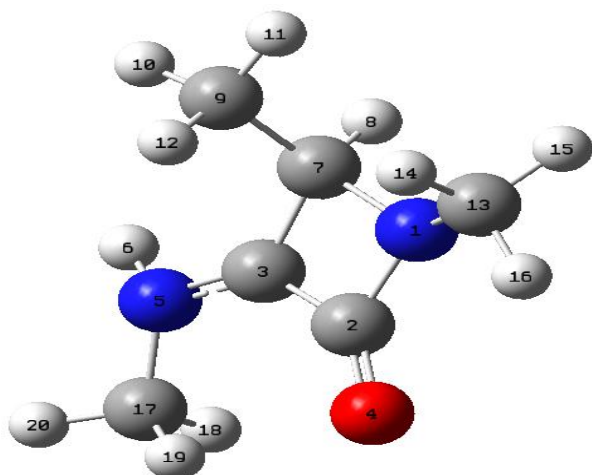


Fig.6. Optimized structure of β -lactam.

Table 2. According to the DFT method energy values.

	Energy (kcal/mol)
Ampicilin	-928.330
Penicillin G	-893.047
Penicillin	-751.029
β -lactam	-263.507

CONCLUSIONS

As a result, decomposition, requires further energy. OH radicals are used to degrade antibiotic substances in water. As seen in our Fragments harmful amoxicillin β -lactam is up fragmented and has become harmless to the environment. Our

objective is that antibiotic substances involved in the water to break down to the smallest harmless and to remove the water. This fragmentation theoretically realized as shown in the results.

Acknowledgements: The authors greatly appreciate Namik Kemal University Research Foundation for financial support. Project number: NKUBAP.00.10.AR.15.14

REFERENCES

1. W. Xu, G. Zhang, S. Zou, X. Li, Y. Liu, *Environ. Pollut.* **145**, 672 (2007).
2. M. Klavarioti, D. Mantzavinos, D. Kassinos, *Environ. Intern.* **35**, 402 (2009).
3. I. Alemzadeh, G. Borghei, L. Vafi, R. Roostaazad, *Chem. Chem. Eng.* **17** (1), 106 (2010).
4. L. Povyakel, O. Boblyiova, S. Snoz, Y. Bardik, *Toxicology Letters*, **180**, 197 (2008).
5. V.G. Buxton, L.C. Greenstock, P.W. Helman, B.A. Ross, *Journal of Physical and Chemical Reference Data*, **17**, 513 (1988).
6. M. Anbar, P. Neta, *Int. J. Radiat Isot*, **18**, 495, (1965).
7. B. Halliwell, M. Grootveld, J.M.C. Gutteridge, (1988), *Methods of Biochemical Analysis*, **33**, 59-90.
8. M.J. Frisch, G.W. Trucks, H.B. Schlegel, G.E. Scuseria, M.A. Robb, J.R. Cheeseman, J.A. Montgomery Jr., T. Vreven, K.N. Kudin, J.C. Burant, J.M. Millam, S.S. Iyengar, J. Tomasi, V. Barone, B. Mennucci, M. Cossi, G. Scalmani, N. Rega, G.A. Petersson, H. Nakatsuji, M. Hada, M. Ehara, K. Toyota, R. Fukuda, J. Hasegawa, M. Ishida, T. Nakajima, Y. Honda, O. Kitao, H. Nakai, M. Klene, X. Li, J.E. Knox, H.P. Hratchian, J.B. Cross, C. Adamo, J. Jaramillo, R. Gomperts, R.E. Stratmann, O. Yazyev, A.J. Austin, R. Cammi, C. Pomelli, J.W. Ochterski, P.Y. Ayala, K. Morokuma, G.A. Voth, P. Salvador, J.J. Dannenberg, V.G. Zakrzewski, S. Dapprich, A.D. Daniels, M.C. Strain, O. Farkas, D.K. Malick, A.D. Rabuck, K. Raghavachari, J.B. Foresman, J.V. Ortiz, Q. Cui, A.G. Baboul, S. Clifford, J. Cioslowski, B.B. Stefanov, G. Liu, A. Liashenko, P. Piskorz, I. Komaromi, R.L. Martin, D.J. Fox, T. Keith, M.A. Al-Laham, C.Y. Peng, A. Nanayakkara, M. Challacombe, P.M.W. Gill, B. Johnson, W. Chen, M.W. Wong, C. Gonzalez, J.A. Pople, Gaussian 09, Revision B.04, Gaussian, Inc., Pittsburgh, PA, 2009.
9. N. San, M. Kilic, Z. Cinar, *J. Adv. Oxid. Technol.* **10**(1), 51 (2007).
10. J.P. Stewart, *J. Comput. Chem.* **10**, 221 (1989).
11. V. Brezová, M. Ceppan, E. Brandsteterova, M. Breza, L. Lapcik, *J. Photochem. Photobiol. A: Chem.* **59**, 385 (1991).

Total phenolic and flavonoid contents and antioxidant activity of extracts from *Vitis vinifera* L.

Y. Yeşiloğlu^{1,*}, S. Gülen²

¹Faculty of Pharmacy, Trakya University, Edirne, Turkey

²Department of Chemistry, Faculty of Science, Trakya University, Edirne, Turkey

Received June 26, 2016, Revised September 10, 2016

Plants naturally are a rich source of secondary metabolites and novel therapeutic compounds. These compounds are well known for their various beneficial effects on human health. In this study, variation in total phenolic and flavonoid contents and antioxidant activities (DPPH radical-scavenging, reducing power, superoxide radical scavenging, hydrogen peroxide scavenging, total antioxidant activity) of water, acetone and methanol extracts from the *Vitis vinifera* L. leaves collected from north Turkey was studied. Results indicated that it was similar total phenolic and flavonoid contents of methanol extract. Total phenolic content varied from 48.67 ± 1.15 to 70.87 ± 1.15 (mg GAE/g dry wt), and total flavonoid content ranged from 45.20 ± 0.86 to 72.90 ± 0.40 (mg CE/g dry matters). Furthermore, results indicated that the extracts have good antioxidant activities. It was concluded that *V. vinifera* might be a potential source of antioxidants.

Key words: Flavonoids, Antioxidant activity, *Vitis vinifera*, Scavenging activity, Phenolic compound.

INTRODUCTION

Free radicals are naturally present in living systems; however, high amounts of free radicals can oxidise biomolecules, leading to tissue damage, cell death or degenerative processes, including aspects of ageing, cancer, cardiovascular diseases, arteriosclerosis, neural disorders, skin irritations and inflammation [1]. Natural antioxidants exist in the leaves, seeds, roots and fruits of most plants. These are the most effective free radical scavengers in living organisms [2].

Vitis vinifera L. (common grape) belong to Vitaceae family, which fruits have been used as a food and for wine or beverage production. In Ayurvedic (Indian) system, grapes leaves are used as a folk remedy for the treatment of diarrhea and vomiting. The grape leaves have been used to stop bleeding, to treat inflammatory disorder, pain, hepatitis, free radical related diseases [3]. The leaves are composed of wide range of polyphenols including anthocyanins, flavonoids and also organic acid [4]. Previous reports showed that leaves, fruits and juice of *V. vinifera* have the hepatoprotective effect on acetaminophen induced hepatic DNA damage, apoptosis and necrotic cell death [5]. In this view, the present study was carried out to evaluate the antioxidant activity of *V. vinifera* leaves.

EXPERIMENTAL

Plant Material

Fresh grape (*V. vinifera* L.) leaves were collected (during February) from Tekirdag, (Tekirdag, Turkey). Plant materials were washed with distilled water and dried at room temperature. For preparation of water extract (WE), 25 g sample was put into a fine powder in a mill and was mixed with 500 mL boiling water by magnetic stirrer for 15 min. The extract was then filtered and evaporated to dryness under reduced pressure and controlled temperature (40–50°C) in a rotary evaporator. For the preparation acetone (AE) and methanol (ME) extracts, 25 g sample was put into a fine powder in a mill and was mixed with 500 mL solvent. The residue was re-extracted until extraction solvents became colorless. The obtained extracts were filtered over Whatman No. 1 paper and the filtrate was collected, then solvent was removed by a rotary evaporator (Buchi R-200, Switzerland) at 40°C to obtain dry extract. All the extracts were kept at -20°C and were dissolved in water or solvent before use.

Determination of total phenolic compounds

Total phenolics in *V. vinifera* extracts were determined according to Folin–Ciocalteu method [6] as described previously [7]. Briefly, 1 mL of the *V. vinifera* extracts (25–125 µg/mL) was transferred into test tubes and their volumes made up to 4.6 mL with distilled water. After addition of 0.1 mL Folin–Ciocalteu reagent (previously diluted 3-fold with distilled water) and 0.3 mL 2% Na₂CO₃

* To whom all correspondence should be sent:
E-mail: yesimyesiloglu@trakya.edu.tr

solution, tubes were vortexed and then allowed to stand for 2 h with intermittent shaking. The absorbance was measured at 760 nm in a spectrophotometer. The total phenolic compounds in the *V. vinifera* extracts were expressed as gallic acid equivalents (GAE) (mg g^{-1}).

Determination of total flavonoid content

Total flavonoid content was determined by using a method described by Wang et al. [8] with minor modification using catechin as standard flavonoid compound. Briefly, 10 mL of the extract ($1000 \mu\text{g/mL}$) or (+)-catechin standard solution ($0\text{--}50 \mu\text{g/mL}$) was mixed with 1 mL of a 5% sodium nitrite solution. After 6 min, 1 mL of a 10% aluminium chloride solution was added and the mixture was allowed to stand for a further 5 min before 10 mL of NaOH (5%) was added. The mixture was brought to 25 mL with distilled water and mixed well. The absorbance was measured immediately at 510 nm using a spectrophotometer. Results were expressed as the average of triplicates. The total flavonoid content was calculated as catechin equivalents (CE) (mg g^{-1}).

Antiradical activity

The DPPH radical scavenging activity of the *V. vinifera* extracts was measured according to the procedure described by Burits, Asresand Bucar [9]. Briefly, 0.1 mM solution of DPPH• in ethanol was prepared and 1 mL of this solution was added to 3 mL of *V. vinifera* extracts at different concentrations ($25\text{--}125 \mu\text{g/mL}$). The mixture was shaken vigorously and allowed to stand in the dark at room temperature for 0.5 h. The decrease in absorbance of the resulting solution was then measured spectrophotometrically at 517 nm against ethanol. All measurements were made in triplicate and averaged. The DPPH radical scavenging activity was calculated using the following equation:

$$\text{Scavenging activity (\%)} = \frac{(A_0 - A_1)}{A_0} \times 100$$

ABTS assay

The ABTS•+ method was based on the procedure described by Siddhuraju and Becker [10]. Briefly, 10 mg of ABTS was diluted in 2.6 mL of potassium persulfate solution (2.45 mM) and final concentration of ABTS•+ was 7 mM. The mixture was left to stand in dark at room temperature for 12–16 h before use. The ABTS•+ was diluted to the absorbance of 0.70 ± 0.02 and stocked for off line and on line assays. 1 mL of diluted extract was added with 3 mL of ABTS•+ solution and stand in dark at room temperature for 60 min. The absorbance was measured at 734 nm.

ABTS scavenging activity is presented as an EC50 value.

Reducing power

Reducing power was determined according to the method proposed by Oyaizu [11] with minor modifications [12]. Stock solutions were diluted. A 500 μL sample solution was mixed with 1.25 mL of 0.2 M phosphate buffer (pH 6.6) and 1.25 mL of 1.0% (w/v) potassium ferricyanide. The resulting mixture was incubated at 50°C for 30 min. After the addition of 1.25 mL of 10% (w/v) trichloroacetic acid, the mixture was centrifuged at $2500 \times g$ for 10 min. A 2.5 mL supernatant was mixed with water (2.5 mL) and 0.5 mL of 0.1% (w/v) ferric chloride before the absorbance was determined at 700 nm. In this assay, the presence of reductants, such as antioxidant compounds in the sample, causes the reduction of the Fe^{3+} /ferricyanide complex to the ferrous form. Standards were used for comparison.

Superoxide anion scavenging activity

Measurement of the superoxide anion scavenging activity of *V. vinifera* extracts was based on the method described by Guo and Wei et al. [13] with slight modifications. Superoxide radicals are generated in PMS-NADH systems by the oxidation of NADH and assayed by the reduction of NBT. In this experiment, superoxide radicals were generated in 3 mL of Tris-HCl buffer (16 mM, pH 8.0) containing 1 mL of NBT ($50 \mu\text{M}$) solution, 1 mL NADH ($78 \mu\text{M}$) solution and the sample solution. The reaction was initiated by adding 1 mL of PMS solution ($10 \mu\text{M}$) to the mixture. The reaction mixture was incubated at 25°C for 5 min, and the absorbance at 560 nm was measured against a blank. A decreased absorbance of the reaction mixture indicates increased superoxide anion scavenging activity. The percentage inhibition of superoxide anion radical generation for three parallel measurements was calculated using the following formula: Inhibition (%) = $[(Ac - As)/Ac] \times 100$. In this formula, Ac is the absorbance of control and As is the absorbance in the presence of the extract or a standard.

Scavenging of hydrogen peroxide

The hydrogen peroxide scavenging ability of extracts was determined according to the method of Ruch et al. [14]. A solution of hydrogen peroxide (40 mM) was prepared in phosphate buffer (pH 7.4). The concentration of hydrogen peroxide was determined by absorption at 230 nm using a

spectrophotometer. *V. vinifera* extracts (125 µg/mL) were added to 1 mL of the hydrogen peroxide (40 mM) solution. The absorbance of hydrogen peroxide at 230 nm was read after ten minutes against a blank solution of phosphate buffer not having hydrogen peroxide. The percentage of hydrogen peroxide scavenged by extracts and standard solutions was calculated as follows: H_2O_2 scavenging activity (%) = $[(A_c - A_s)/A_c] \times 100$, where A_c and A_s are the absorbance values of the control sample and the test sample, at particular times, respectively.

Ferric reducing antioxidant potential (FRAP) assay

The total antioxidant activity of the *V. Vinifera* extracts was determined according to the thiocyanate method described by Mitsuda et al. [15]. For stock solutions, 10 mg of extracts was dissolved in 10 mL deionized water. The solution, which contains the same concentration of extracts or standard samples (75 µg/mL) in 2.5 mL of potassium phosphate buffer (0.04 M, pH 7.0) was added to 2.5 mL of linoleic acid emulsion in potassium phosphate buffer (0.04 M, pH 7.0). Fifty millilitres linoleic acid emulsion contained 175 µg Tween-20, 155 µL linoleic acid and 0.04 M potassium phosphate buffer (pH 7.0). On the other hand, 5 mL control was composed of 2.5 mL linoleic acid emulsion and 2.5 mL, 0.04 M potassium phosphate buffer (pH 7.0). The mixed solution (5 mL) was incubated at 37 °C in a glass flask. At regular intervals during incubation, a 0.1 mL aliquot of the mixture was diluted with 3.7 mL of solvent, followed by the addition of 0.1 mL of 30 % ammonium thiocyanate and 0.1 mL of 20 mM ferrous chloride in 3.5 % hydrochloric acid. The peroxide level was determined by reading the absorbance at 500 nm in a spectrophotometer. This step was repeated every 10 h until the control reached its maximum absorbance value. Therefore, high absorbance indicates high linoleic acid oxidation. All data on total antioxidant activity are the average of triplicate experiments.

RESULTS

Recovery Percent, Total Phenolics, and Flavonoid Contents

It is well known that phenolics and flavonoids are the important antioxidant substances that are obtained from most natural plants. In the present study, the percent yield, total phenolics and flavonoid contents obtained from extracts of *Vitis vinifera* are shown in Table 1

The extraction was carried out with three different solvents, including water, methanol, and acetone, to obtain extracts from dried plant material, which will be used in all assays. The extraction with methanol resulted in the highest amount of total extractable compounds. The extraction yields were found to be 118.8, 131.2, and 61.2 mg/g dried leaf for the water, methanol, and acetone extracts, respectively. These extraction yields indicated that the solvents used for extract preparation from *V. vinifera* leaves showed different capacities to extract the leaf compounds and probably different compositions of the extracts.

Among the different leaf extracts, the methanol extract of *V. vinifera* showed the highest total phenolic content (70.87 ± 1.15 mg GAE/g extract) when compared to other extracts. Moreover, we determined the total flavonoid contents of the *V. Vinifera* extracts. Flavonoids are important secondary metabolites in plants with high antioxidant activity properties. In our study they were estimated using the linear regression equation obtained from the standard catechin curve (absorbance = $0.013 [CE] \times 0.003$), $r^2 = 0.9990$ as catechin equivalents per 1 mg of extract (CE/mg extract). The methanol extract of *V. vinifera* showed the highest total flavonoid content (72.90 ± 0.40 mg CE/g extract). The total flavonoid contents exhibited the descending order among: methanol extract > water extract > acetone extract. In different studies, various amounts of flavonoids have been detected in vegetables. For example, 11.88 ± 1.46 µg epicatechin equivalent was detected in the water extracts of chard [16].

Antiradical activity

Antiradical activity of extracts was carried out by measuring the decolourisation of DPPH solution at 517 nm. The scavenging effects of extracts on DPPH increased with the increase in concentration. The highest inhibition ratio was 55.2% at 125 µg mL⁻¹ for methanol extract. Ascorbic acid had an activity of 64.2% at 125 µg mL⁻¹ and BHA had an activity of 61.7% (Fig. 1). *V. vinifera* extracts, on interacting with DPPH, might have transferred an electron to it, thus neutralizing its free radical nature as observed by Oyaizu [11].

ABTS assay

The antioxidant capacity of leaf extracts was determined by the ABTS method. The antioxidant ability of *V. vinifera* extracts to scavenge the blue-green colored ABTS⁺ radical cation was measured. ABTS⁺ scavenging activity increased with increasing concentration.

Table 1. Extraction yields and contents of total phenols, total flavonoids in *Vitis vinifera* extracts.

Extracts	Extraction yield ^a (mg g ⁻¹ dry wt)	Total phenols ^b (GAE) (mg g ⁻¹)	Total flavonoids ^c (CE) (mg g ⁻¹)
Water extract	118.8	60.33 ± 0.58	59.87 ± 0.23
Acetone extract	61.2	48.67 ± 1.15	45.20 ± 0.86
Methanol extract	131.2	70.87 ± 1.15	72.90 ± 0.40

Note: The data are expressed as mean ± SD (*n* = 3). ^aExpressed as milligram of extract per gram dry material. ^bExpressed as milligram of gallic acid per gram dry extract. ^cExpressed as milligram of catechin per gram dry extract.

The EC50 values of the extracts were between 12.32±0.16 and 45.87±0.47µg/mL. It was found that the ABTS+ scavenging activity of water extract of chard increased with increasing concentration, reaching 18.56 ± 1.77% at 400 µg mL⁻¹ [16].

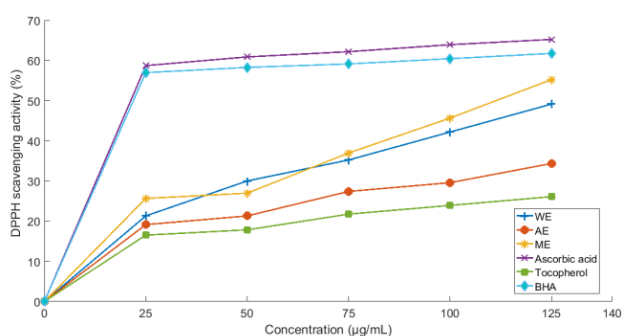


Fig. 1 DPPH radical scavenging activity of the *V. vinifera* extracts. BHA, ascorbic acid and α -tocopherol were used as reference antioxidants.

Reducing power

The reducing capacity of a compound may serve as a significant indicator of its potential antioxidant activity [17]. Fig. 2 shows, the extent of the reduction, in terms of absorbance values at 700 nm. The reducing power of *V. vinifera* extracts was not concentration dependent and was found to be below those of ascorbic acid (1.617), BHA (1.042) and BHT (1.004) at 250 µg mL⁻¹. The extracts showed lower reducing power than the standards. Reducing power of extracts and standards decreased in order of ascorbic acid > BHA > BHT > methanol extract > water extract > acetone extract. Previous studies have correlated the reducing capacity of phytochemicals to their electron-donating ability [13]. Hence it can be started that the effective electron (hydrogen) donating ability of the *V. vinifera* extracts contributed to the observed overall antioxidant property.

Superoxide anion scavenging activity

Superoxide radical is known to be very harmful to cellular components as a precursor of more reactive oxidative species, such as single oxygen and hydroxyl radicals. It is considered to play an

important role in the peroxidation of lipids [18]. Figure 3 shows the superoxide radical scavenging activity of *V. vinifera* extracts (50 and 125 µg mL⁻¹) in comparison with the same doses of standard antioxidants BHA, BHT and ascorbic acid. Ascorbic acid had stronger superoxide radical scavenging activity than BHA and BHT. The inhibition of superoxide radical formation by *V. vinifera* extracts and standard antioxidants decreased in the following order: Ascorbic acid (37.3 %), BHA (9 %), BHT (11.1%), water extract (18.2 %), acetone extract (28.9 %) and methanol extract (9.2 %) in presence of 125 µg mL⁻¹ test sample.

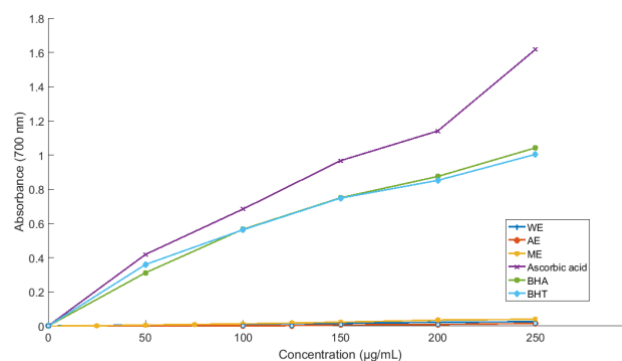


Fig. 2 Reducing power of the extracts from *V. vinifera*. BHA, BHT and ascorbic acid were used as reference antioxidants.

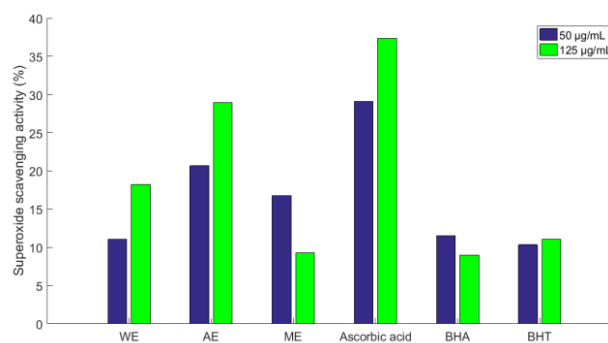


Fig. 3 Superoxide anion scavenging activity of the extracts from *V. vinifera*. BHA, BHT and ascorbic acid were used as reference antioxidants.

Hydrogen peroxide scavenging activity

The highest percentage H₂O₂ scavenging activity of 94.7% was obtained with BHT followed by α -tocopherol which had 91.4% scavenging activity. BHA, acetone extract, ascorbic acid and trolox had 66.95, 50.0, 47.97, 30.68% H₂O₂ scavenging activities respectively (Fig. 4). Hydrogen peroxide can accept protons (H⁺) or electrons and by so doing be reduced to H₂O. In a H₂O₂ scavenging activity, the acetone extract act as hydrogen peroxide scavengers by donating hydrogen atoms to reduce the hydrogen peroxide to H₂O.

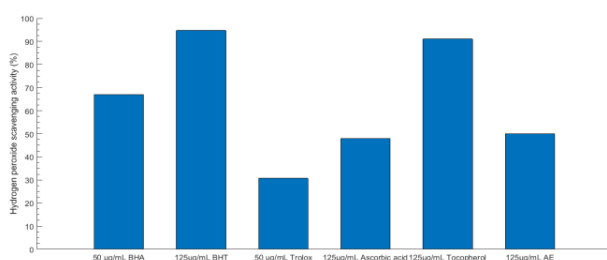


Fig. 4 H₂O₂ scavenging activity of the acetone extract from *V. vinifera*. BHA, BHT, ascorbic acid, trolox and α -tocopherol were used as reference antioxidants.

Total antioxidant activity

Total antioxidant activity of *V. vinifera* extracts was determined by the thiocyanate method. All of extracts exhibited effective antioxidant activity. The effects of same amounts of *V. vinifera* extracts of (75 µg/mL) on peroxidation of linoleic acid emulsion are shown in Fig. 5. The effects on lipid peroxidation of linoleic acid emulsion of extracts and standards decreased in that order: water extract > acetone extract > methanol extract > ascorbic acid > tocopherol > BHT > BHA. The total antioxidant capacity of plant extract may be attributed to their chemical composition and phenolic acid content.

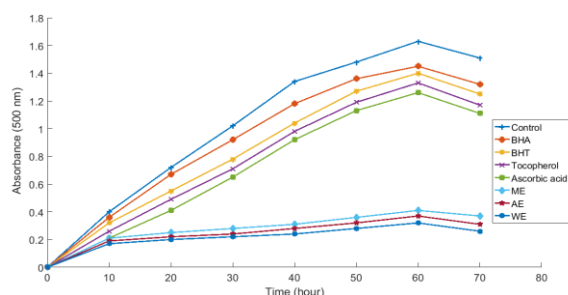


Fig. 5 Inhibitory effect of the extracts from *V. vinifera* on lipid peroxidation. BHA, BHT, ascorbic acid and α -tocopherol were used as reference antioxidants. Values are means \pm SD (n = 3).

CONCLUSION

The extracts of *V. vinifera* leaves exhibited different levels of antioxidant activity in all the models studied. The results from various free radical-scavenging systems revealed that the *V. vinifera* had significant antioxidant activity and free radical-scavenging activity. The free radical-scavenging property may be one of the mechanisms by which this drug is useful as a foodstuff as well as a traditional medicine. However, further investigation of individual compounds, their *in vivo* antioxidant activities and in different antioxidant mechanisms is warranted.

Acknowledgements: The authors are thankful to the Trakya University Research Fund, Edirne-Turkey (Project number: TUBAP-2012-37).

REFERENCES

1. E. Bursal, İ Gülçin, *Food Res. Int.*, **44**, 1482 (2011).
2. J. K. Jacob, F. Hakimuddin, G. Paliyath, H. Fisher, *Food Res. Int.*, **41**, 419 (2008).
3. A. Lardos, M. H. Kreuter, *Fitoterapia*, **3**, 1 (2000).
4. E. Bombardelli, P. Morazzonni, *Fitoterapia*, **66**, 291 (1995).
5. M. K. Gharib Naseri, M. Navid Hamidi, A. Heidari, *Iranian J. Pharm. Res.*, **2**, 93 (2005).
6. V. L. Singleton, R. Orthofer, R. M. Lamuela-Raventós, *Methods in Enzymology*, **299**, 152 (1999).
7. Y. Yeşiloğlu, L. Şit, *Spectrochim. Acta A.*, **95**, 100 (2012).
8. J. Wang, X. Yuan, Z. Jin, Y. Tian, H. Song, *Food Chem.*, **104**, 242 (2007).
9. M. Burits, K. Asres, F. Bucar, *Phytother. Res.*, **15**, 103 (2001).
10. P. Siddhuraju, K. Becker, *Food Chem.*, **101**, 10 (2007).
11. M. Oyaizu, *J. Nutr. (Japan)*, **44**, 307 (1986).
12. Y. Yeşiloğlu, H. Aydın, *Asian J. Chem.*, **25**, 7199 (2013).
13. T. Guo, L. Wei, J. Sun, C-L. Hou, L. Fan, *Food Chem.*, **127**, 1634 (2011).
14. R. J. Ruch, S. J. Cheng, J. E. Klaunig, *Carcinogenesis*, **10**, 1003 (1989).
15. H. Mitsuda, K. Yuasumoto and K. Iwami, *J. Soc. Nutri. Food Sci. (Japan)*, **19**, 210 (1996).
16. O. Sacan, R. Yanardag, *Food Chem. Toxicol.*, **48**, 1275 (2010).
17. M. R. Bhandari, M. Kawabata, *Food Chem.*, **88**, 163 (2004).
18. M. K. Dahl, T. Richardson, *J. Dairy Sci.*, **61**, 400 (1978).

Control of adiabatic continuous stirred tank reactor at an unstable operating point

S. Altuntaş^{1*}, H. Hapoğlu²

^{1*}Provincial Directorate of Environment and Urbanization, 55070 Samsun, Turkey

²Department of Chemical Engineering, Ankara University, 06500 Ankara, Turkey

Received June 26, 2016, Revised September 10, 2016

This paper describes application of temperature control to an unstable reactor. A non-adiabatic continuous stirred tank reactor simulation program was run in Matlab at a predetermined unstable operating point to attain closed loop performances. Jacket temperature was chosen as a manipulated variable. The simulated program having mass and energy balances for reactor inlet and cooling system was used to apply proportional control and to design the tuning parameters of conventional and advance control systems. A sinusoidal set point change for a small time interval was introduced to the simulated process, the reactor temperature oscillation with a constant amplitude was monitored for proportional only control. The numerical value of the proportional controller coefficient that produces oscillatory system response was varied to rich the well-suited ultimate reactor temperature changes versus time. Ziegler-Nichols and Tyreus-Luyben evaluation technique was utilized to evaluate Proportional Integral Derivative controller parameters. Whilst retaining the computational simplicity of Matlab and the conventional control parameter evaluation techniques, the proposed method was made temperature response to follow an unstable operation set-point successfully. It is significant to note that integral action in the controller provides saddle point steady-state following without offset even if the values of the parameters of the system or of the controller change. Self-tuning Proportional Integral Derivative controller tuning parameters were also evaluated by using the proportional, integral and derivative constants and the second order parametric system model. The success of the various control actions were compared by using two performance criterions.

Keywords: Experimental Self-tuning PID application, pH control, kefir yeast, cheese whey

INTRODUCTION

All industrial chemical reactions which are either exothermic or endothermic require energy manipulation to maintain a constant temperature or a predetermined temperature profile in various types of processes [1]. Exothermic reactions in many industrial reactors which have the similar characteristic may have very interesting behaviour to investigate because of potential safety problems. A mean conversion of a reactant can be realized at a single unstable equilibrium point that can be obtained by determining the eigenvalues of this system Jacobian matrix [2]. The chemical processes such as exothermic styrene polymerization reactors are exposed to various disturbances [3]. To maintain certain set point in face of load disturbances, conventional or advance controller must be applied to a process with well-tuned control parameters [4-5]. Nonlinear oscillation of

outputs, sensitivity of system parameters, ignition/extinction and interaction of responses may occur for open-loop cases in continuous stirred tank reactors (CSTR's). A steady-state analysis was used to determine operation and design parameters effects on CSTR performance [6]. The processes steady-state and dynamic characteristic behaviours and the reactor design parameters were investigated to improve feedback control efficiency. Several techniques based on process simulation were proposed to demonstrate the difficulty of control at a certain steady-state set point in some regions of operation [7].

Although the system is simulated by a set of differential equations, some applicable parametric models which include the relationship between manipulated and controlled variables were usually written in discrete-time domain for advance process control applications. The parameters identification of these models is one of the effective procedures to define the systems in a certain operation range by utilizing the best estimates of model degree and all the unknown variables of operation [8]. There are several

* To whom all correspondence should be sent:
E-mail: seminaltuntas@hotmail.com

methods including strategies for the tuning of the conventional controller and the selection of the best model for control application. A multi-model control strategy was proposed to identify the delay without turning the system unstable [9]. Some researchers improve control strategies to obtain a better method than conventional proportional integral derivative (PID) controllers. Several combined advance and conventional control were proposed as a novel PID controller. The performance was evaluated for the set point tracking and disturbance rejection [10].

Nomenclature	
A_R	heat transfer area
a_i	coefficients of monic polynomial in the z-domain
b_i	coefficients of polynomial in the z-domain
C_A	inlet concentration of the reactant
C	reactant concentration of the reaction mixture
C_p	average heat capacity of the reaction mixture
E_1	activation energy
e	error
F_1	feed rate to the reactor
K_c	steady-state gain for three-term controller
K_u	ultimate gain
k_0	pre-exponential for the rate constant
P_u	ultimate period
R_1	ideal gas constant
TD	derivative time
TI	integral time
T	temperature of the reaction mixture
T_1	inlet feed temperature
T_c	coolant temperature
T_s	temperature set point
$r(t)$	set point at time t
$u(t)$	input variable at time t
us	input value at initial steady-state point
U_R	overall heat transfer coefficient
V_R	volume of reaction mixture
ρ	density of the reaction mixture
$(-\Delta H_R)$	heat of reaction
$y(t)$	output variable at time t

An objective of this paper is to overcome the difficulty of feedback control of the CSTR when it is operated at a saddle point. PID control action was executed throughout-being considered the most likely type of control action for this application. The controller parameters were estimated using three different closed loop response tuning criteria for discrete controllers, viz. those due to Tyreus–Luyben [11] (denoted by T-L), Ziegler-Nichols [2]

(denoted by Z-N), and the increased gain approach was combined by considering an application from [12]. Self-tuning proportional integral derivative (STPID) control [13-14] was also achieved by adjusting three tuning parameters with three-term PID parameters proposed by Z-N and second order system model parameters. A controlled auto regressive moving average (CARMA) model was utilized and its parameters were determined with Bierman computation procedure [15] in which data obtained by enforcing the system with a pseudo random binary sequence (PRBS).

CONVENTIONAL AND SELF-TUNING CONTROLLER

The conventional three-term (PID) feedback control is the highly applied feedback control strategy because of its robustness, ease of operation and the lack of specified process knowledge required for the initial controller position or velocity form designs. When the controller parameters have been determined, sufficient and effective control is usually obtained by detuning such as increase gain approach for stability and non-oscillatory behaviour over the whole range of operating conditions. The discrete-time equivalent of three term control action may be written:

$$\frac{\Delta u}{e} = K_c \left\{ \left(1 + \frac{\Delta t}{2TI} + \frac{TD}{\Delta t} \right) + \left(\frac{\Delta t}{2TI} - 1 - \frac{2TD}{\Delta t} \right) z^{-1} + \left(\frac{TD}{\Delta t} \right) z^{-2} \right\} \quad (1)$$

Rearranging equation (1)

$$\Delta u = s_0 e(t) + s_1 e(t-1) + s_2 e(t-2), \quad (2)$$

In order to convert the position form of the PID algorithm into a self-tuning equivalent, the following equations can be written:

$$u(t) - us = e[s_0 + (s_0 + s_1)z^{-1} + (s_0 + s_1 + s_2)z^{-2}], \quad (3)$$

The properties of the STPID closed-loop can be varied by placing the poles of the characteristic equation (T) that is the denominator of equation (4).

$$y(t) = \left[\frac{z^{-1} b_0 (s_0 + s_1 z^{-1} + s_2 z^{-2})}{1 + t_1 z^{-1} + t_2 z^{-2} + t_3 z^{-3}} \right] r(t), \quad (4)$$

The system CARMA type model without control and the controller coefficients are defined respectively as:

$$y(t) = \left[\frac{z^{-1}b_0}{1+a_1z^{-1}+a_2z^{-2}} \right] u(t), \quad (5)$$

$$s_0 = \frac{t_1-a_1+1}{b_0}; \quad s_1 = \frac{t_2-a_2+a_1}{b_0}; \quad s_2 = \frac{t_3-a_2}{b_0}, \quad (6)$$

All the coefficients of the characteristic third order T polynomial should be user defined. They can be initially determined by using the system model parameters (a_1, a_2, b_0) and Kc, TI and TD constants.

RESULTS AND DISCUSSION

To investigate the steady-state and unsteady-state behaviour of a adiabatic CSTR, the system is the model obtained from the set of the mass and energy balance equations [16]. The system parameters given in [2] are utilized as $k_0 = 9703 \cdot 3600 \text{ hr}^{-1}$, $(-\Delta H_R) = 5960 \text{ kcal kmol}^{-1}$, $E_1 = 11843 \text{ kcal kmol}^{-1}$, $\rho \cdot C_p = 500 \text{ kcal m}^{-3} \text{ K}^{-1}$, $T_1 = 298 \text{ K}$, $CA = 10 \text{ kmol m}^{-3}$, $V_R = 1 \text{ m}^3$, $F_1 = 1 \text{ m}^3 \text{ hr}^{-1}$, $(U_R \cdot A_R \cdot V_R^{-1}) = 150 \text{ kcal m}^{-3} \text{ K}^{-1} \text{ hr}^{-1}$, $R_1 = 1.987 \text{ kcal kmol}^{-1} \text{ K}^{-1}$. The jacket and the reactor are assumed to be perfectly mixed and the jacket temperature is lower than the reactor temperature, T. The feasible steady-state solutions were obtained for the coolant temperature of 293 K by means of the fsolve function in Matlab software with various initial C and T values (see Table 1). The eigenvalues for the stability of a particular operating point are determined by using the eig(amat) command in Matlab (see Table 1).

At a constant coolant temperature of 293K, the phase-plane plot was obtained by using ode45 function with many initial conditions (see Fig 1). In this figure, the feasible high and low reactor temperature steady-states are also shown as 'o'. The intermediate reactor temperature steady state was presented with the symbol '+' which is unstable, since all initial conditions have diverged from it. This saddle point was chosen as the operation condition of CSTR for control cases studied.

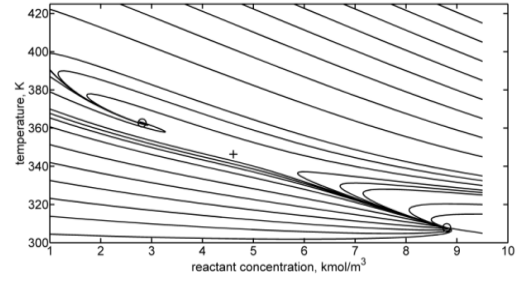


Fig. 1. Phase-plane plot for coolant temperature $T_c=293\text{K}$ (o: stable nodes, +: saddle point).

Table 1. The steady-state solution and the eigenvalues of the continuous stirred tank reactor.

Initial values, C, kmol/m ³ , T, K	The feasible solution of the steady-state equations for coolant temperature, $T_c=293\text{K}$	
9 300	C=8.79	T=307.85
8 310	C=8.79	T=307.85
7 320	C=8.79	T=307.85
6 330	C=4.60	T=346.30
5 350	C=4.60	T=346.30
4 360	C=2.81	T=362.73
3 370	C=2.81	T=362.73

The eigenvalues: -0.88, -0.65 Sink (stable node)	✖
The eigenvalues: -0.76, 0.48 Saddle point (unstable)	✖
The eigenvalues: -0.48+0.70i, -0.48-0.70i Spiral sink (stable focus)	✖

2	380		C=2.81	T=362.73
1	390		C=2.81	T=362.73
1	450		C=2.81	T=362.73

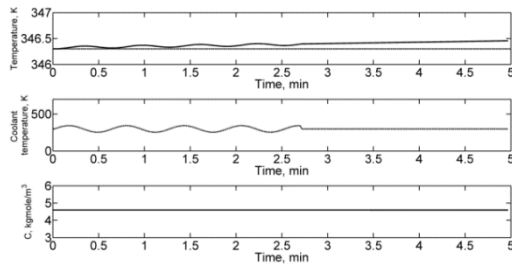


Fig. 2. The reactor temperature response of proportional only control with $K_C=0.5$ in the face of the set-point change as $90 \sin(600t)$

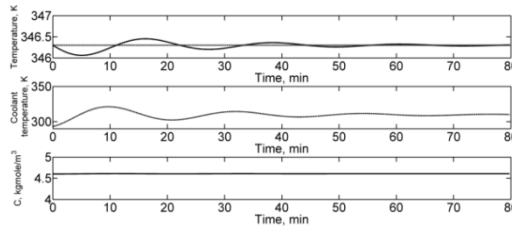


Fig. 3. PID control of the reaction temperature (the T-L settings with increase gain applied as $K_C=22.5$, $TI=1.37\text{min}$, $TD=0.1\text{min}$).

The conventional controller settings were estimated based on the continuous cycling method. To obtain the ultimate gain (K_u) and period (P_u) at the middle operation point, a sinusoidal temperature set point change ($T_s = 346.3+90*\sin(600t)$) was introduced to the closed loop system with various steady-state gain (K_c) for proportional controller in a short time interval. The well suited K_c value of 0.5 that produces continuous cycling within a certain range was found by monitoring coolant temperature and reactor temperature changes versus time (see Fig 2). The K_u and P_u values are evaluated as 0.5 and 0.6228min respectively. The Ziegler-Nichols and Tyreus-Luyben settings were evaluated based on K_u

and P_u values. These numerical values of K_c multiplied by 100 to obtained the well-suited increase gain for PID controller.

For the simulation of the closed loop behaviour of the controlled reactor at the saddle point, the PID controllers based on the T-L settings with increase gain ($K_C=22.5$, $TI=1.37\text{min}$, $TD=0.1\text{min}$) and the Z-N settings with increase gain ($K_C=30$, $TI=0.3\text{min}$, $TD=0.08\text{min}$) were used. The controlled temperate of reactor and the manipulated coolant temperature changes versus time were shown in Fig 3 and Fig 4 respectively. The magnitude of temperature sampling time was 1.08s which influences the stability of the controlled output. Comparison of PID performances using two different parameter settings were made by considering set point following in Figures 3-4. The control algorithm using the Z-N settings with increase gain were preferred to bring the reactor temperature to the set point.

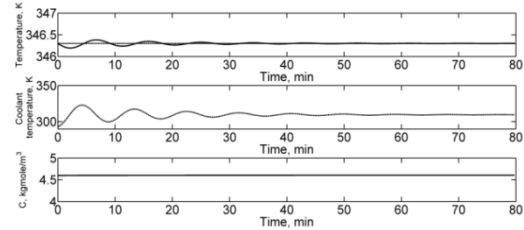


Fig. 4. PID control of the reaction temperature (the Z-N settings with increase gain applied as $K_C=30$, $TI=0.3\text{min}$, $TD=0.08\text{min}$)

A pole-placement based STPID algorithm application was also achieved to obtain better performance. Firstly, a second order system transfer function of the CARMA form was considered. Secondly, the PRBS of the certain magnitude given in Fig. 5 was applied to the coolant temperature. The simultaneous input and output data were obtained for the system model parameters identification. Finally, Bierman algorithm in Matlab was utilized to evaluate the three model parameters as given in the equation below:

$$y(t) = \frac{0.00003 u(t-1)}{1+0.669z^{-1}+0.332z^{-2}}, \quad (7)$$

These system model parameters $a_1 = 0.669$, $a_2 = 0.332$, $b_0 = 0.0003$ and the Z-N settings as $K_c=0.3$, $TI=0.3\text{min}$, $TD=0.08\text{min}$ were used to determine the closed loop real denominator

coefficients as $t_1=-0.33$, $t_2=-0.337$, $t_3=-0.33$ for the STPID controller tuning. Figure 6 shows the STPID control of reactor temperature in the face of an exothermic reaction in unstable operation condition with $t_1=-0.33$, $t_2=-0.337$ and $t_3=-0.33$ for the CSTR.

For comparison of the performances of the all controllers applied, the integral square of the error (ISE) and the integral of absolute value of error (IAE) criteria were evaluated by using the following formula:

$$ISE = \sum(T - T_s)^2, \quad (8)$$

$$IAE = \sum|T - T_s|, \quad (9)$$

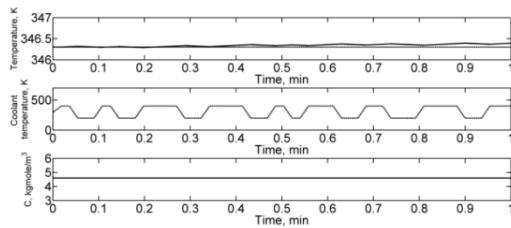


Fig. 5. The temperature response obtained in the face of the pseudo-random binary sequence given to the coolant temperature.

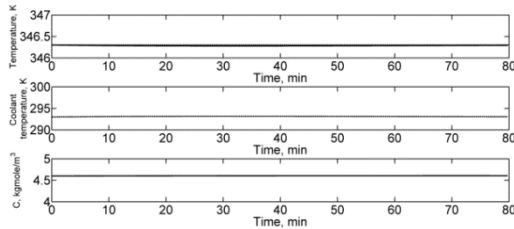


Fig. 6. Self-tuning PID control of reactor temperature by using the coolant temperature as the controlling variable.

Table 2. ISE and IAE values obtained for PID and Self-tuning PID control of the reaction temperature.

Controller	ISE	IAE	Figure number
PID with Tyreus-luyben increased gain	29.7	248.5	Fig 3
PID with Ziegler-Nichols increased gain	3.5	72.7	Fig 4
Self-tuning PID with second order ARMAX model	1.1	67.1	Fig 6

Table 2 lists the ISE and IAE criteria values for each controlled variable response. By using STPID, improvement in the control is clearly seen in Fig 6. There is no doubt that the introduction of STPID reduces the ISE and

IAE values for the controlled reactor temperature response (see Table 2).

CONCLUSION

The modelling equations of the CSTR were solved simultaneously by using ode45 function in Matlab. For the identification, the magnitude and generation of PRBS forcing function was well-determined for operating conditions of the system. The simulation result obtained without control was used for the system model parameters identification. The PID control parameters were estimated by using the proportional control response in the face of a momentary sinusoidal set point change with well-chosen amplitude and radian frequency. Both sets of parameters were found by using the data obtained in a sort time domain. These parameters were used successfully to evaluate the tuning parameters of STPID controller. The position form of PID and STPID controller were applied to the CSTR by accepting the heat release during the reaction as a disturbance of the system. Although the control was stable in all cases the STPID action was found to give smaller closed-loop ISE and IAE values than the PID action when applied to the CSTR at an unstable operating saddle point.

For the operating point studied, the performance of the position form STPID control have been shown in Fig 6 to be superior to the velocity form of STPID control results given in Fig 7. It was found that the performance of velocity form controller algorithm was unacceptably poor (see Appendix A).

Appendix A. Velocity form of STPID control application to a adiabatic CSTR

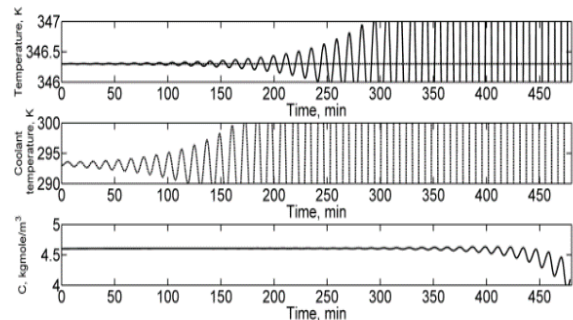


Fig. 7. Velocity form self-tuning PID control of reactor temperature by using the coolant temperature as the controlling variable.

The velocity form STPID control was applied to the CSTR. The controller tuning parameters were used as $t_1 = -0.33$, $t_2 = -0.337$, $t_3 = -0.33$. Fig 7 shows the reactor temperature response during the velocity form control application at the unstable operating saddle point.

Acknowledgements: Financial support from the scientific and technical research council of Turkey is gratefully acknowledge (TUBITAK, project MISAG-85).

REFERENCES

- 1.S. Çetinkaya, H. H. Durmazuçar, Z. Zeybek, H. Hapoğlu, M. Alpbaz, *Journal of the Faculty of Engineering and Architecture of Gazi University*, **28**(2), 383 (2013).
- 2.B. W. Bequette, *Process Dynamics*, Prentice Hall, New Jersey, 1998.
- 3.F. P. P. Manuel, P. M. Manuel, *Journal of Process Control*, **23**, 778 (2013).
- 4.A. Altinten, F. Ketevanlioğlu, S. Erdoğan, H. Hapoğlu, M. Alpbaz, *Chemical Engineering Journal*, **138**, 490 (2008).
- 5.A. Aldemir, H. Hapoğlu, *Journal of Polytechnic*, **19**(1), 9 (2016).
- 6.L. P. Russo, W. Bequette, *Comput. Chem. Eng.*, **20**, 417 (1996).
- 7.L. P. Russo, W. Bequette, *Chem. Eng. Sci.*, **53**, 27 (1998).
- 8.A. Altinten, S. Altindal, S. Erdoğan, H. Hapoğlu, *Journal of the Faculty of Engineering and Architecture of Gazi University*, **26**(3), 613 (2011).
- 9.J. Herrera, A. Ibeas, S. Alcatara, R. Vilanova, in: Proceedings of IEEE International Symposium on Intelligent Control Part, IEEE Multi Conference on Systems and Control in Japan, Yokohama, 2010, p.767.
- 10.H. Li, J. Zhang, *Chemometrics and Intelligent Laboratory Systems*, **151**, 95 (2016).
- 11.D. E. Seborg, D. A. Mellichamp, T. F. Edgar, F. J. Doyle, *Process Dynamics and Control*, John Wiley and Sons, 2011.
- 12.A.P. Wardle, S. M. Heathcock, in: Proceedings of Proc. Int. Conf. on Intelligent Control and Instrumentation in Singapore, 1992, p.317.
- 13.P. E. Wellstead, M. B. Zarrop, *Self-tuning systems-control and signal processing*, Willey, Sussex United Kingdom, 1991.
- 14.M. Alpbaz, H. Hapoğlu, G. Özkan, S. Altuntaş, *Chemical Engineering Journal*, **116**, 19 (2006).
- 15.G. J. Bierman, *Automatica*, **12**, 375 (1976).
- 16.H. Hapoğlu, *Computers and Chemical Engineering*, **26**, 1427 (2002).

Synthesis, spectroscopic studies and electrochemical properties of Schiff bases derived from 5-chloro-2-hydroxybenzaldehyde with methyl 2-amino-6-methyl-4,5,6,7-tetrahydrobenzo[b]thiophene-3-carboxylate

N. Çolak^{1*}, A. B. Gündüzalp², S. Mamaş², D. Akkaya², K. Kaya³

¹Hitit University, Faculty of Art & Science, Department of Chemistry, Çorum

²Gazi University, Faculty of Science, Department of Chemistry, Ankara

³Istanbul Technical University, Faculty of Art & Science, Department of Chemistry, İstanbul

Received June 26, 2016, Revised September 10, 2016

Schiff base; methyl 2-((5-chloro-2-hydroxybenzylidene)amino)-6-methyl-4,5,6,7-tetrahydrothieno[2,3-c]pyridine-3-carboxylate was synthesized by the reaction of methyl 2-amino-6-methyl-4,5,6,7-tetrahydrothieno[2,3-c]pyridine-3-carboxylate with 5-chloro-2-hydroxybenzaldehyde in excellent yield. This compound was characterized by elemental analysis, NMR (¹H and ¹³C-APT), FT-IR and X-ray diffraction methods. The electrochemical behavior of Schiff base was investigated using cyclic voltammetry (CV), controlled potential electrolysis and chronoamperometry (CA) techniques. The number of electrons transferred (n), diffusion coefficient (D) and standard heterogeneous rate constants (k_s) were also determined by electrochemical methods.

Key words: Schiff base, 2-aminothiophene, X-ray diffraction, electrochemical behavior

INTRODUCTION

Multi-substituted 2-aminothiophenes are a kind of important privileged structures used as a scaffold to construct a series of natural products. In particular, 2-aminothiophene derivatives have been demonstrated in a number of applications such as in pesticides, dyes [1], agrochemical applications [2,3] and pharmaceuticals [1,4], anti-inflammatory [5,6], analgesic, antidepressant, antioxidant [7], antitumor [8], antimicrobial, antibacterial [9], antifungal [10] and anticonvulsant activities [11-19]. Substituted 2-aminothiophenes are active as allosteric enhancers at the human A1 adenosine receptor [3,20,21]. Some of them are serve as potential some kinase inhibitors and adenosine agonists [22-25].

Schiff bases are an important class of organic compounds both synthetically and biologically. These compounds show antibacterial, antifungal, anticancer and herbicidal activities [26-29]. Furthermore, it is known that Schiff bases are utilized as starting materials in the synthesis of organic or inorganic compounds for industrial usage. There are many studies on the electrochemical behaviors of Schiff bases (imines) by cyclic voltammetry (CV). Their reduction potentials are dependent on the types of substituent attached to the aromatic ring [30-34], the size of the

aromatic groups on either sides of the imine (–C=N–) group [30-32,35] and the amount of intramolecular hydrogen bonds [36,37].

In this work, Schiff base: methyl 2-((5-chloro-2-hydroxybenzylidene) amino) -6-methyl -4,5,6,7-tetrahydrothieno[2,3-c]pyridine-3-carboxylate was synthesized by the reaction of methyl 2-amino-6-methyl-4,5,6,7-tetrahydrothieno [2,3-c] pyridine-3-carboxylate and 5-chloro-2-hydroxybenzaldehyde. Synthesized compounds were characterized by elemental analysis, NMR (¹H and ¹³C-APT), ATR and X-ray diffraction methods. The electrochemical behavior of Schiff base was evaluated by cyclic voltammetry (CV), controlled potential electrolysis and chronoamperometry (CA) techniques.

EXPERIMENTAL

Elemental analysis was carried out Elementar Vario Cube Pro, Germany. NMR (¹H and ¹³C-APT) spectrum were obtained in CDCl₃ on a Bruker Fourier 300 MHz spectrometer. IR spectrum were measured on Nicolet 6700 spectrometer with ATR apparatus. Crystal structure of Schiff base was characterized by using Bruker D8 VENTURE diffractometer. Voltametric measurements were carried out with IVIUM Stat Electrochemical Analyzer.

* To whom all correspondence should be sent.
E-mail: nakicolak@hitit.edu.tr

Synthesis of methyl 2-amino-6-methyl-4,5,6,7-tetrahydrothieno[2,3-c]pyridine-3-carboxylate (1)

A mixture of 1-methylpiperidin-4-one (1.13 g, 10 mmol), methyl 2-cyanoacetate (0.99 g, 10 mmol), sulfur (0.32 g, 10 mmol) in absolute ethanol (15 mL) and Et₃N (1.01 mL, 10 mmol) was stirred at room temperature for 6 h (Scheme 1) until TLC showed complete disappearance of the starting materials. The crude product which precipitated at the end of the reaction was separated by filtration [38-40], dried *in vacuo* and then recrystallized from ethanol. The chemical analysis gave the following results: Yield: 78 %, m.p. 208-210 °C; Elemental analysis for C₁₀H₁₄N₂O₂S: Calc. C, 53.08; H, 6.24; N, 12.38; S, 14.17. Found: C, 52.61; H, 6.02; N, 12.08; S, 13.97. FT-IR (ATR, cm⁻¹); 3399-3282 (NH₂); 2926 (aliph. C-H), 1699 (C=O). ¹H NMR (300 MHz, CDCl₃, ppm); δ= 5.99 (br, 2H, NH₂); 3.80 (s, 3H, OCH₃); 3.41 (s, 2H, CH₂); 2.82 (t, 2H, CH₂); 2.64 (t, 2H, CH₂); 2.47 (s, 3H, NCH₃). ¹³C-APT (75 MHz, CDCl₃, ppm); δ= 27.26 (C3); 45.44 (NCH₃); 50.67 (OCH₃); 52.36 (C4); 53.23 (C5); 114.48 (C7); 130.60 (C6); 162.25 (C=O); 166.33 (C1).

Synthesis of methyl 2-((5-chloro-2-hydroxybenzylidene)amino)-6-methyl-4,5,6,7-tetrahydrothieno[2,3-c]pyridine-3-carboxylate (2)

To a solution of methyl 2-amino-6-methyl-4,5,6,7-tetrahydrothieno[2,3-c]pyridine-3-carboxylate (2.26 g, 10 mmol) in 20 mL of ethanol, 5-chloro-2-hydroxybenzaldehyde (1.56 g, 10 mmol) was added dropwise with constant stirring. The mixture was refluxed for 4 hours and yellow precipitate was obtained (Scheme 1). Then, the crude product was dissolved in ethanol and single crystals for X-ray diffraction studies were grown by the slow evaporation method. The chemical analysis gave the following results: Yield: 75%, m.p. 208-210 °C; Elemental analysis for C₁₇H₁₇N₂O₃SCl: Calc. C, 55.96; H, 4.70; N, 7.68; S, 8.79. Found: C, 55.74; H, 4.48; N, 7.47; S, 8.62. FT-IR (ATR, cm⁻¹): 3050 (Ar-H); 2943 (aliph. C-H); 1667 (C=O); 1622 (CH=N). ¹H NMR (300 MHz, CDCl₃, ppm); δ= 12.88 (s, 1H, Ar-OH); 8.41 (s, 1H, CH=N); 7.15 (m, 2H, Ar-H); 6.79 (d, 1H, Ar-H); 3.88 (s, 3H, OCH₃); 3.41 (s, 2H, CH₂); 2.82

(t, 2H, CH₂); 2.64 (t, 2H, CH₂); 2.47 (s, 3H, NCH₃). ¹³C APT (75 MHz, CDCl₃, ppm); δ= 26.77 (C3); 45.49 (NCH₃); 51.71 (OCH₃); 52.12 (C4); 53.98 (C5); 119.14 (C10); 119.88 (C8); 123.77 (C12); 124.53 (C2); 129.45 (C7); 130.95 (C13); 133.37 (C11); 134.60 (C6); 153.04 (C1); 157.45 (C9); 159.58 (C=O); 163.34 (CH=N).

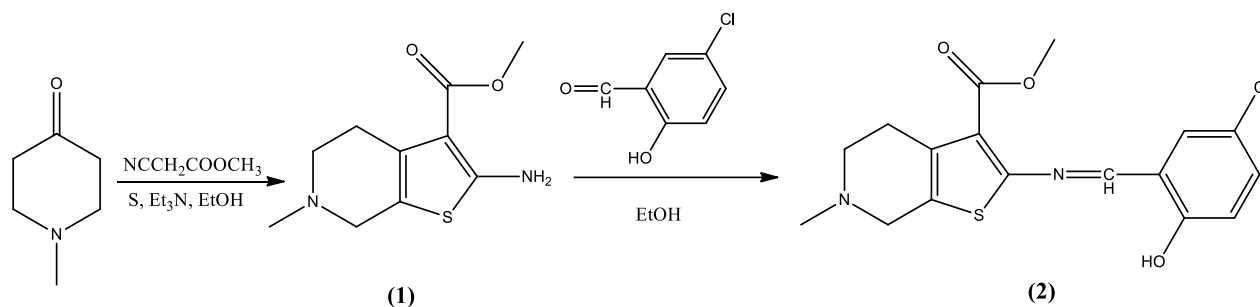
X-Ray crystallography

The rod shaped dark orange single crystal of Schiff base with dimensions 0.05x0.1x0.5mm was grown by slow evaporation of ethanolic solution. Crystal was mounted on a micromount and attached to a goniometer head on a Bruker D8 VENTURE diffractometer equipped with PHOTON100 detector using graphite monochromated Mo-Kα radiation (λ = 0.71073 Å) and scanned with 1° Φ-rotation frames at room temperature. Crystal parameters of Schiff base are summarized in Table 1. The structure was solved by intrinsic method SHELXS-1997 [41,42] and refined by using SHELXL-2014/7 (Sheldrick, 2014) [43]. ORTEP drawings with the atomic numbering is given in Fig. 2. and the crystal packing motif is shown in Fig. 3. All the molecular drawings were generated using OLEX2. Ver. 1.2-dev [44]. Thermal ellipsoids were plotted at the 50% probability level. Geometric values for the hydrogen bond are given in Table 2. Selected bond and torsion angles of molecule are given in the Table 3 (CCDC number is 1477724).

Electrochemical studies

In voltammetric measurements, glassy carbon electrode (BAS MF-2012), bulk electrolysis electrode (BAS MF-1056) and 11 μm-ultramicro carbon electrode (BAS MF-2007) were used as a working electrode. A platinum wire was used as the auxiliary electrode (BAS MW-1032). The reference electrode was a silver wire in contact with 0.01 M AgNO₃ in dimethylsulfoxide (BAS MF-2052).

The number of electrons transferred (n), the diffusion coefficient (D) and the heterogeneous rate constant (k_s) of Schiff base were determined by ultramicro electrode CV technique of Baranski method and Klingler-Kochi method.



Scheme 1. Synthesis method of Schiff base

Table 1. Crystal data for Schiff Base

Empirical formula	C ₁₇ H ₁₇ ClN ₂ O ₃ S (FW. 364.85)
T(K)	300(0)
λ(Å)	0.71073
Crystal system (space group)	Monoclinic (P 1 21/c 1)
Unit cell dimensions: (Å, °)	
a, b, c	11.2530(7), 10.4582(5), 28.7130(16)
V(Å ³)	3379.1(3)
α, β, γ	90, 90.289(2), 90

Table 2. H bonding distances

Donor---Hydrogen...Acceptor	D--H [Å]	H--A [Å]	D--A [Å]	D--H----A
O6---H13...N4	0.820(4)	1.884(9)	2.606(12)	2.606(12)

Table 3. Selected bond lengths (Å)

O6	C15	1.3428(1)	C6	C9	1.5030(1)	C16	C14	1.3742(1)
Cl2	C16	1.7428(1)	C9	N3	1.4562(1)	C14	C13	1.4013(1)
N4	C1	1.3743(1)	N3	C10	1.4624(1)	N1	C28	1.4616(1)
N4	C12	1.2813(1)	C15	C17	1.3859(1)	C23	O2	1.2003
C1	S2	1.7421(1)	C17	C18	1.3779(1)	C23	O1	1.3318(1)
S2	C6	1.7225(1)	C18	C16	1.3775	O1	C24	1.4418

Table 4. Selected bond and torsion angles (°)

bond angles (°)				torsion angles (°)				
S2	C1	C2	111.14	N1	C27	C25	C20	-51.8(2)
S2	C6	C5	113.09	C20	C19	S1	C22	1.1(2)
N1	C27	C25	111.03	C21	O2	C23	O1	-179.0(3)
N1	C26	C19	110.28	C22	N2	C29	C30	-175.7(2)
C23	O2	O1	30.18					
C21	C23	O2	123.83					
C23	O1	C24	116.44					
C4	O5	C3	114.52					

Table 5. Reduction peak potentials (E_p^c, V) of Schiff base at different scan rates

0.01 V/s	0.05 V/s	0.1 V/s	0.5 V/s	1 V/s	5 V/s
-1.15	-1.17	-1.19	-1.20	-1.21	-1.28
-2.14	-2.15	-2.17	-2.18	-2.19	-2.21
-2.60	-2.62	-2.64	-2.66	-2.69	-

Table 6. Electrochemical results of Schiff base*

D (cm ² /s) x 10 ⁷ <i>D</i> ± ts/√N	UME Limit current (i. A)x10 ¹⁰	n (Baranski method)	n (Bulk electrolysis)	k _s (cm/s)x10 ⁴ k _s ± ts/√N
8.85 ± 0.08	2.95 ± 0.02	1.96 ± 0.01	2.01 ± 0.01	9.12 ± 0.05

*Results are average of three measurements and standard deviation.

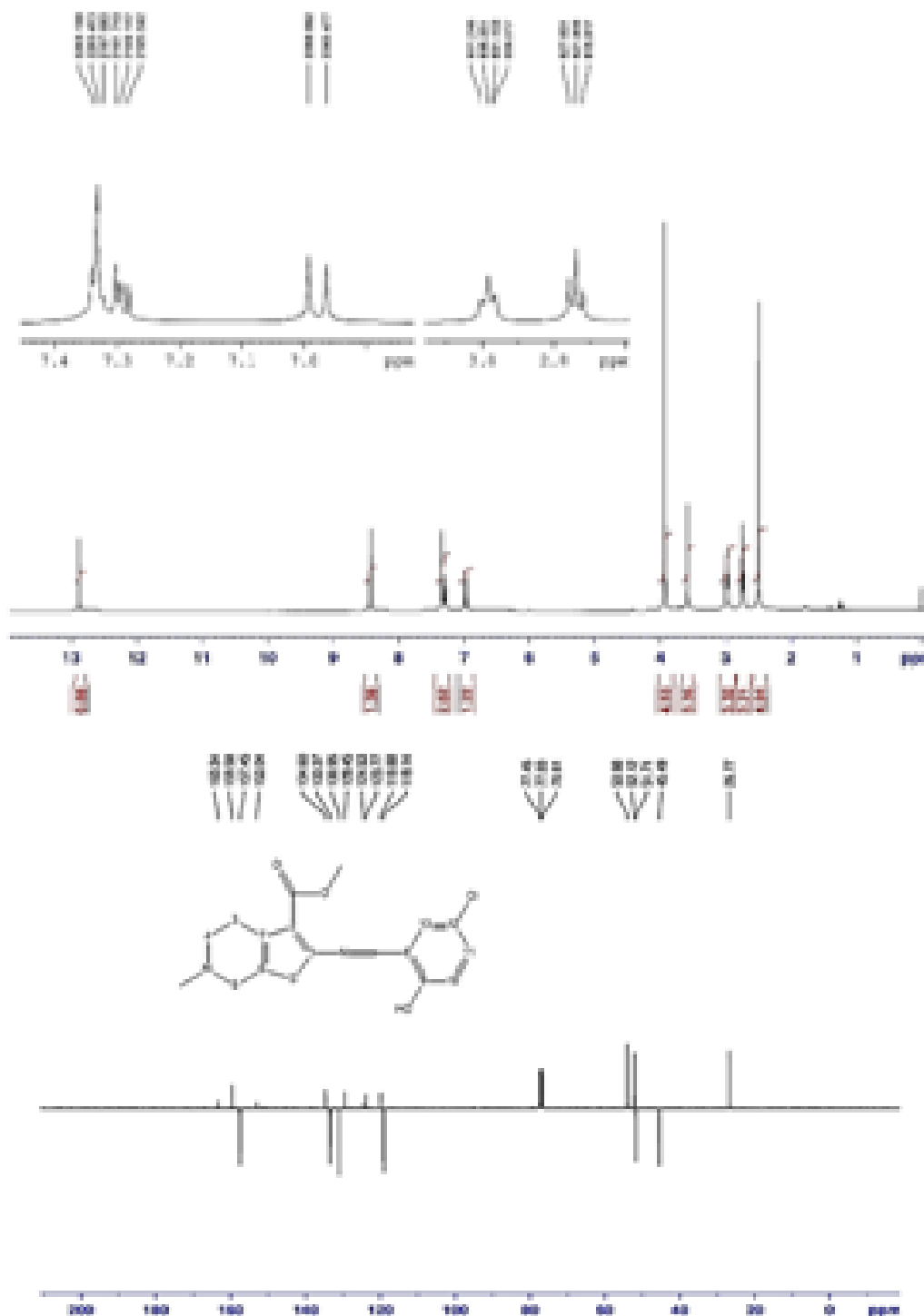


Fig. 1. ¹H(left side) and ¹³C-APT (right side) NMR spectrum of Schiff base.

RESULTS AND DISCUSSION

Structural characterization

^1H NMR spectra of methyl 2-((5-chloro-2-hydroxybenzylidene)amino)-6-methyl-4,5,6,7-tetrahydrothieno[2,3-c]pyridine-3-carboxylate shows the following signals in CDCl_3 solution. The peak observed at 12.88 ppm is the characteristic of intra-molecular hydrogen bonding of enolic proton (Ar-OH). The signal of imine (CH=N) hydrogen is observed at 8.41 ppm [45]. The signal of the aromatic protons are observed at 7.15 ppm and 6.79 ppm, respectively. The signal appearing at 3.88 ppm corresponds to the methoxy (OCH_3) protons, the signals at 3.41 ppm, 2.82 ppm and 2.64 ppm are belong to CH_2 protons of piperidine ring, the signal at 2.47 ppm may be attributed to the methyl group bounded to nitrogen in piperidine. In APT spectra, we observed signals at 26.77 (C3), 52.12 (C4), 53.98 (C5), 119.88 (C8), 123.77 (C12), 124.53 (C2), 129.45 (C7), 134.60 (C6), 153.04 (C1), 159.58 (C=O), 163.34 (CH=N) correspond to positive phases and the signals at 45.49 (NCH_3), 51.71 (OCH_3), 119.14 (C10), 130.95 (C13), 133.37 (C11), 157.45 (C9) correspond to negative phases, respectively. These results are coherent with the literature knowledge. ^1H and ^{13}C -APT spectrum of Schiff base are given in Fig. 1.

Crystal structure

According to crystal data (Table 1), -C=N- double bond distance of the imine moiety of 1.281 Å (1) is close to corresponding literature values [46]. The molecule is stabilized by medium strength intra-molecular hydrogen bonding that occurs between hydroxyl proton and imine nitrogen as shown in Fig. 2 and Table 2. The angle between the planes forming thiophene ring and phenyl unit is only 6.57° which shows that two units are nearly on the same plane. The piperidine ring exhibits a slightly distorted chair conformation [47]. Crystal packing of Schiff base is exhibited in Fig. 3, selected bond lengths (Å), bond and torsion angles ($^\circ$) are given in Table 3 and 4.

Electrochemical behavior

The electrochemical behavior of Schiff base was evaluated by cyclic voltammetry (CV), controlled potential electrolysis and chronoamperometry (CA) techniques. The cyclic voltammogram of Schiff base was taken at different scan rate (0.01-5 V/s) as seen in Fig. 4. Schiff base is also electrochemically active and its reduction potentials (E_p^c) are given in Table 5.

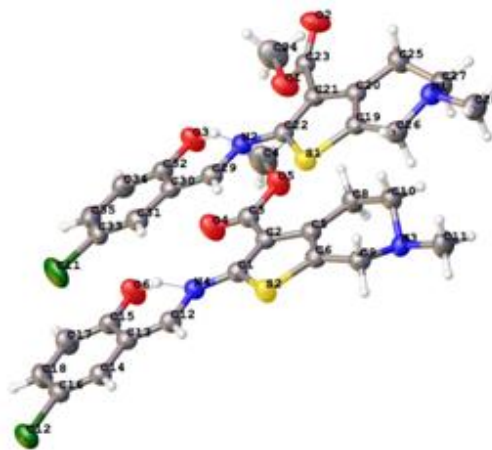


Fig. 2. The labeled diagram of asymmetric unit (intra-molecular hydrogen bonding)

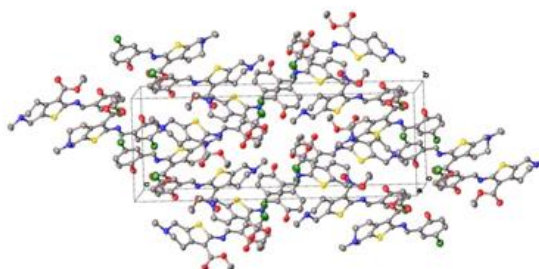


Fig. 3. Crystal packing of Schiff base (hydrogen atoms are omitted for clarity)

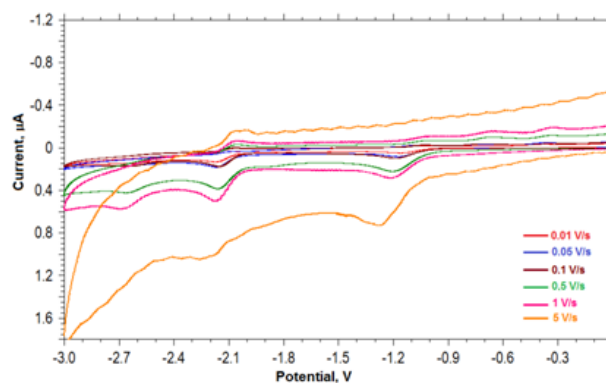


Fig. 4. Cyclic voltammogram of Schiff base in DMSO containing 0.1 M TBATFB on glassy carbon electrode at a scan rate of 0.01 V s^{-1} (vs. Ag/Ag^+)

The number of electrons transferred (n) and the diffusion coefficient (D) related with the diffused amount of compound to the electrode surface were determined (Table 6) by using ultramicro electrode and chronoamperometry methods [48-50]. The heterogeneous standard rate constant (k_s) is also found by Klingler-Kochi method (as seen Table 6).

The scan rate, reduction peak potential (E_p^c) and peak width ($E_{p/2}$) affect the value of k_s [51-54].

The electrochemical studies show that the electron transfer follows electrochemical reduction (EC) mechanism. It is supposed that EC mechanism occurs over $2e^-$ transferring through imine ($-CH=N$) group. The action mechanism of Schiff base can be useful for pharmacokinetic and pharmacodynamic purposes in biological systems as drugs.

CONCLUSIONS

Schiff base has been synthesized by the reaction of methyl 2-amino-6-methyl-4,5,6,7-tetrahydrothieno [2,3-c]pyridine-3-carboxylate with 5-chloro-2-hydroxybenzaldehyde and characterized by elemental analysis, ATR, 1H and ^{13}C APT methods. Crystal studies show that our molecule has intra-molecular hydrogen bonding between hydroxyl proton and imine nitrogen atoms.

Based on the electrochemical results, the reaction mechanism of Schiff base can conveniently be claimed as electrochemical reduction (EC) mechanism. The number of electrons transferred calculated with the use of UME is in good accordance with the number of electrons determined from bulk electrolysis. The electron transferred follows EC mechanism which contributes to the suggestion of the biochemical behavior of Schiff base.

Acknowledgments: We thank for financially supported by Hitit University (No. FEF19004.13.001).

REFERENCES

1. M. S. Yen, I. J. Wang, *Dyes Pigm.*, **61**, 243 (2004).
2. R.W. Sabnis, D.W. Rangnekar, N.D. Sonawane, *J. Heterocycl. Chem.*, **36**, 333 (1999).
3. H. Lütjens, A. Zickgraf, H. Figler, J. Linden, R.A. Olsson, P.J. Scammells, *J. Med. Chem.*, **46**, 1870 (2005).
4. Z. Puterova, A. Krutosikova, D. Vegh, *Arkivoc*, **i**, 209 (2010).
5. I.M.I. Fakhr, M.A.A. Radwan, S. El-Batran, M.E. Omar, A. El-Salam, S.M. El-Shenawy, *Eur. J. Med. Chem.*, **44**, 1718 (2009).
6. M.H.M. Helal, M.A. Salem, M.S.A. El-Gaby, M. Aljahdali, *Eur. J. Med. Chem.*, **65**, 517 (2013).
7. K.P. Kumar, S. Mohan, J. Saravanan, K.V. Prakash, N.A. Raju, J.V. Rao, *Int. J. Chem. Sci.*, **5**, 1284 (2007).
8. R. Narlawar, J.R. Lane, M. Doddareddy, J. Lin, J. Brussee, A.P. Jzerman, *J. Med. Chem.*, **53**, 3028 (2010).
9. W. Kemnitzer, N. Sirisoma, C. May, B. Tseng, J. Drewe, S.X. Cai, *Bioorg. Med. Chem. Lett.*, **19**, 3536 (2009).
10. J. Katada, K. Iijima, M. Muramatsu, M. Takami, E. Yasuda, M. Hayashi, M.Hattori, Y. Hayashi, *Bioorg. Med. Chem. Lett.*, **9**, 797 (1999).
11. (a) G.A. Elmegeed, W.W. Wardakhan, M. Younis, N.A. Louca, *Arch. Pharm.*, **337**, 140 (2004). (b) K.S.M. Shetty, V. Somashekar, S. Mohan, *Asian J. Chem.*, **16**, 623 (2004). (c) K. Harza, J. Saravanan, S. Mohan, *Asian J. Chem.*, **19**, 3541 (2007). (d) D. Singh, S. Mohan, P.C. Sharma, J. Saravanan, *Acta Pharm. Sci.*, **49**, 29 (2007).
12. R. Kulandasamy, A. V. Adhikari, P. J. Stables, *Eur. J. Med. Chem.*, **44**, 4376 (2009).
13. K. I. Molvi, K. K. Vasu, S. G. Yerande, V. Sudarsanam, N. Haque, *Eur. J. Med. Chem.*, **42**, 1049 (2007).
14. N. S. Rai, B. Kalluraya, B. Lingappa, S. Shenoy, V. G. Puranic, *Eur. J. Med. Chem.*, **43**, 1715 (2008).
15. B. V. Asthalatha, B. Narayana, K. K. Vijaya Raj, N. S. Kumari, *Eur. J. Med. Chem.*, **42**, 719 (2007).
16. A. Foroumadi, S. Mansouri, Z. Kiani, A. Rahmani, *Eur. J. Med. Chem.*, **38**, 851 (2003).
17. F.C. Meotti, D.O. Silva, A.R.S. dos Santos, G. Zeni, J.B.T. Rocha, C.W. Nogueira, *Environ. Toxicol. Pharmacol.*, **37**, 37 (2003).
18. S. Gobbi, A. Rampa, A. Bisi, F. Belluti, L. Piazzini, P. Valenti, A. Caputo, A. Zampiron, M. Carrara, *J. Med. Chem.*, **46**, 3662 (2003).
19. (a) D.M. Barnes, A.R. Haight, T. Hameury, M.A.M. Laughlin, J. Mei, J.S. Tedrowand, J.D.R. Toma, *Tetrahedron*, **62**, 11311 (2006). (b) G. Nikolakopoulos, H. Figler, J. Linden, P. Scammells, *J. Bioorg. Med. Chem.*, **14**, 2358 (2006). (c) A. D. Pillai, S. Rani, P. R. Rathod, F. P. Xavier, K. K. Vasu, H. Padh, V. Sudarsanam, *Bioorg. Med. Chem.*, **13**, 1275 (2005).
20. A. Cannito, M. Perrisin, C. Luu-Duc, F. Huguer, C. Gaultier, G. Narcisse, *Eur. J. Med. Chem.*, **25**, 635 (1990).
21. G. Nikolakopoulos, H. Figler, J. Linden, P. Scammells, *Bioorg. Med. Chem.*, **14**, 2358 (2006).
22. A. Gopalsamy, M. Shi, Y. Hu, F. Lee, L. Feldberg, E. Frommer, S. Kim, K. Collins, D. Wojciechowicz, R. Mallon, *Bioorg. Med. Chem. Lett.*, **20**, 2431 (2010).
23. H. H. D. Showalter, A. J. Bridges, H. Zhou, A. D. Sercel, A. McMichael, D. W. Fry, *J. Med. Chem.*, **42**, 5464 (1999).
24. Y. Dai, Y. Guo, R. R. Frey, Z. Ji, M. L. Curtin, A. A. Ahmed, D. H. Albert, L. Arnold, S. S. Arries, T. Barlozzari, J.L. Bauch, J. J. Bouska, P. F. Bousquet, G. A. Cunha, K. B. Glaser, J. Guo, J. Li, P. A. Marcotte, K. C. Marsh, M. D. Moskey, L. J. Pease, K. D. Stewart, V.S. Stoll, P. Tapang, N. Wishart, S. K. Davidsen, M. R. J. Michaelides, *Med. Chem.*, **48**, 6066 (2005).
25. A. G. Waterson, K. G. Petrov, K. R. Hornberger, R. D. Hubbard, D.M. Sammond, S. C. Smith, H. D. Dickson, T. R. Caferro, K. W. Hinkle, K. L. Stevens, S. H. Dickerson, D. W. Rusnak, G. M. Spehar, E. R. Wood, R. J. Griffin, D. E. Uehling, *Bioorg. Med. Chem. Lett.*, **19**, 1332 (2009).
26. S. B. Desai, P. B. Desai, K. R. Desai, *Heterocycl. Commun.*, **7**, 83 (2001).

27. F. D. Karia, P. H. Parsania, *Asian J. Chem.*, **11**, 991 (1999).
28. S. Samadhiya, A. Halve, *Orient. J. Chem.*, **17**, 119 (2001).
29. W. M. Singh, B. C. Dash, *Pesticides*, **22**, 33 (1988).
30. L. V. Kononenko, V. D. Bezuglyi, V. N. Dmitrieva, *Zh. Obshch. Khim.*, **38**, 2153 (1968).
31. P. Martinet, J. Simonet, J. Tendil, *C. R. Acad. Sci. C*, **268**, 303 (1969).
32. V. N. Dmitrieva, L. V. Kononenko, V. D. Bezuglyi, *Teor. Eksp. Khim.*, **1**, 456 (1965).
33. V. D. Bezuglyi, L. V. Kononenko, A. F. Forunova, V. N. Dmitrieva, B. L. Timan, *Zh. Obshch. Khim.*, **39**, 1680 (1969).
34. V. N. Dmitrieva, N. A. Rozanel'skaya, B. M. Krasovitskii, B. I. Stepanov, V. D. Bezuglyi, *Zh. Obshch. Khim.*, **41**, 60 (1971).
35. J. M. V. Scott, W. H. Jura, *Can. J. Chem.*, **45**, 2375 (1967).
36. V. N. Dmitrieva, V. B. Smelyakova, B. M. Krasovitskii, V. D. Bezuglyi, *Zh. Obshch. Khim.*, **36**, 405 (1966).
37. N. F. Levchenko, L. S. Afanasiadi, V. D. Bezuglyi, *Zh. Obshch. Khim.*, **37**, 666 (1967).
38. Y. Huang, A. Dömling, *Mol Divers.*, **15**, 3 (2011).
39. K. Gewalt, E. Schinke, H. Botcher, *Chem. Ber.*, **99**, 94 (1966).
40. K. Gewalt, *Chem. Ber.*, **98**, 3571 (1965).
41. G. M. Sheldrick, SHELXS-97, Program for Crystal Structure Solution, University of Göttingen, 1997.
42. G. M. Sheldrick, *Acta Cryst. A*, **64**, 112 (2008).
43. G. M. Sheldrick, SHELXTL Version 2014/7. <http://shelx.uni-c.gwdg.de/SHELX/index.php>.
44. O.V. Dolomanov, L.J. Bourhis, R.J. Gildea, J.A.K. Howard, H. Puschmann, *J. Appl. Cryst.*, **42**, 339 (2009).
45. Ü. Özmen Özdemir, A. Altuntaş, A. Balaban Gündüzalp, F. Arslan, F. Hamurcu, *Spectrochimica Acta Part A*, **128**, 452 (2014).
46. A.V. Metelitsa, A.S. Burllov, S.O. Bezugly, I.G. Borodkina, V.A. Bren, A.D. Garnovskii, V.I. Minkin. *Russ. J. Coord. Chem.*, **32**, 858 (2006).
47. J. Ellena, G. Punte, B. E. Rivero, M. V. Remedi, E. B. de Vargas, R. H. de Rossi, *J. Chem. Crystallogr.*, **25**, 801 (1995).
48. A.J. Bard, L.R. Faulkner, *Electrochemical Methods: Fundamentals and Applications*, John Wiley and Sons. Inc., New York, 2001.
49. A. Balaban Gündüzalp, Ü. Özdemir Özmen, B.S. Çevrimli, S. Mamaş, S. Çete, *Med. Chem. Res.*, **23**(7), 3255 (2014).
50. F. Hamurcu, S. Mamaş, U. Ozmen Ozdemir, A. Balaban Gündüzalp, O. Sanlı Senturk, *J. Mol. Struc.*, **1118**, 18 (2016).
51. R.J. Klingler, J.K. Kochi. *J. Phys. Chem.*, **85**, 1731 (1981).
52. A.S. Baranski, W.R. Fawcett, C.M. Gilbert, *Anal. Chem.*, **57**(1), 170 (1985).
53. A. Demirel Özel, Z. Durmuş, A. Çukurovalı, İ. Yılmaz, E. Kılıç, *Acta Chim Slov.* **56**, 797 (2009).
54. Fatma Hamurcu, S. Mamaş, U. Ozmen Ozdemir, A. Balaban Gündüzalp, O. Sanlı Senturk, *J. Mol. Struc.* **1118**, 18 (2016).

Synthesis and application of conducting polymers and their nanocomposites as a corrosion protection performances

M. Ates*, N. Uludag

Department of Chemistry, Faculty of Arts and Sciences, Namik Kemal University,
Degirmenalti Campus, 59030, Tekirdag, Turkey

Received August 25, 2016

Corrosion is explained as metal or alloy changes by chemical or electrochemical process or physical changes because of environmental effects. Corrosion occurs with oxidation and reduction reactions. In this study, Some general informations were given in the introduction section. And then, monomer synthesis, conducting polymers, nanocomposites, copolymers, and applications of corrosion protection performances were examined as a review article in recent papers.

Keywords: Corrosion, nanocomposites, EIS, Ag nanoparticles, copolymer.

INTRODUCTION

We introduce the some formulas, which are used in corrosion science as shown in Table 1. P is the protection efficiency (PE %) [1]. i_0 is the current density of an uncoated film, and i is the current density of the coated film. C_{corr} is the corrosion rate (CR mmy^{-1}) [2]. EW shows equivalent weight (g/eq), A is surface area (cm^2), and d represents density (g/cm^3). Similarly, corrosion rate was also calculated using the following expression

$$R_{corr} = 0.032 \times i_{corr} \times M \times n \times d, \quad (1)$$

where i_{corr} defines corrosion current density, M is molar mass (g/mol), n represents charge number, and d is density of tested metal (g/mol). Polarization resistance (R_p) was obtained by applying the Stern-Geary formula [3].

$$R_p = (\beta_a + \beta_c) / 2.303 \times i_{corr} (\beta_a + \beta_c), \quad (2)$$

where i_{corr} is corrosion current density β_a denotes Tafel slope of the anode and β_c is the Tafel slope of cathode. C_{sp} was obtained from Nyquist plot [4], which was obtained from the slope of a plot of the imaginary component (Z'') of the impedance at low frequency (f), where $\pi=3.14$, $f=0.01$ Hz and Z'' is the imaginary impedance.

Table 1. Some formulas are used in corrosion science.

$P = (i_0 - i) / i_0 \times 100$	$C_{corr} = 0.13 \times i_{corr} (EW) / A_d$
$R_{corr} = 0.032 \times i_{corr} \times M \times n \times d$	$R_p = (\beta_a + \beta_c) / 2.303 \times i_{corr} (\beta_a + \beta_c)$
$C_{sp} = -1 / (2 \times \pi \times f \times Z'')$	$C_{dl} = 1 / Z $

* To whom all correspondence should be sent:
E-mail: mates@nku.edu.tr

C_{dl} was obtained from Bode-magnitude plot [5], which gives the extrapolating line to the logZ axis at $w=1$ ($\log w=0$).

Monomer synthesis for corrosion protection performances

Rodriquez et al [6] have studied cationic polymerization of *N*-vinylcarbazole, initiated by $\text{Ph}_3\text{C}^+ \text{AsF}_6^-$ and $\text{Ph}_3\text{C}^+ \text{PF}_6^-$ in methylene dichloride at 20 °C and 0 °C. In addition, novel coral-like polyaniline sub-micrometer particles were synthesized by chemical polymerization. The obtained conductivity of PANI can obtain 2.7 Scm^{-1} [7]. 4-methylcarbazole-3-carboxylic acid was synthesized electrochemically on a stainless steel (316L) surface with lithium perchlorate/acetonitrile as the supporting electrolyte [8]. The corrosion performance of poly(4-methylcarbazole-3-carboxylic acid) (PCz) was examined by potentiodynamic polarization curves, open circuit potentials, and electrochemical impedance spectroscopy. The results show that PCz has an effective anodic protection in corrosive test solution. 4-(2-Thienyl) benzenamine (TBA) was synthesized by a simple method by Shahhosseini et al [9]. Structure of the synthesized monomer was characterized by IR, $^1\text{H-NMR}$, GC-MS and elemental analysis techniques. The TBA monomer was electrochemically synthesized in acidic aqueous solution by CV method. The corrosion tests in 3.5 wt % NaCl solution was performed by potentiodynamic polarization test and EIS. The results of PTBA were obtained to show enhanced corrosion protection effect on stainless steel electrode compared to PANI and polythiophene. Michel et al [10] have studied to test the controlling the concrete-reinforcement interfacial conditions.

This study focuses on the relation between macroscopic damage at the concrete-steel interface and corrosion initiation of reinforcement embedded in plain and fibre reinforced concrete.

Conducting polymers for corrosion protection performances

PANI are mostly used in corrosion protection of metals. Mostly, electropolymerization method was used to polymerize of the monomer due to its economical process [11]. It is necessary to passivate the metal before the electropolymerization method [12]. PANI has a large amount of amine and imine functional groups, which can interact with metal ions [13]. Grubac et al [14] have studied the reactive surface of Mg alloy which was coated with the nontoxic biocompatible polypyrrole film synthesized by electrochemical oxidation from an aqueous salicylate solution. The chemical polymerization of polyaniline (PANI) on cellulose fiber is used for various applications [15]. PANI by itself has poor mechanical properties but, by incorporation of micro or nanoparticles, its physical properties can be improved. The cellulose / PANI composite combines the properties of cellulose and conducting polymer of PANI, having application in corrosion protection of metals [16, 17]. Polyaniline (PANI), Polypyrrole (PPy) nanofilms, PANI/TiO₂ and PPy/TiO₂ nanocomposites were synthesized electrochemically on Al1050 electrode [18]. Perrin et al [19] have synthesized PANI dispersions consisting of 270 to 380 nm sized particles which were obtained by oxidation with ammonium peroxydisulfate (APS) in n-dodecylphosphonic acid (DPA) micellar solutions.

Bilal et al [20] have reported a sophisticated emulsion polymerization route for the synthesis of PANI. They work with two dopants i.e., dodecylbenzenesulfonic acid (DBSA) and sulfuric acid (H₂SO₄). Potentiodynamic measurements show that coatings of PANI can supply extra ordinary resistance to the steel surfaces particularly against the harsh corrosive environment of the oceans. In literature, a novel polyurea containing oligoaniline pendants (PU-p-OA) was synthesized by one step reaction way [21]. The inhibition effect of the electroactive PU-p-OA coatings on the cold rolled steel (CRS) in 5 wt % sodium chloride solution was examined by Tafel plot analysis and EIS method. Düdükçü et al have prepared poly(5-nitroindole)(P5NI) on 316L stainless steel (SS) [22]. P5NI coating against SS corrosion was studied in 3.5% NaCl solution by EIS, anodic polarization and the open circuit potential time

(E_{ocp}-t) diagrams. Billaud and co-worker [23] and Xu et al [24] studied the tests of polymerization of 5-nitroindole and showed that poly(5-nitroindole) films have easily electrodeposited by direct anodic oxidation of 5NI when certain conditions were applied. Polyaniline doped a phosphomolybdic acid was synthesized on stainless steel (SS304) by electropolymerization method [25]. The corrosion resistance of the coating was used in 1 M H₂SO₄ solution by electrochemical methods.

Recently, the inorganic materials added to the PPy coatings improved the mechanical and barrier properties of the coatings as corrosion inhibitor hosts [26-28]. Lei et al [29] have studied the polypyrrole films which were deposited on copper from "green" inhibitor of phytic acid solution for corrosion protection of copper. As a result, PPy coating prepared in the phytic acid solution at pH 4 show the most protective property against copper solution. Corrosion protection behaviour of poly(*N*-methylpyrrole) coated steel was examined in 0.5 M HCl solution by potentiodynamic polarization and EIS methods [30]. The results indicate that the P(NMPy)-DS coating supply effective protection for the stainless steel against to corrosion because of the fact that the large negatively charged dodecyl sulphate dopant in the polymer structure electrostatically repels corrosive chloride ions and delays their access to metal surface. A novel electroactive hyperbranched poly(aryl-ether keton) with oligoaniline segments has been synthesized by K₂CO₃-mediated nucleophilic aromatic polycondensation [31].

In literature, polycarbazole, polycarbazole/nanoclay and polycarbazole/Zn nanoparticles were chemically and electrochemically synthesized on a stainless steel (SS304) electrode [32]. The modified films was performed on SS304 by open circuit potential monitoring, potentiodynamic polarization and electrochemical impedance spectroscopic measurements to test the corrosion protection efficiency against 3.5 % NaCl solution. The highest protection efficiency (PE= 99.81%) was found for chemically synthesized PCz films. In literature, carbazole and *N*-vinylcarbazole were electrochemically polymerized in copper electrode and corrosion ability was studied in 0.5 M NaCl solution [33]. Strong adherent electro-active polymer films of poly(*N*-vinylcarbazole) (PVCz) and its nanocomposites with P(VCz)/nanoclay and P(VCz)/Zn nanoparticle have been electrodeposited on stainless steel (SS304) by chronoamperometric method using 0.3 M oxalic acid/butanol solution [34]. Conducting polymers have been extensively studied as protection for corrosion of metals in

recent years. Previous research on the corrosion protective properties of some conducting polymers is listed in Table 2.

Düdükçü et al [40] have studied the use of electrochemically synthesized polyindole (PIN) film, which was investigated for protective coating on 304 stainless steel. Corrosion tests demonstrated that PIN coating had important barrier effect to SS for significant immersion times in aggressive medium.

Thiophene, 3-hexylthiophene and its nanocomposites with TiO₂ were electropolymerized on Al1050 electrode by chronoamperometric technique [41]. Tüken et al [42] have electropolymerized poly(thiophene) on nickel coated mild steel (MS) electrode, in LiClO₄ containing acetonitrile medium (ACN-LiClO₄). The nickel coating showed like a physical barrier and supplied some protection to MS against corrosion. The corrosion behaviour of PPy/PTh film coated copper was tested in 3.5% NaCl solution [43]. EIS, anodic polarization curves and open circuit potential-time (E_{OCP}-t) diagrams were examined. The PPy/PTh coating provides important protection against copper corrosion for considerable immersion times. Silva et al [44] have studied the effect of thermal annealing of poly(3-octylthiophene) (P3OT) coatings on the corrosion inhibition of stainless steel in an NaCl solution.

Nanocomposites for corrosion protection performances

Poly(vinylacetate) (PVAc) coating over carbon steel was prepared by addition of emulsion nanoparticles in different concentrations (1%, 2% and 1.5%) in PVAc [45]. 2% of PANI/TiO₂ nanocomposite in PVAc has the best corrosion

protection in HCl. The growth of conducting polymers in the interlayer region of the clays has shown to dramatically improve the properties of conducting polymers [46]. Polypyrrole / Ni organic-inorganic hybrid materials were synthesized by electrochemically on carbon steel (AISI 1018) by combining potentiostatic and potentiodynamic methods [47]. Ashassi-Sorkhabi et al [48] have studied the effect of co-incorporation of a kind of nanomaterials and organic additives in a polymer matrix coating on corrosion performance of St-12 steel. Sonoelectrochemically the PPy, PPy-chitosan, PPy/MWCNTs and PPy/MWCNTs/chitosan films were studied on the base alloy.

The results show that PPy/MWCNTs/chitosan nanocomposite coating shows better corrosion protection than others. Valença et al [49] have synthesized polypyrrole/Zn nanoparticles hybrid nanocomposites and used them as additives in an epoxy paint to protect SAE 1020 carbon steel from corrosion.

Alhummade et al [50] have investigated the polyetherimide-graphene composites (PEI/G) which is used in corrosion inhibition coatings on copper substrates. In literature, a soluble terpolymer of aniline, 2-pyridylamine (PA) and 2,3-xylydine (XY), poly(AN-co-PA-co-XY) and its nanocomposite with ZnO nanoparticles were chemically synthesized by oxidative polymerization method with ammonium persulfate as an oxidant [51]. Polyaniline (PANI) and its nanocomposites containing TiO₂, Ag and Zn nanoparticles were electrocoated on an Al1050 electrode by cyclic voltammetry [52].

Table 2. Corrosion properties of some conducting polymer films obtained from literature.

Polymer	Measurement Technique	Solution	Results
PPy	Impedance spectroscopy	H ₂ SO ₄	PPy doesn't provide anodic protection of mild steel electrode. After short immersion time, PPy has in contact with H ₂ SO ₄ become undoped [35, 36].
PANI	Tafel extrapolation	H ₂ SO ₄	Corrosion of copper electrode occurs for synthesis from aniline in presence of H ₂ SO ₄ or from aniline sulphate without using H ₂ SO ₄ in the reaction medium [37].
PPy	Potentiodynamic method	H ₂ SO ₄	The corrosion resistance of the substrates was reduced after longer immersion times [38].
PTh	EIS and anodic polarization curves	LiClO ₄ /ACN	PTh top coat was improved the barrier efficiency and anodic polarization curves [39].

Copolymers for corrosion protection performances

Govindaraju et al [53] have studied the corrosion performance of zinc modified poly(aniline-co-pyrrole) coatings in 1 M HCl solution, using potentiodynamic polarization and EIS techniques. The interfacial co-polymerization of aniline and m-aminobenzene sulfonic acid in the presence of Cloisite 30B was performed in Sc-CO₂/water to produce the SPANI-clay nanocomposites [54]. Ozyilmaz et al [55] have studied zinc-iron-cobalt (ZnFeCo) particles which were electrochemically deposited on carbon steel (CS) electrode applying current of 3 mA with chronoamperometric technique. They have studied poly(aniline-co-o-anisidine), poly(aniline-co-pyrrole), poly(aniline-co-N-methylpyrrole) and poly(o-anisidine-co-pyrrole) copolymer coatings in 3.5% NaCl solution which was investigated by using AC impedance spectroscopy (EIS) technique, anodic polarization and the E_{OCP}-time curves. As a result, copolymer films showed important physical barrier on ZnFeCo plated carbon steel, in longer exposure time. In addition, poly(aniline-co-o-bromoaniline) copolymer has been synthesized using chemical oxidation method in HCl medium [56]. The electrical conductivity of the copolymers is found in the range of 10⁻⁵ Scm⁻¹. These organic semiconductor materials are used in optoelectronic devices that will replace the conventional inorganic semiconductors. Raotole et al [57] have studied poly(aniline-co-anisidine) (PAOA) coatings, which were used as corrosion protection on mild steel. The results of the potentiodynamic polarization measurements indicated that the PAOA coatings had more effective corrosion protection to mild steel than the respective homopolymers. Gopi et al [58] have studied the electrochemical synthesis of poly(indole-co-thiophene) copolymer on low-nickel stainless steel (LN-SS) with CV method in acetonitrile medium containing lithium perchlorate. As a result, a 1:1 ratio of indole to thiophene obtained the most stable and corrosion protective copolymer coating. Gopi et al [59] have studied the methacrylate based copolymers which have been synthesized by free radical solution polymerization technique from different mole ratios of N-vinylcarbazole and glycidyl methacrylate.

Application of corrosion protection performances

There are many metals, such as iron and its alloys which widely used in corrosion resistance in various neutral and aggressive environments [60, 61]. Polycarbazoles have been used in many areas,

such as electroluminescent devices, sensors, redox catalysts, and electrochromic displays [62-64]. Lei et al [65] have studied the effect of benzotriazole addition on polypyrrole film formation on copper and its corrosion protection. In 400 h of immersion, copper dissolution was protected with 80% inhibition efficiency relative to that of bare copper. Aravindan et al [66] found that after 300 h of immersion period, the Cu-PPy coating prepared from a solution containing 1:4 water to methanol volume ratio showed a better corrosion protection to SS than coatings prepared from other compositions.

Magnesium and its alloys are used in the applications, such as aerospace and automotive industry because of their excellent properties, such as high damping capacity, castability, weldability and recyclability [67]. The big problem is to have their high corrosion susceptibility [68, 69]. Electrochemically synthesized PPy coating on AZ31 magnesium alloy in a solution containing sodium salicylate and monomer of pyrrole through CV technique. Ma et al [70] have investigated the mechanism for localised corrosion in AA 2029-T83 alloy during immersion in 3.5 % NaCl solution. A model is suggested to explain the development of the localised corrosion in the alloy by taking into account heterogeneous plastic deformation during cold working and preferential precipitation of T1 phase at crystallographic defects within deformed grains. Polymer alloys show excellent coating properties. Palraj et al [71] have studied the corrosion resistant interpenetrating polymer networks (IPNs) were synthesized from immiscible resins (epoxy, silicone and thiophene).

CONCLUDING REMARKS

In this review article, new synthesis of monomers, polymers, nanocomposites and copolymers have used for corrosion protection on potential usefulness of other cheap metals or alloys in various medium. New monomer synthesis and new conducting polymer or nanocomposites or copolymer synthesis are important effect for corrosion synthesis are important effect for corrosion protection. Therefore, we analyze which material affect to this process.

Acknowledgments: Authors acknowledges to Namik Kemal University for financial support at 2nd AIOC ICNTC 2016 Conference in Zagreb, Croatia.

REFERENCES

1. M. Pehpour, S.M. Choreishi, N. Soltani, M. Salavati-Niasari, M. Hamadani, A. Gandami, *Corros. Sci.*, **50**, 2172 (2008).
2. J.M. Yeh, S.J. Liou, H.J. Lu, H.Y. Huang, *J. Appl. Polym. Sci.*, **92**, 2269 (2004).
3. E. Pooquasemi, O. Abootalebi, M. Peikari, F. Haqdar, *Corros. Sci.*, **51**, 1043 (2009).
4. M. Ates, T. Karazehir, F. Arican, N. Eren, *Iran. Polym. J.*, **22**, 199 (2013).
5. E. Sezer, B. Ustamethmetoglu, A.S. Sarac, *Synth. Met.*, **107**, 7 (1999).
6. M. Rodriguez, L.M. Leon, *European Polymer J.*, **19**, 585 (1983).
7. J.R. Zhang, X. Wang, G.C. Qi, B.H. Li, J.L. Qiao, X.H. Zhang, *Acta Polymerica Sinica*, **2**, 149 (2016).
8. M. Düdükçü, Y.A. Ergun, K. Pekmez, G. Okay, A. Yildiz, *Electrochem Days*, **6**, 76 (2005).
9. L. Shahhosseini, M.R. Nateghi, S. SheikhSivandi, *Synth. Met.*, **211**, 66 (2016).
10. A. Michel, A.O.S. Solgaard, B.J. Pease, M.R. Geiker, H. Stang, J.F. Olesen, *Corrosion Science*, **77**, 308 (2013).
11. P. Pawar, B. Gaikawad, P.P. Patil, *Sci. Technol. Adv. Mater.*, **7**, 732 (2006).
12. A. Nautiyal, S. Parida, *Prog. Org. Coat.*, **94**, 28 (2016).
13. N. Jiang, Y. Xu, Y. Dai, W. Luo, L.J. Dai, *Hazard Mater.*, **215-216**, 17 (2012).
14. Z. Grubac, I.S. Roncevic, M. Metikos-Hukovic, *Corros. Sci.*, **102**, 310 (2016).
15. B.H. Lee, H.J. Kim, H.S. Yang, *Curr. Appl. Phys.*, **12**, 75 (2012).
16. C. Borsoi, A.J. Zattera, C.A. Ferreira, *Appl. Surf. Sci.*, **364**, 124 (2016).
17. D.Y. Liu, G.X. Sui, D. Bhattacharyya, *Compos. Sci. Technol.*, **99**, 31 (2014).
18. M. Ates, O. Kalender, E. Topkaya, L. Kamer, *Iran. Polym. J.*, **24**, 607 (2015).
19. F.X. Perrin, T.A. Phan, D.L. Ngyen, *J. Polym. Sci. Part A: Polym. Chem.*, **53**, 1606 (2015).
20. S. Bilal, S. Gul, R. Holze, A.H.A. Shah, *Synth. Met.*, **206**, 131 (2015).
21. M. Chi, F. Li, M. Zhou, K. Zhao, D. Chao, C. Wang, *Colloid Polym. Sci.*, **293**, 2217 (2015).
22. M. Düdükçü, F. Köleli, *Prog. Org. Coat.*, **62**, 1 (2008).
23. H. Talbi, D. Billaud, *Synth. Methods*, **97**, 239 (1998).
24. J. Xu, W. Zhou, J. Hou, S. Pu, L. Yan, J. Wang, *Mater. Lett.*, **59**, 2412 (2005).
25. Y. Gao, J.A. Syed, H. Lu, X. Meng, *Appl. Surf. Sci.*, **360**, 389 (2016).
26. I.A. Kartsonakis, A.C. Balaskas, E.P. Koumoulos, C.A. Charitidis, G. Kordas, *Corros. Sci.*, **65**, 481 (2012).
27. D.V. Andreeva, E.V. Skorb, D.G. Shchukin, *ACS Appl. Mater. Interfaces*, **2**, 1954 (2010).
28. D. Borisova, H. Mohwald, D.G. Shchukin, *ACS Nano*, **5**, 1939 (2011).
29. Lei Y, Sheng N, Hyono A, M. Ueda, T. Ohtsuka, *Prog. Org. Coat.*, **77**, 774 (2014).
30. B. Zeybek, E. Aksun, *Prog. Org. Coat.*, **81**, 1 (2015).
31. F. Li, M. Zhou, J. Wang, X.Liu, C.Wang, D. Chao, *Synth. Met.*, **205**, 42 (2015).
32. M. Ates, A.T. Özyilmaz, *Prog. Org. Coat.*, **84**, 50 (2015).
33. C.T. Wang, S.H. Chen, H.Y. Ma, C.S. Qi, *J. Appl. Electrochem.*, **33**, 179 (2003).
34. M. Ates, *J. Solid State Electrochem.*, **19**, 533 (2015).
35. N.V. Krstajic, B.N. Grgur, *Electrochim. Acta*, **42**, 1685 (1997).
36. B.N. Grgur, N.V. Krstajic, *Prog. Org. Coat.*, **33**, 1 (1998).
37. S. Bhandari, D. Khastgir, *Int. J. Polym. Mater. Polym. Biomater.*, **65**, 543 (2016).
38. A.A. Ganash, *J. Compos. Mater.*, **48**, 2215 (2014).
39. T. Tüken, B. Yazici, M. Erbil, *Appl. Surf. Sci.*, **239**, 398 (2005).
40. M. Düdükçü, F. Köleli, *Prog. Org. Coat.*, **55**, 324 (2006).
41. M. Ates, A. Dolapdere, *Polymer-Plastics Technology and Engineering*, **54**, 1780 (2015).
42. T. Tüken, B. Yazici, M.Erbil, *Appl. Surf.Sci.*, **239**, 398 (2005).
43. T. Tüken, B. Yazıcı, M. Erbil, *Prog. Org. Coat.*, **53**, 38 (2005).
44. U. Leon-Silva, M.E. Nicho, J.G. Gonzalez-Rodriguez, J.G. Chacon-Nava, N.M. Salinas-Bravo, *J. Solid State Electrochem.*, **14**, 1089 (2010).
45. M. Khademian, H. Eisazadeh, *J. Polym. Eng.*, **35**, 597 (2015).
46. U. Riaz, S.M. Ashraf, A. Verma, *Current Org. Chem.*, **19**, 1275 (2015).
47. A.M. Torres-Huerta, M.A. Dominguez-Crespo, A. Alanis-Valdelamar, E. Onofre-Bustamonte, M.L. Escudero, M.C. Garcia-Alonso, J.A. Lois-Correa, *Metallurgical and Materials Transactions A*, **46A**, 1741 (2015).
48. H. Ashassi-Sorkhabi, R. Bagheri, B. Rezaei-Maghadam, *J. Mater. Eng. Performance.*, **24**, 385 (2015).
49. D.P. Valença, K.G.B. Alves, C.P. Neto, N. Bouchonreau, *Materials Research*, **18**, 273 (2015).
50. H. Alhumade, A. Abdala, A. Yu, A. Elkamel, L. Simon, *The Canadian J. Chem. Eng.*, **94**, 896 (2016).
51. R. Alam, M. Mobin, *J. Aslam, Appl. Surf. Sci.*, **368**, 360 (2016).
52. M. Ates, E. Topkaya, *Prog. Org. Coat.*, **82**, 33 (2015).
53. K.M. Govindaraju, V.C.A. Prakash, *Colloids and Surfaces A: Physicochem. Eng. Aspects*, **465**, 11 (2015).
54. T. Mousavinejad, M.R. Bagherzadeh, E. Akbarinezhad, M. Ahmadi, M.J.F. Guinel, *Prog. Org. Coat.*, **79**, 90 (2015).
55. A.T. Ozyilmaz, B. Avsar, G. Ozyilmaz, İH. Karahan, T. Camurcu, F. Colak, *Appl. Surf. Sci.*, **318**, 261 (2014).
56. A. Mahudeswaran, J. Vivekanandan, P.S. Vijayanand, T. Kojima, S. Kato, *Int. Modern Phys. B.*, **30**, Article number: 1650008.

57. P.M. Raotole, P. Koinkar, B. Joshi, S.R. Patil, *J. Coat. Technol. Res.*, **12**, 757 (2015).
58. D. Gopi, R. Saraswathy, L. Kavitha, D.K. Kim, *Polym. Int.*, **63**, 280 (2014).
59. D. Gopi, K.M. Govindaraju, L. Kavitha, K.A. Basha, *Prog. Org. Coat.*, **71**, 11 (2011).
60. D. Gopi, K.M. Govindaraju, V.C.A. Prakash, V. Manivannan, L. Kavitha, *J. Appl. Electrochem.*, **39**, 269 (2009).
61. D. Gopi, K.M. Govindaraju, V.C.A. Prakash, D.M.A. Sakila, L. Kavitha, *Corros. Sci.*, **51**, 2259 (2009).
62. Y. Diamant, J. Chen, H.Han, B. Kamenev, L. Tsybeskov, H.Grebel, *Synth. Met.*, **151**, 202, 2005.
63. G. Nie, J. Xu, S. Zhang, T. Cai, X. Han, *J. Appl. Polym. Sci.*, **102**, 1877, 2006.
64. M. Düdükçü, Y.A. Udum, Y. Ergün, F. Köleli, *J. Appl. Polym. Sci.*, **111**, 1496 (2009).
65. Y.H. Lei, N. Sheng, A. Hyono, M. Ueda, T. Ohtsuka, *Prog. Org. Coat.*, **77**, 339 (2014).
66. N. Aravindan, M.V. Sangaranarayanan, *Prog. Org. Coat.*, **95**, 38 (2016).
67. E. Ghali, Magnesium and Magnesium alloys, Uglig's Corrosion Handbook, John Wiley & Sons, New York, 2000.
68. E. Aghion, B. Bronfin, *Mater. Sci. Forum*, **350**, 19 (2000).
69. H. Tsubakino, A. Yamamoto, K. Sugahara, S. Fukumoto, *Mater. Sci. Forum*, **419**, 915 (2003).
70. Y. Ma, X. Zhou, Y. Liao, Y. Yi, H. Wu, Z. Wang, W. Huang, *Corros. Sci.*, **107**, 41 (2016).
71. S. Palraj, M. Selvaraj, M. Vidhya, G. Rajagopa, *Prog. Org. Coat.*, **75**, 356 (2012).

A comparative DNA binding study for heteroleptic platinum (II) complexes of pip and hpip

U. Yildiz*, B. Coban

Department of Chemistry, Bulent Ecevit University, Zonguldak 67100, Turkey

Received August 25, 2016

In this study, G-quadruplex DNA (Q-DNA) binding abilities of two platinum complexes ([Pt(bpy)(pip)](NO₃)₂ (1) and [Pt(bpy)(hpip)](NO₃)₂ (2) (bpy is 2,2'-bipyridine; pip is 2-phenylimidazo[4,5-f][1,10]phenanthroline; hpip is 2-(2-hydroxyphenyl)imidazo[4,5-f][1,10]phenanthroline) those previously reported were compared with double stranded DNA (ds-DNA) binding abilities. The interactions of both derivatives with human telomere Q-DNA (both the antiparallel basket and the mixed-hybrid G-quadruplex) and ds-DNA have been comparatively studied by UV-visible (UV-Vis), fluorescent intercalator displacement (FID) assays and thermal melting methods. The results show that both derivatives can stabilize Q-DNA and they show different binding affinities for different Q-DNA and ds-DNA. All spectroscopic studies have shown that the derivatives have a modest selectivity for Q-DNA vs ds-DNA. Increase in melting temperature was detected for both DNA forms but increase in Q-DNA melting temperature was significantly higher.

Keywords: Pt(II); G-Quadruplex DNA; ds-DNA; DNA binding

INTRODUCTION

Guanine-rich regions of genomic DNA are suggested to fold into non-canonical secondary structures known as G-quadruplexes (GQ). GQs are formed by π - π stacking of G-quartets, which are composed of four planar guanines held together by Hoogsteen hydrogen-bonds. Since the demonstration of G-quadruplexes and G-tetraplexes telomeric DNA [1-3], the conformations and functions of G-quadruplexes have gained considerable research interest [4]. During the replication in normal cell proliferation, telomeres erode by about 100 bp with each cell division which finally triggering cellular senescence [5, 6]. However, in most cancer cells, telomere cannot be shortened because of high telomerase enzyme activity. The formation of stable G-quadruplex from G-rich strands of telomere inhibits catalytic functions of the telomerase enzyme. Therefore, molecules those can stabilize G-rich strands to form G-quadruplexes have gained considerable research interest because quadruplex stabilizers could serve as antitumor agents [7-9].

As common structural features, G-quadruplex binders generally share a large, flat, aromatic surface, and the presence of protontable side chains. Most known G-quadruplex binders such as BRACO-19, RHSP4, and telomestatin [10-12] are polycyclic planar aromatic compounds with at least one substituent terminating in a cationic group.

Some metal complexes also have been used to target G-quadruplexes due to their planar aromatic ligands and cationic metal center [13-15].

Several metal complexes and cationic form of pip and hpip ligands have been synthesized and their ds-DNA binding properties have extensively been studied [16-22]. In this study, double stranded and G-quadruplex DNA (Q-DNA) binding abilities of two platinum complexes (fig.1) those previously synthesized [18] has been discussed.

MATERIALS AND METHODS

All reagents and solvents were of commercial origin and used without further purification unless otherwise noted. Solutions of calf thymus DNA (CT-DNA; purchased from Sigma) in 100 mM KCl, 10 mM Tris (pH 7.0) had a UV-Vis absorbance ratio of 1.8–1.9: 1 at 260 and 280 nm ($A_{260}/A_{280} = 1.9$), indicating that the DNA was sufficiently free of protein [23]. The concentration of ds-DNA was determined spectrophotometrically using a molar absorptivity of $6600 \text{ M}^{-1} \text{ cm}^{-1}$ (260 nm).

HTG21 (5'-GGGTTAGGGTTAGGGTTAGGG-3') Q-DNA oligomer (purchased from thermo) extinction coefficients were calculated from mononucleotide data using a nearest-neighbour approximation [24]. Double-distilled water was used to prepare buffers. Stock solutions of ds-DNA and Q-DNA were stored at 4 °C and used within 4 days. The formation of intramolecular Q-DNA was

* To whom all correspondence should be sent:
E-mail: ufyildiz@gmail.com

carried out as follows: the oligonucleotide samples, dissolved in different buffers, were heated to 90 °C for 5 min, gently cooled to room temperature, and then incubated at 4 °C overnight. Solutions of the compounds were prepared by dissolving a weighed amount in 0.5 mL DMSO for solubility reasons and were then diluted (up to 150 times without precipitation) with 100 mM KCl, 20 mM Tris (pH 7.5) to the required concentration.

Physical measurements

UV-Vis spectra were recorded with a Varian Cary 100 spectrophotometer and emission spectra were recorded with a PerkinElmer LS 55 spectrofluorophotometer at room temperature.

Absorption titrations

For the absorption and emission titrations, compounds were dissolved in a minimum amount of DMSO, and were then diluted in buffer (100 mM KCl, 20 mM Tris (pH 7.5)) to a final concentration of 20 μM. Titrations were performed in a 10-mm stoppered quartz cell by using a fixed concentration of the complexes (20 μM), to which the CT-DNA stock solution was added in increments of 1 μL to a DNA-to-compound concentration ratio of 2.4:1 for ds-DNA and 0.003:1 for Q-DNA. Complex-DNA solutions were incubated for 10 min each time before the spectra were recorded. A control solution of 20 μM compound in the same buffer

was also treated in the same manner. Cell compartments were thermostated at 25 ± 0.1 °C.

UV melting studies

For UV thermal melting studies, solutions of the Q-DNA and ds-DNA in the absence and presence of the complexes [DNA/complex = 1/1] were prepared in a buffer solution (20 mM Tris-HCl, pH 7.5, 100 mM KCl). The temperature of the solution was increased at a 1 °C min⁻¹ interval, and the absorbance at 295 nm was continuously monitored. The *T_m* values were determined graphically from the plots of absorbance vs temperature.

FID studies

The competitive behavior of each compound with thiazole orange (TO) was investigated by fluorescence spectroscopy in order to examine whether the compound is able to displace TO from the Q-DNA-TO complex.

DNA was pretreated with TO at a TO to DNA concentration ratio of 2:1 for 30 min at 27 °C to prepare the initial complex. The intercalating effect of the complexes with the Q-DNA-TO complex was studied by adding a certain amount of a solution of the compound in increments to the solution of the Q-DNA-TO complex. The influence of each addition of complex to the solution of the Q-DNA-TO complex was obtained by recording the change in the fluorescence spectrum. To study the competitive binding of the compound with TO, TO was excited at 504 nm.

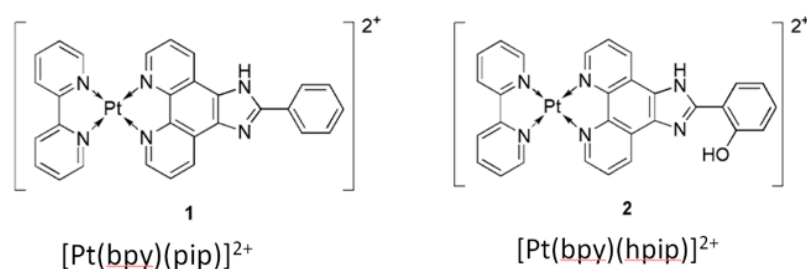


Fig. 1. Platinum complexes used in this study ($[\text{Pt}(\text{bpy})(\text{pip})](\text{NO}_3)_2$ (**1**) and $[\text{Pt}(\text{bpy})(\text{hpi})](\text{NO}_3)_2$ (**2**)).

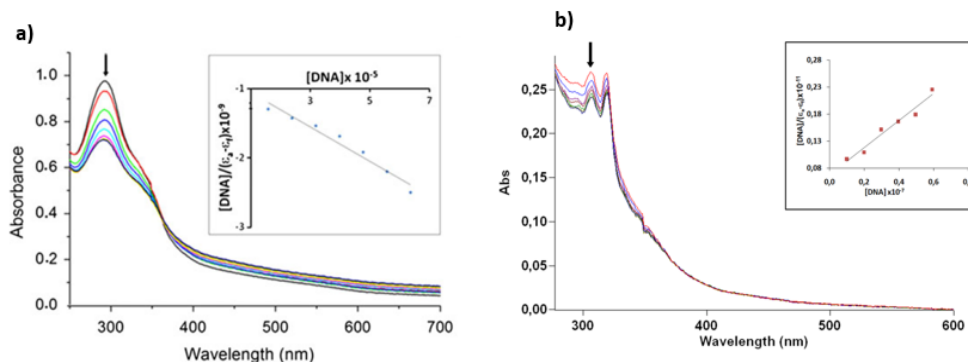


Fig. 2. UV-vis spectra of **1** (20 μM) in Tris/KCl buffer (100 mM KCl, 20 mM Tris-HCl, pH 7.5) with increasing amounts of ds (a) Q-DNA (b) ds-DNA.

RESULTS AND DISCUSSION

Synthesis of ligands and complexes

Synthesis and characterization of ligands and complexes was discussed in detail in our previous study [18].

Electronic absorption titration

The application of electronic absorption spectroscopy in DNA binding studies is one of the most useful techniques. Electronic spectra are a useful way to investigate the interactions of complexes with DNA. A complex bound to DNA through intercalation usually results in hypochromism and red shift (bathochromism) owing to the intercalation mode involving a strong stacking interaction between an aromatic chromophore and the base pairs of DNA. The extent of the hypochromism in the visible metal-to-ligand charge transfer band is commonly consistent with the strength of the intercalative interaction [25].

The high energy band around 292 nm is attributed to the $\pi \rightarrow \pi^*$ transitions corresponding to the phenanthroline moiety of the ligands. Absorption spectra titrations were performed to determine the binding affinity of complex to Q-DNA. DNA sample was added in aliquots sequentially to complex solutions, with absorbance spectra recorded after each addition. The changes in the spectral profiles during titration were shown in Fig. 2. When both Q-DNA and ds-DNA is added into complex 1 solutions, significant hypochromism is observed in absorption spectra. Similar hypochromism is observed for complex 1 upon addition of the lower rate of Q-DNA than ds-DNA under the same conditions. R_{\max} values can be seen in table 1. When the amount of DNA was

increased, the decreases in the intensities of the $\pi \rightarrow \pi^*$ transitions of complex 1 were 27.9 % for ds-DNA at a DNA-to-Pt concentration ratio of 4.8 and 12.2 % for Q-DNA at a DNA-to-Pt concentration ratio of 0.03. The similar case could be seen for complex 2. Hypochromism at low R values for Q-DNA indicated strong interactions between the G-quadruplex form of DNA and the complexes. In order to compare quantitatively the binding strength of complexes to Q- DNA and ds-DNA, the intrinsic binding constants K_b with each DNA at 25 °C were obtained using the following equation;

$$[DNA]/(\varepsilon_A - \varepsilon_f) = [DNA]/(\varepsilon_B - \varepsilon_f) + 1/K_b (\varepsilon_B - \varepsilon_f) \quad (1)$$

where [DNA] is the concentration of the nucleic acid in base pairs, ε_a is the apparent absorption coefficient obtained by calculating $A_{\text{obs}}/[Pt]$, and ε_f and ε_B are the absorption coefficients of the free and the fully bound platinum complex, respectively. In the $[DNA]/(\varepsilon_A - \varepsilon_f)$ versus [DNA] plot, K_b is given by the ratio of the slope to the intercept. The values of the intrinsic binding constants K_b of 1 were derived to be $2.88 (\pm 0.4) \times 10^4$ and $3.58 (\pm 0.3) \times 10^7$ for ds-DNA and Q-DNA respectively. As seen in results, K_b for Q-DNA is bigger than ds-DNA. This indicates that complex 1 is more selective for G-quadruplex form of DNA. K_b of 2 were derived to be $5.38 (\pm 0.4) \times 10^4$ and $3.83 (\pm 0.5) \times 10^7$ for ds-DNA and Q-DNA respectively.

Similar binding trend to complex 1 has been observed for complex 2 with a greater binding constant value for Q-DNA (Fig. 3). Both complexes can bind to G-quadruplex form more selective. The difference between K_b values of complexes for different DNA forms was approximately 10^3 results from complexes can interact with Q-DNA at much lower R values than ds-DNA.

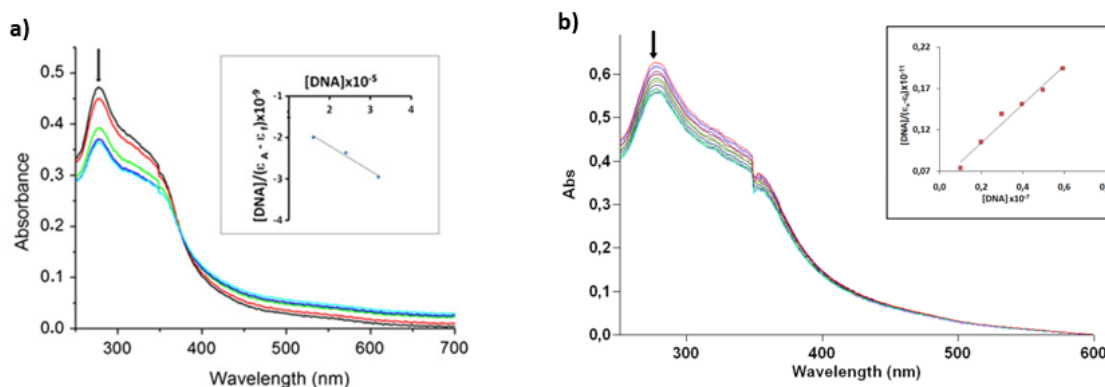


Fig. 3. UV-vis spectra of 2 (20 μ M) in Tris/KCl buffer (100 mM KCl, 20 mM Tris-HCl, pH 7.5) with increasing amounts of ds (a) Q-DNA (b) ds-DNA

Table 1. UV titration results

Titration results for ds-DNA				Titration results for Q-DNA		
Complex	ΔA (%)	K_b (M^{-1})	R	ΔA (%)	K_b (M^{-1})	R
1	27.9	$2.88 (\pm 0.4) \times 10^4$	4.8	12.2	$3.58 (\pm 0.3) \times 10^7$	0.03
2	23.4	$5.38 (\pm 0.4) \times 10^4$	2.4	11.5	$3.83 (\pm 0.5) \times 10^7$	0.03

UV melting studies

The DNA thermal melting is a measure of the stability of the DNA double helix with temperature an increase in the thermal melting temperature (T_m) indicates an interaction between ds-DNA and the metal complex [26]. Like ds-DNA, an increase in T_m of Q- DNA can be observed as a result of interaction between Q- DNA and metal complexes [27]. In the present case, thermal melting studies were carried out and T_m values were determined by monitoring the absorbance of ds-DNA at 260 nm and Q-DNA at 295 nm as a function of temperature. Usually, classical intercalation gives rise to higher ΔT_m values than either groove binding or outside stacking [28]. The T_m of ds-DNA in the absence of any added complex was found to be $78 \text{ }^\circ\text{C} \pm 0.20$, under our experimental conditions. Under the same set of conditions, ds-DNA structure degraded at $82 \text{ }^\circ\text{C} \pm 0.32$ and $83 \text{ }^\circ\text{C} \pm 0.24$ in the presence of complexes 1 and 2, respectively. The observed ΔT_m value of $2 \text{ }^\circ\text{C}$ and $3 \text{ }^\circ\text{C}$ for 1 and 2 respectively indicates that complex 2 binds to ds-DNA stronger than complex 1. These are consistent with the determined K_b values, further stressing that intercalation took place (Fig. 4).

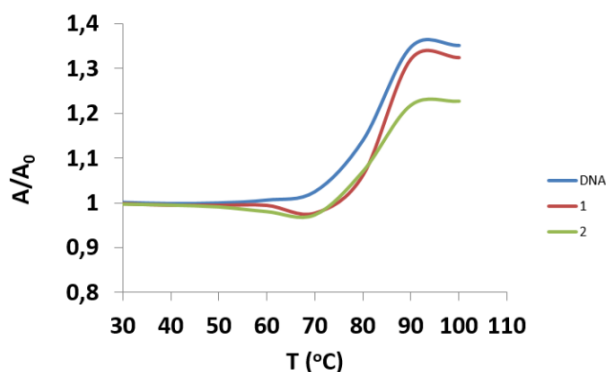


Fig. 4. UV melting curves for (—) ct-DNA, (—) ct-DNA + 1 and (—) ct-DNA + 2.

The T_m of Q-DNA in the absence of any added complex was found to be $45 \text{ }^\circ\text{C} \pm 0.40$, under our experimental conditions. It is uprised to $62 \text{ }^\circ\text{C} \pm 0.34$ and $67 \text{ }^\circ\text{C} \pm 0.28$ by addition of complex 1 and 2, respectively (fig.5). The great increase in T_m values indicates that both complexes bind to Q-DNA stronger than ds-DNA. Also ΔT_m value of 22

$^\circ\text{C}$ for complex 2 shows that it can stabilize the Q-DNA better than complex 1 with a ΔT_m value of 17 $^\circ\text{C}$.

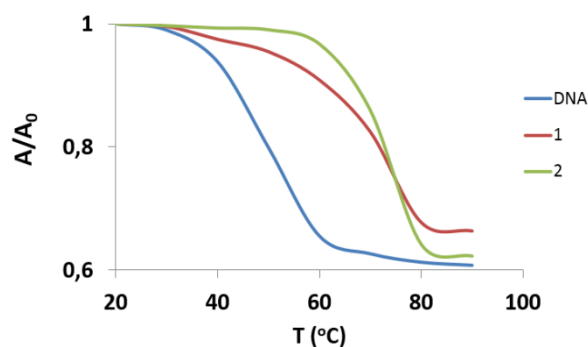


Fig. 5. UV melting curves for (—) HTG21, (—) HTG21 + 1 and (—) HTG21 + 2.

FID studies

To further clarify the nature of the interaction between the complex and Q-DNA and ds-DNA FID was carried out. FID is a simple and fast method to evaluate the affinity of a compound for Q-DNA [29, 30]. This assay is based on the loss of fluorescence of thiazole orange (TO) upon competitive displacement from DNA by a putative ligand. Upon interaction with Q-DNA, TO exhibits high affinity ($K = 3.0 \times 10^6 M^{-1}$) [31] and displays a significant increase in its fluorescence, whereas when free in solution, the fluorescence is quenched. Therefore, displacement of TO by another molecule provides an approximate measure of the affinity of the given compound for duplex and quadruplex DNA by evaluating the DC_{50} which corresponds to the required concentration of complex to induce a 50% fluorescence decrease.

We were first interested in comparing the Q-DNA binding abilities of the complex 1. The emission spectra of TO bound to ds-DNA and Q-DNA in the absence and the presence of complex 1 are shown in Fig. 6.

DC_{50} value of complex 1 for Q-DNA that can be seen in table 2 was lower than ds-DNA. This indicates that 1 can kick out TO molecules from Q-DNA easier due to stronger binding. The emission spectra of TO bound to ds-DNA and Q-DNA in the absence and the presence of complex 2 are shown in Fig. 7. DC_{50} of complex 2 for Q-DNA is lower than DC_{50} for ds-DNA. To discuss the G-

quadruplex selectivity of complexes, DC_{50} values can be compared.

The selectivity of both complexes for Q-DNA versus ds-DNA was calculated and both complexes showed prominent G-quadruplex binding affinity, a modest selectivity for G-quadruplex over double stranded was observed. However, calculated selectivity of complex **2** is nearly 2 times better than complex **1**.

Table 2. DC_{50} values

Complex	DC_{50} (ds-DNA (μM))	DC_{50} (Q-DNA (μM))	Selectivity ($DC_{50}\text{-ds}/$ $DC_{50}\text{-Q}$)
1	11.70	7.87	1.49
2	11.23	4.53	2.65

CONCLUSION

Q-DNA selectivities of two previously synthesized platinum complexes have been compared with different spectroscopic methods. All methods are consistent with each other and demonstrate that complex **2** is a more selective complex for Q-DNA as supposed. Such a difference in the DNA-binding affinities between **1** and **2** can be reasonably explained by the intramolecular hydrogen bond between the ortho phenolic group and the nitrogen atom of the imidazole ring. The extended co-planarity of the hpip ligand leads to enhanced DNA-binding affinity of the hpip complex. Q-DNA binding affinity was more significantly enhanced because Q-DNA has a larger surface area due to four guanine bases.

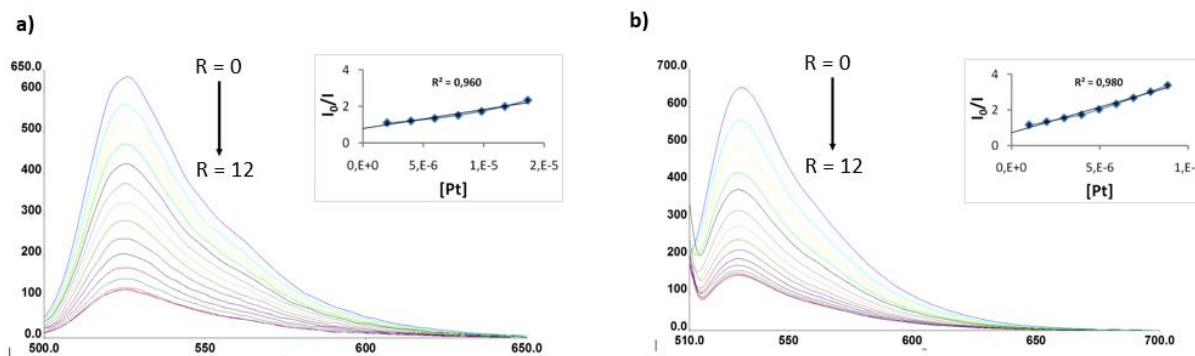


Fig. 6. Fluorescence spectra of TO (2 μM) with (a) ds-DNA (30 μM) (b) Q-DNA (1 μM) in Tris/KCl buffer (100 mM KCl, 20 mM Tris-HCl, pH 7.5) with increasing amounts of **1**.

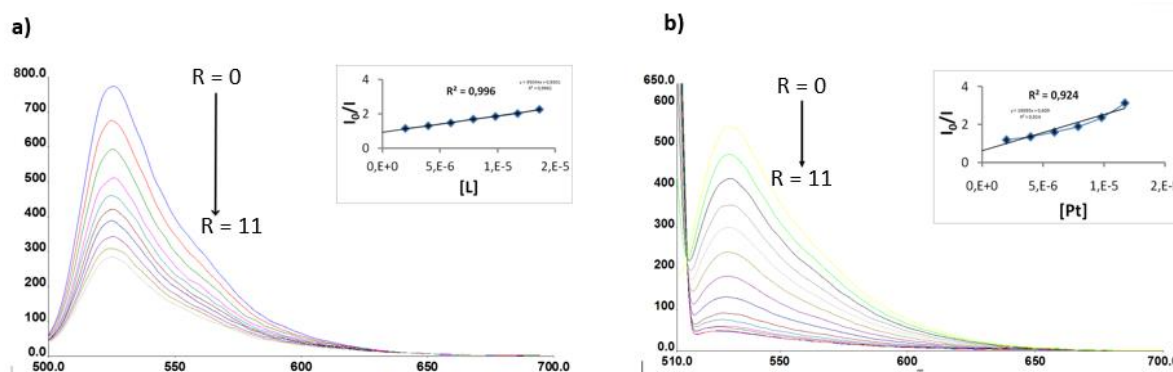


Fig. 7. Fluorescence spectra of TO (2 μM) with (a) ds-DNA (30 μM) (b) Q-DNA (1 μM) in Tris/KCl buffer (100 mM KCl, 20 mM Tris-HCl, pH 7.5) with increasing amounts of **2**.

Acknowledgements: We are grateful for the support of Bulent Ecevit University with grant 2014-72118496-04 and 2016-YKD-72118496-04.

REFERENCES

1. E. Henderson, C.C. Hardin, S.K. Walk, I. Tinoco Jr, E.H. Blackburn, *Cell*, **51**, 899 (1987).
2. D. Sen, W. Gilbert, *Nature*, **334**(6180), 364 (1988).
3. J.R. Williamson, M.K. Raghuraman, T.R. Cech, *Cell*, **59**, 871 (1989).
4. S. Neidle, G. Parkinson, *Nat. Rev. Drug. Discov.*, **1**, 383 (2002).
5. C.B. Harley, A.B. Futcher, C.W. Greider, *Nature*, **345**(6274), 458 (1990).
6. E.H. Blackburn, *Cell*, **106**, 661 (2001).
7. J.-L. Mergny, C. Helene, *Nat. Med.*, **4**, 1366 (1998).
8. L. Guittat, A. De Cian, F. Rosu, V. Gabelica, E. De Pauw, E. Delfourne, J.L. Mergny, *Biochim. Biophys. Acta, Gen. Subj.*, **1724**, 375 (2005).
9. Y. Mikami-Terao, M. Akiyama, Y. Yuza, T. Yanagisawa, O. Yamada, T. Kawano, M. Agawa, H. Ida, H. Yamada, *Exp. Eye Res.*, **89**, 200 (2009).
10. A.M. Burger, F. Dai, C.M. Schultes, A.P. Reszka, M.J. Moore, J.A. Double, S. Neidle, *Canc. Res.*, **65**, 1489 (2005).
11. T. Tauchi, K. Shin-ya, G. Sashida, M. Sumi, S. Okabe, J.H. Ohyashiki, K. Ohyashiki, *Oncogene*, **25**, 5719 (2006).
12. P. Phatak, J.C. Cookson, F. Dai, V. Smith, R.B. Gartenhaus, M.F.G. Stevens, A.M. Burger, *Br. J. Cancer*, **96**, 1223 (2007).
13. G.-B. Jiang, Y.-Y. Xie, G.-J. Lin, H.-L. Huang, Z.-H. Liang, Y.-J. Liu, *J. Photochem. Photobiol.*, **129**, 48 (2013).
14. J.-T. Wang, X.-H. Zheng, Q. Xia, Z.-W. Mao, L.-N. Ji, K. Wang, *Dalton Trans.*, **39**, 7214 (2010).
15. T. Wilson, P.J. Costa, V. Félix, M.P. Williamson, J.A. Thomas, *J. Med. Chem.*, **56**, 8674 (2013).
16. B. Coban, I.O. Tekin, A. Sengul, U. Yildiz, I. Kocak, N. Sevinc, *J. Biol. Inorg. Chem.*, **21**, 163 (2016).
17. B. Coban, U. Yildiz, *Analogs. Appl. Biochem. Biotechnol.*, **172**, 248 (2014).
18. B. Coban, U. Yildiz, A. Sengul, *J. Biol. Inorg. Chem.*, **18**, 461 (2013).
19. I. Kocak, U. Yildiz, B. Coban, A. Sengul, *J. Solid State Electrochem.*, **19**, 2189 (2015).
20. C.M. Che, M.S. Yang, K.H. Wong, H.L. Chan, W. Lam, *Eur. J. Chem-a*, **5**, 3350 (1999).
21. M. Cusumano, M.L. Di Pietro, A. Giannetto, *Inorg. Chem.*, **45**, 230 (2006).
22. L. Messori, P. Orioli, C. Tempi, G. Marcon, *Biochem. Biophys. Res. Commun.*, **281**, 352 (2001).
23. Z. Liu, H. Lv, H. Li, Y. Zhang, H. Zhang, F. Su, S. Xu, Y. Li, Y. Si, S. Yu *et al*, *Chemother.*, **57**, 310 (2011).
24. C. Zimmer, E. Birch-Hirschfeld, R. Weiss, *Nucleic Acids Res.*, **1**, 1017 (1974).
25. J.K. Barton, A. Danishefsky, J. Goldberg, *J. Am. Chem. Soc.*, **106**, 2172 (1984).
26. V. Gabelica, E. De Pauw, F. Rosu, *J. Mass Spectrom.*, **34**, 1328 (1999).
27. P.A. Rachwal, K.R. Fox, *Methods*, **43**(4), 291 (2007).
28. C. Uslan, B. Şebnem Sesalan, *Dyes and Pigments*, **94**, 127 (2012).
29. D. Monchaud, C. Allain, M.-P. Teulade-Fichou, *Bioorg. Med. Chem. Lett.*, **16**, 4842 (2006).
30. K. Suntharalingam, A.J.P. White, R. Vilar, *Inorg. Chem.*, **48**, 9427 (2009).
31. J. Nygren, N. Svanvik, M. Kubista, *Biopol.*, **46**, 39 (1998).

Symmetric device performances of carbon based nanostructures for supercapacitors

M. Ates*

Department of Chemistry, Faculty of Arts and Sciences, Namik Kemal University,
Degirmenalti Campus, 59030, Tekirdag, Turkey

Received June 26, 2016, Revised September 10, 2016

In this review article, symmetric device performances of carbon based nanostructures were reviewed and presented for supercapacitors. There are many important parameters to affect the supercapacitor device performances. The most important one is the formation of active materials used for electrodes. Nowadays, graphene based nanostructures have been used as an active electrode material due to their storage capability of more charges compared to other carbon materials. Supercapacitors divide two main parts: pseudocapacitors and electrical double layer capacitors (EDLCs). Conducting polymers are also used as important active material components due to their good conductivity. Some techniques were also presented to obtain information about capacitance, such as electrochemical impedance spectroscopy (EIS) etc.

Keywords: Carbon nanostructures, nanomaterials, conducting polymers, supercapacitors, double-layer capacitance, graphene.

INTRODUCTION

Graphene is used in many applications, such as energy storage, environmental protection, chemical conversion, electrocatalysis, nanoelectronics etc. Graphene facile stacking nature caused by the strong π - π interaction and van der Waals forces between graphene layers [1]. 3D porous graphene significantly enhanced the energy storage performance because of increasing surface area and effective pores to transport or store electrons / ions for bulk use in many devices [2, 3]. Zhao et al have studied Ni(OH)₂ nanocrystals which have been synthesized via a gas liquid diffusion method at room temperature in the absence of any template or organic surfactant [4]. Supercapacitors have much attention over the past decade due to their extremely high power density, long cycle life and short changing time [5]. Supercapacitors divide into two categories, namely pseudocapacitors [6], and electrical double layer capacitors (EDLCs). EDLC stores electric charges at the interface between the electrode and the electrolytes. Electroactive materials have been made from carbon materials with high surface area, such as graphene, carbon nanotubes and porous carbon [7]. Modern electronic devices, such as electric/hybrid vehicles, mobile communication devices has high-performance energy storage resources [8]. The illustration of supercapacitor device was given in Figure 1.

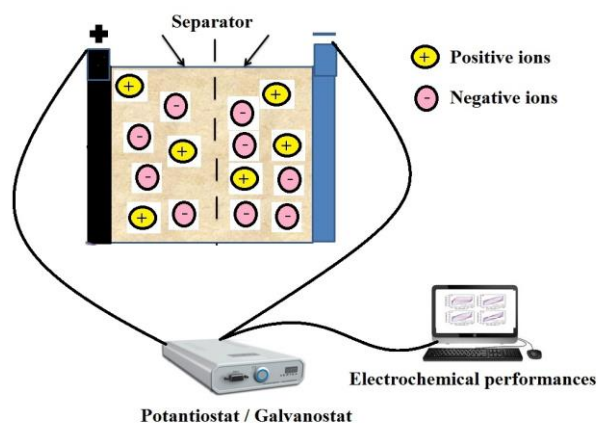


Fig. 1. The illustration of supercapacitor device with all components.

PSEUDOCAPACITORS

Pseudocapacitors have transition metals (Ru, Co, Fe, Mn etc.) oxides higher capacitance and energy density because of the fast and reversible faradaic reactions [9-11]. Among the transition metal oxides, manganese (Mn) compounds have been used due to its multi-oxidation states for charge transfer and reversible adsorption [12]. Mei et al [13] presented that MnO₂-graphene composite has the specific capacitances of $C_{sp} = 112 \text{ Fg}^{-1}$ in 1 M Na₂SO₄ and $C_{sp} = 165 \text{ Fg}^{-1}$ in 6 M KOH electrolyte, respectively. In addition, multiwalled carbon nanotubes / α -MnO₂ coaxial nanocable films through electrophoretic deposition process shows a high mass specific capacitance of $C_{sp} = 327 \text{ Fg}^{-1}$ and good cycle stability [14]. MnO₂ nanorods / graphene composite was synthesized a specific

* To whom all correspondence should be sent:
E-mail: mates@nku.edu.tr

capacitance of $C_{sp} = 268 \text{ Fg}^{-1}$ at a current density of 0.5 Ag^{-1} [15]. The PANI-5% acetylene black (AB) hallowed hybrids show much better electrochemical performance ($C_{sp} = 520 \text{ Fg}^{-1}$ at 1 Ag^{-1}) than that of pure PANI pseudocapacitors ($C_{sp} = 271 \text{ Fg}^{-1}$ at 1 Ag^{-1}). In addition, the high power density of $P = 1361 \text{ Wkg}^{-1}$ and energy density of $E = 17.8 \text{ Whkg}^{-1}$ at current density of 2 Ag^{-1} even 6.32 kWkg^{-1} and 14.1 Whkg^{-1} at high current density of 10 Ag^{-1} [16]. The fabricated flexible and transport pseudocapacitor of ultrafine Co_3O_4 nanocrystal shows a high capacitance of $C_{sp} = 177 \text{ Fg}^{-1}$ on a mass basis and $C_{sp} = 6.03 \text{ mFcm}^{-2}$ based on the area of the active material at a scan rate of 1 mVs^{-1} , as well as a super-long cycling life with 100% retention rate after 20,000 cycles [17]. One of the highest capacitance value was obtained as $C_{sp} = 2105 \text{ Fg}^{-1}$ for $\text{Ni}_{10}\text{Co}_5$ LDH NSs/CNs electrode at a current density of 2 Ag^{-1} as well as an excellent cyclic stability as a pseudocapacitive electrode material [18]. Ren et al have reported metallic cobalt pyrite (CoS_2) nanowires (NWs) prepared directly on current collecting electrodes, e.g., carbon cloth or graphite disc, for high-performance supercapacitors [19].

Electrical double layer capacitors

Electrochemical capacitors (ECs) are used for an electrode of a given polarity, opposite charges stored on the electrode surface. Two parallel plates constitute capacitor and the consequent device are called as electrical double layer capacitors (EDLCs) [20]. In literature, Zhou et al have studied highly porous nanostructures with large surface areas, which are typically employed for EDLCs to increase gravimetric energy storage capacity; however, carbon based electrodes with high surface area show in poor volumetric capacitance due to the low packing density of porous materials. They found ultrahigh volumetric capacitance of $C_{sp} = 521 \text{ Fcm}^3$ in aqueous electrolytes for non-porous carbon microsphere electrodes codoped with fluorine and nitrogen, which is synthesized by low temperature solvothermal route. The carbon nanostructures including CNTs-based networks, graphene based architectures, hierarchical porous carbon based nanostructures and other even more complex carbon based 3D configurations were studied in literature [21].

Active materials

Active materials were obtained many polymeric and composite materials which include carbon based nanostructures. Composite materials with polymeric matrix consist of a fiber material, which

is used as the core and a matrix material [22]. The fiber reinforced materials have more advantages than the other composite materials due to their low weight, resistance against the corrosion, heat sound and electric isolation [23, 24]. Active materials are synthesized by two ways, such as chemical and electrochemical synthesis. The active materials were characterized by FTIR-ATR, $^1\text{H-NMR}$, $^{13}\text{C-NMR}$, CV, SEM-EDX, and AFM analysis. Symmetric device was fabricated to examine supercapacitor device performances with CV, constant current (CC), and EIS analysis. To understand the more information about energy density, power density and charge transfer resistance (R_{ct}), Warburg impedance etc, Ragone plot and equivalent circuit models were analyzed obtained from electrochemical measurements. The high performance capacitive behaviour depends on the total mass (current collectors, electrolyte type, separator, etc.), thus, the greater percentage of active materials in the electrode material results in more energy storage in the supercapacitor device [25]. Carbons are used to fabricate supercapacitor active electrode materials due to the low cost, easy availability, nontoxic nature, environmental friendless, and stability [26].

Conducting polymers

Conducting polymers were used in many usage areas, such as energy storage (batteries and supercapacitors), electrochromic devices (smart windows, mirrors IR and microwave shutters), antistatic coatings (displays, flat TV screens), semiconductor devices (solar cells), corrosion protection, mechanical actuators, bioapplication (drug delivery systems, artificial muscles, biosensors). A novel synthesis of Cz-EDOT comonomers and their copolymers (EDOTTsCz, EDOTVBCz, and EDOTMetac) were synthesized in our previous studies. The aim of these syntheses is to obtain capacitance performances of the active materials [27]. Three-dimensional (3D) material shows great attention all the time because it exhibits the enhanced capacitive performance comparing with the low dimensional nanoscale building blocks [28].

There are many parameters affecting the conducting polymers, such as current density, used methods, type of solvent and electrolytes, monomer concentration, monomer structure and applied potential etc. The performance of a supercapacitor depends on many factors, such as the active material used as the electrode, the nature of electrolyte, and the interface between electrode and electrolyte [29]. In literature, PANI-based

supercapacitor by designed the PANI-acetylene black (PANI-AB) hybrid nanostructures supported by MnO₂ nanotubes have good long-term cycling stability and 86% of the capacitance after 1000 cycles by CV test at a scan rate of 50 mVs⁻¹ compared to that of pure PANI based supercapacitors [30]. Li et al have studied PANI/carbon nanotubes with ternary coaxial structures as supercapacitor electrodes via a simple wet chemical method [31].

Electrochemical impedance spectroscopy

Electrochemical impedance spectroscopic analysis (EIS) were examined using Nyquist plots, which show the frequency response of the electrode/electrolyte system, graph the imaginary component (*Z'*). Nyquist plots show three parts. In the first part, a semicircle in the high to medium frequency region, with the starting cross-point at the *Z'* axis, consists of the combined series resistance of electrolyte, electrode and current collectors, such as stainless steel, in the second part; a straight line with a slope of 45° in the low-frequency range which representative to the semi-infinite Warburg impedance, resulting from the frequency dependence of the ion diffusion / transport in the electrolyte, in the third part; a vertical line at very low frequencies, which is obtained by the accumulation of ions at the bottom of the pores of the electrode [32]. A vertical line proves a good capacitive behaviour without diffusion limitations [33]. A low frequency capacitive value can be calculated from the Nyquist plot according to the following equation 1.

$$C_{sp} = -1 / (2\pi \times f \times Z''), \quad (1)$$

where *f* is the frequency and *Z''* (*f*) is the imaginary part of the impedance. The relationship between the specific capacitance and frequency shows the penetration of the alternating current into the bulk pores of the electrode material, which can indicate how many electrolyte ions have reached the pore surfaces at a specific frequency [34]. EIS, CV and CC analysis of different types of polymers and nanocomposites were analyzed in literature [35-37]. Mn₃O₄ samples were prepared in 0.05 M Mn(NO₃)₂ solution for 30 min delivered a large gravimetric specific capacitance of *C_{sp}*= 210 Fg⁻¹ at a current density of 0.5 Ag⁻¹, and a good rate capability over other samples [38].

The symmetrical supercapacitors based on the porous silicon carbide spheres (PSiCS) electrode with an aqueous electrolyte (1 M KCl) or an organic electrolyte (1 M tetraethyl ammonium tetrafluoroborate) in acetonitrile were designed in

literature [39]. There are many usage areas of supercapacitors from portable electronic devices to electric vehicles. The study written by Niesson et al have mentioned about the steady-state impedance measurements, cross-correlated with cyclic voltammetry, which show discharging of the electrical double layer capacitance [40].

CONCLUDING REMARKS

Supercapacitors have lower energy than batteries but higher power density with fast charge/discharge rates and a much larger cycle life than rechargeable batteries. In this review article, we firstly classified the electrochemical capacitors as pseudocapacitors and EDLCs. Secondly, we investigated the active materials used in supercapacitor devices, conducting polymers, and electrochemical impedance spectroscopy. Symmetric supercapacitor devices were fabricated by carbon based nanostructures, such as graphene, carbon nanotubes, carbon fibers, etc. Not only the specific capacitance (*C_{sp}*) performance but also the energy (*E*) and power density (*P*) values should be higher for supercapacitors. To obtain the higher *C_{sp}*, *E* and *P* performances, the active electrode materials should be fabricated by higher conductive and higher surface area materials.

Acknowledgments: Dr. Murat Ates acknowledges to Namik Kemal University for financial support at 2nd AIOC ICNTC 2016 Conference in Zagreb, Croatia.

REFERENCES

1. J.L. Shi, H.F. Wang, X. Zhu, C.M. Chen, X. Huang, X.D. Zhang, B.Q. Li, C. Tang, Q. Zhang, *Carbon*, **103**, 36 (2016).
2. S. Mao, G.H. Lu, J.H. Chen, *Nanoscale*, **7**, 6924 (2015).
3. J.L. Shi, H.F., Wang, X. Zhu, C.M. Chen, X. Huang, X.D., Zhang, B.Q. Li, C. Tang, Q. Zhang, *Carbon*, **103**, 36 (2016).
4. J. Zhou, Z. Shi, Q. Zhang, *J. Alloys Compounds*, **668**, 176 (2016).
5. B.P. Bastakoti, H.S., Huang, L.C. Chen, K.C.W. Wu, Y. Yamauchi, *Chem. Commun.*, **48**, 9150 (2012).
6. I. Shakir, M. Nadeem, M. Shahid, D.J. Kang, *Electrochim. Acta*, **118**, 138 (2014).
7. M.F. Warsi, I. Shakir, M. Shahid, M. Sarfraz, M. Nadeem, Z.A. Gilahi, *Electrochim. Acta*, **135**, 513 (2014).
8. J. Li, X. Zhang, J. Guo, R. Peng, R. Xie, Y. Huang, Y. Qi, *J. Alloys Comp.*, **674**, 44 (2016).
9. W. Li, K. Xu, B. Li, J. Sun, F. Jiang, Z. Yu, R. Zou, Z. Chen, J. Hu, *Chem. Electrochem.*, **1**, 1003 (2014).
10. J. Huang, J. Zhu, K. Qheng, Y. Xu, D. Cao, G. Wang, *Electrochim. Acta*, **75**, 273 (2012).

11. R.B. Rakhi, W. Chen, M.N. Hedhili, D. Cha, H.N. Alshareef, *ACS Appl. Mater. Interfaces*, **6**, 4196 (2014).
12. S. He, W. Chen, *J. Power Sources*, **294**, 150 (2015).
13. J. Mei, L. Zhang, *J. Solid State Chem.*, **221**, 178 (2015).
14. H. Fang, S. Zhang, X. Wu, W. Liu, B. Wen, Z. Du, T. Jiang, *J. Power Sources*, **235**, 95 (2013).
15. Y. Cao, Y. Xiao, Y. Gong, C. Wang, F. Li, *Electrochim. Acta*, **127**, 200 (2014).
16. Y. Xi, G. Wei, X. Liu, M. Pang, L. Liu, Y. Yang, Y. Ji, V.Y. Izotov, N.I. Klyui, W. Han, *Chem. Eng. J.*, **290**, 361 (2016).
17. X. Liu, Y.Q. Gao, G.W., Yang, *Nanoscale*, **8**, 4227 (2016).
18. G. Nagaraju, G.S.R. Raju, Y.H. Ko, J.S. Yu, *Nanoscale*, **8**, 812 (2016).
19. R. Ren, M.S. Faber, R. Dziedzic, Z.H. Wen, S. Jin, S. Mao, J.H. Chen, *Nanotechnology*, **26**, Article number: 494001 (2015).
20. P.R. Bandaru, H. Yamada, R. Narayanan, M. Hoefler, *Materials Science and Engineering R*, **98**, 1 (2015).
21. H. Jiang, P.S. Lee, C.Z. Li, *Energy & Environmental Science*, **6**, 41 (2013).
22. C. Misirli, N. Becenen, M. Sahin, *Applied Mechanics and Materials*, **555**, 406 (2014).
23. N. Becenen, *Tekstili Obleklo*, **57**, 8 (2009).
24. N. Becenen, B. Eker, M. Sahin, *J. Reinforced Plastics and Composites*, **29**, 3637 (2010).
25. S.H. Kazemi, M.A. Kiani, M. Ghaemmaghami, H. Kazemi, *Electrochim. Acta*, **197**, 107 (2016).
26. P.V. Adhyapak, T. Maddanimath, S. Pethkar, A.J. Chandwadkar, Y.S. Negi, K. Vijayamohanon, *J. Power Sources*, **109**, 105 (2002).
27. M. Ates, N. Uludag, T. Karazehir, F. Arican, *Ovidius University Annals of Chemistry*, **23**, 63 (2012).
28. Y. Zhang, Z. Hu, Y. An, B. Guo, N. An, Y. Liang, H.Wu, *J. Power Sources*, **311**, 121 (2016).
29. A.G. Pandolfo, A.F. Hollenkamp, *J. Power Sources*, **157**, 11 (2006).
30. Y. Xi, G. Wei, X. Liu, M. Pang, L. Liu, Y. Yang, Y. Ji, V.Y. Izotov, N.I. Klyui, W. Han, *Chemical. Eng. J.*, **290**, 361 (2016).
31. Q. Li, J. Liu, J. Zou, A. Chunder, Y. Chen, L. Zhai, *J. Power Sources*, **196**, 565 (2011).
32. M.J. Kim, J.H. Kim, *Phys. Chem. Chem. Phys.*, **16**, 11323 (2014).
33. M.J. Kim, J.H. Kim, *ACS Appl. Mater. Interfaces*, **6**, 9036 (2014).
34. W. Xing, S.Z. Qiao, R.G. Ding, F. Li, G.Q., Lu, Z.F. Yan, H.M. Cheng, *Carbon*, **44**, 216 (2006).
35. A.S. Sarac, S. Sezgin, M. Ates, C.M. Turhan, *Adv. Polym. Technol.*, **28**, 120 (2009).
36. M. Ates, A.S. Sarac, *Prog. Org. Coat.*, **65**, 28 (2009).
37. M. Ates, J. Castillo, A.S. Sarac, W. Schuhmann, *Microchim. Acta*, **160**, 247 (2008).
38. Z. Qi, A. Younis, D. Chu, S. Li, *Nano-Micro Letters*, **8**, 165 (2016).
39. K. Myeongjin, O. Ilgeun, K. Jooheon, *Phys. Chem. Chem. Phys.*, **17**, 16367 (2015).
40. A.H. Niessen, J. De Jonge, P.H.L. Notten, J. *Electrochem. Soc.*, **153**, A1484 (2006).

Synthesis and cyclization reactions of novel benzo[a]phenazine- and phenoxazine-5-ones derivatives

S. Kurban, N. Gulsah Deniz, C. Sayil*

Istanbul University, Engineering Faculty, Department of Chemistry, Division of Organic Chemistry, 34320, Avcilar, Istanbul, Turkey

Received August 25, 2016

In the present study we reported the cyclization reactions of 2-(alkylthio)-1,4-naphthoquinones to 6-(alkylthio)benzo[a]phenazine- and phenoxazine-5-ones derivatives **5a-c** and **7b-c**, respectively and their structural studies. The reactions of 2-(alkylthio)-3-chloro-1,4-naphthoquinone **3a-c** with phenyl-1,2-diamine **4** and 2-aminophenol **6** in ethanol in the presence of sodium carbonate (Na_2CO_3) were investigated. All new compounds were characterized on the basis of nuclear magnetic resonance spectroscopy (^1H - and ^{13}C -NMR), mass spectrometry (MS), and fourier transform infrared spectroscopy (FT-IR). A probable mechanism for the formation of all reaction products was presented and detailed spectroscopic data of all compounds were given.

Keywords Phenazine; Phenoxazine; Phenyl-1,2-diamine; 2-Aminophenol; Quinones

INTRODUCTION

Quinone imines are useful for medicine, dyestuffs and others in the wide of industries. Some phenoxazone and phenothiazone derivatives containing stable quinone imine systems have been synthesized to study the biological and pharmaceutical activities, e.g. antitumor activities, and to obtain the useful pigments [1-3]. Quinones are well known in biological systems as reactive centers of transporting both electrons and protons across biological membranes. The evaluation of the redox chemistry and electrochemical properties of quinones are a useful way for identifying their biological evolutions. Most of the reported methods for the synthesis of phenoxazones [4-6] from quinones and *o*-aminophenols involve the initial attack of the amino group of the *o*-aminophenol on the quinone substituent (OH, OCH_3 , Cl, etc.) and subsequent ring closure. An *o*-aminophenol exchange reaction or a rearrangement leads finally to the phenoxazone system.

In this work, we synthesized novel 6-(alkylthio)benzo[a]phenazine-5(7H)-ones (compounds **5a-c**) and 6-(alkylthio)-5H-benzo[a]phenoxazine-5-ones (compounds **7b-c**) by the condensation of phenyl-1,2-diamine **4** or 2-aminophenol **6** with 2-(alkylthio)-3-chloro-1,4-naphthoquinone compounds (**3a-c**). The condensations between **3a-c** and **4** or **6** were carried out in ethanol in the presence of sodium carbonate (Na_2CO_3). The conversion of the substituents of the resulting products, the reduction and the dehalogenation

were carried out. Their structures were characterized by using micro analysis, FT-IR, ^1H -NMR, ^{13}C -NMR, MS spectroscopy.

EXPERIMENTAL

Reagents and apparatus

Micro analyses were performed on a Thermo Finnigan Flash EA 1112 Elemental analyser. Infrared (FT-IR) spectra were recorded in KBr pellets in Nujol mulls on a Perkin Elmer Precisely Spectrum One FTIR spectrometry. ^1H - and ^{13}C NMR spectra were recorded on Varian UNITYINOVA operating at 500 MHz. Chemical shifts δ (ppm) were reported relative to tetramethylsilane (TMS) with the solvent resonance employed as the internal standard. ^1H - and ^{13}C NMR spectra in CDCl_3 refer to the solvent signal center at $\delta = 7.26$ and $\delta = 77.0$ ppm, respectively. Mass spectra were obtained on a Thermo Finnigan LCQ Advantage MAX LC/MS/MS spectrometer using an ESI probe. Products were isolated by column chromatography on Silica gel (Fluka Silica gel 60, particle size 63-200 μm). Melting points were measured on a Buchi B-540 melting point apparatus.

Analytical thin layer chromatography (TLC) was purchased from Merck KGaA (silica gel 60 F254) based on Merck DC-plates (aluminum based). Visualization of the chromatogram was performed by UV light (254 nm). Moisture was excluded from the glass apparatus using CaCl_2 drying tubes.

Solvents, unless otherwise specified, were of reagent grade and distilled once prior to use, and all

* To whom all correspondence should be sent:
E-mail: sayil@istanbul.edu.tr

other chemicals (reagent grade) were used without further purification.

General procedure for the synthesis 2-(alkylthio)-3-chloro-1,4-naphthoquinone compounds as a starting material (3a-c)

2-(Ethylthio)-3-chloro-1,4-naphthoquinone (**3a**) [7], 2-(hexadecylthio)-3-chloro-1,4-naphthoquinone (**3b**) [8] and 2-(octadecylthio)-3-chloro-1,4-naphthoquinone (**3c**) [9] were synthesized from the reactions of compound **1** with **2a-c** for using as a starting material according to the literatures [7-9]

General procedure for the synthesis of new phenazine and phenoxazine compounds (5a-c and 7b-c)

Sodium carbonate was dissolved in ethanol (50 mL), and equimolar amounts of 2-(alkylthio)-3-chloro-1,4-naphthoquinone (**3a-c**) and nucleophilics (**4** and **6**) were added slowly. The mixture was heated at 40°C and stirred in a single reaction vessel for 18 h. The color of the solution quickly changed (from yellow to red color), and the extent of the reaction was monitored by TLC. Chloroform (30 mL) was added to the reaction mixture. The organic layer was separated, washed with water (4 × 30 mL), and dried with Na₂SO₄. After the solvent was evaporated, the residue was purified by column chromatography on silica gel.

6-(Ethylthio)-benzo[a]phenazine-5(7H)-one (5a)

Compound **5a** was synthesized from reaction of 2-(ethylthio)-3-chloro-1,4-naphthoquinone (**3a**) (0.5 g, 1.978 mmol) with phenyl-1,2-diamine **4** (0.213 g, 1.978 mmol) according to the general procedure.

Orange solid. Yield: 18.4% (0.111 g). m.p.: 86.1-88.5°C. R_f [PET/CHCl₃(3:1)]: 0.52. FT-IR (KBr): ν (cm⁻¹)= 2925-2853 (C-H_{aliph}), 3018 (C-H_{arom}), 1600 (C=N), 1588 (C=O), 1522 (C=C), 3295 (N-H). ¹H-NMR (499.74 MHz, CDCl₃): δ = 0.79-0.83 (t, 3H, J= 6.81 Hz, CH₃), 2.97-3.04 (q, 2H, J= 7.32 Hz, S-CH₂), 2.87 (bs, H, -NH), 7.00-7.07, 7.18-7.21 (m, 2H, CH_{arom}), 7.46-7.48, 7.27-7.29 (m, 2H, CH_{arom}), 7.73-7.78 (m, 2H, CH_{naph}), 8.29-8.33 ppm (m, 2H, CH_{naph}). ¹³C-NMR (125.66 MHz, CDCl₃): δ = 13.5 (-CH₃), 28.8 (SCH₂-), 118.6 (S-C_{naph}), 141.6 (NH-C_{naph}), 131.3, 131.4, 131.9, 132.5 (CH_{naph}), 134.0, 135.1 (C_{naph}), 118.7, 127.9, 128.1, 129.3 (CH_{arom}), 135.2 (N-C_{arom}), 142.0 (NH-C_{arom}), 178.5 (C=O), 142.1 (C=N). MS [+ESI]: m/z = 307.1 [M+H]⁺, Micro analysis: C₁₈H₁₄N₂OS, (M_A= 306.38 g/mol). Calculated: C, 70.56; H, 4.61; N, 9.14; S, 10.46%. Found: C, 70.83; H, 4.92; N, 9.17; S, 10.45%.

6-(Hexadecylthio)benzo[a]phenazine-5(7H)-one (5b)

Compound **5b** was synthesized from reaction of 2-(hexadecylthio)-3-chloro-1,4-naphthoquinone (**3b**) (0.2 g, 0.445 mmol) with phenyl-1,2-diamine **4** (0.048 g, 0.445 mmol) according to the general procedure.

Red solid. Yield: 10.4% (0.023 g). m.p.: 112.1-113.9°C. R_f [PET/CHCl₃(5:2)]: 0.60. FT-IR (KBr): ν (cm⁻¹)= 2926-2854 (C-H_{aliph}), 3019 (C-H_{arom}), 1601 (C=N), 1590 (C=O), 1525 (C=C), 3335 (N-H). ¹H-NMR (499.74 MHz, CDCl₃): δ = 0.78-0.82 (t, 3H, J= 7.11 Hz, CH₃), 1.11-1.54 (m, 28H, CH₂), 2.97-3.00 (t, 2H, J= 7.31 Hz, S-CH₂), 2.84 ppm (bs, H, -NH), 7.74-7.84 (m, 2H, CH_{arom}), 8.23-8.28 (m, 2H, CH_{arom}), 8.30-8.36 (m, 2H, CH_{naph}), 9.32-9.34 ppm (m, 2H, CH_{naph}). ¹³C-NMR (125.66 MHz, CDCl₃): δ = 14.1 (-CH₃), 22.7- 31.9 (-CH₂-), 35.2 (SCH₂-), 123.8 (S-C_{naph}), 142.7 (NH-C_{naph}), 129.2, 129.5, 129.9, (CH_{naph}), 130.0, 131.8 (C_{naph}), 123.9, 125.5, 128.8, 129.3 (CH_{arom}), 140.0 (N-C_{arom}), 144.0 (NH-C_{arom}), 174.4, (C=O), 140.1 (C=N). MS [+ESI]: m/z = 503.5 [M+H]⁺, Micro analysis: C₃₂H₄₂N₂OS, (M_A= 502.75 g/mol). Calculated: C, 76.45; H, 8.42; N, 5.57; S, 6.38%; Found: C, 76.63; H, 9.01; N, 5.62; S, 6.35%.

6-(Octadecylthio)benzo[a]phenazine-5(7H)-one (5c)

Compound **5c** was synthesized from reaction of 2-(octadecylthio)-3-chloro-1,4-naphthoquinone (**3c**) (0.4 g, 0.838 mmol) with phenyl-1,2-diamine **4** (0.090 g, 0.838 mmol) according to the general procedure.

Dark orange solid. Yield: 9.3 (0.041 g)%. m.p.: 117.6-118.4°C. R_f [PET/CHCl₃(5:2)]: 0.58. FT-IR (KBr): ν (cm⁻¹)= 2920-2850 (C-H_{aliph}), 2957 (C-H_{arom}), 1649 (C=N), 1727 (C=O), 1591 (C=C), 3355 (N-H). ¹H-NMR (499.74 MHz, CDCl₃): δ = 0.81-0.84 (t, 3H, J= 7.46 Hz, CH₃), 1.13-1.61 (m, 32H, CH₂), 3.21 ppm (bs, H, -NH), 3.37-3.42 (t, 2H, J= 7.32 Hz, S-CH₂), 7.82-7.87 (m, 2H, CH_{arom}), 7.87-7.91 (m, 2H, CH_{arom}), 8.30-8.35 (m, 2H, CH_{naph}), 9.28-9.32 ppm (m, 2H, CH_{naph}). ¹³C-NMR (125.66 MHz, CDCl₃): δ = 14.1 (-CH₃), 22.8-31.9 (-CH₂-), 38.7 (SCH₂-), 125.7 (S-C_{naph}), 143.1 (NH-C_{naph}), 129.5, 130.5, 130.7, 130.9 (CH_{naph}), 131.5, 132.5 (C_{naph}), 123.2, 125.9, 128.8, 129.8 (CH_{arom}), 141.6 (N-C_{arom}), 144.8 (NH-C_{arom}), 167.8 (C=O), 141.9 (C=N). MS [+ESI]: m/z = 553.3 [M+Na]⁺, Micro analysis: C₃₄H₄₆N₂OS, (M_A= 530.33 g/mol). Calculated: C, 76.93; H, 8.74; N, 5.28; S, 6.04%. Found: C, 77.05; H, 8.99; N, 5.33; S, 6.01%.

6-(Hexadecylthio)-5H-benzo[a]phenoxazine-5-one
(**7b**)

Compound **7b** was synthesized from reaction of 2-(hexadecylthio)-3-chloro-1,4-naphthoquinone (**3b**) (0.4 g, 0.890 mmol) with aminophenol **6** (0.097 g, 0.890 mmol) according to the general procedure.

Red solid. Yield: 13.7% (0.061 g). m.p.: 80.6-81.9°C. R_f [PET/CHCl₃(3:1)]: 0.61. FT-IR (KBr): ν (cm⁻¹)= 2924-2852 (C-H_{aliph}), 3018 (C-H_{arom}), 1595 (C=N), 1633 (C=O), 1542 (C=C). ¹H-NMR (499.74 MHz, CDCl₃): δ = 0.89-0.91 (t, 3H, J = 7.09 Hz, CH₃), 1.21-1.68 (m, 28H, CH₂), 3.12-3.17 (t, 2H, J = 7.48 Hz, S-CH₂), 7.38-7.47 (m, 2H, CH_{arom}), 7.52-7.84 (m, 2H, CH_{arom}), 7.71-7.81 (m, 2H, CH_{naph}), 8.35-8.75 ppm (m, 2H, CH_{naph}). ¹³C-NMR (125.66 MHz, CDCl₃): δ = 14.1 (-CH₃), 22.7-32.0 (-CH₂-), 33.4 (SCH₂-), 117.2 (S-C_{naph}), 146.5 (O-C_{naph}), 128.7, 129.6, 131.1, 131.8 (CH_{naph}), 132.1, 132.4 (C_{naph}), 115.9, 124.3, 125.7, 127.0 (CH_{arom}), 133.0 (N-C_{arom}), 150.2, (O-C_{arom}), 183.0 (C=O), 144.0 (C=N). MS [+ESI]: m/z = 504.84 [M+H]⁺, Micro analysis: C₃₂H₄₁NO₂S, (M_A= 503.74 g/mol). Calculated: C, 76.30; H, 8.20; N, 2.78; S, 6.37% Found: C, 76.72; H, 8.77; N, 2.84; S, 6.30%.

6-(Octadecylthio)-5H-benzo[a]phenoxazine-5-one
(**7c**)

Compound **7c** was synthesized from reaction of 2-(octadecylthio)-3-chloro-1,4-naphthoquinone (**3c**) (0.4 g, 0.838 mmol) with aminophenol **6** (0.091 g, 0.838 mmol) according to the general procedure.

Red solid. Yield: 11.9% (0.053 g). m.p.: 88-89°C. R_f [PET/CHCl₃(3:1)]: 0.62. FT-IR (KBr): ν (cm⁻¹)= 2918-2849 (C-H_{aliph}), 3019 (C-H_{arom}), 1596 (C=N), 1628 (C=O), 1541 (C=C). ¹H-NMR (499.74 MHz, CDCl₃): δ = 0.87-0.91 (t, 3H, J = 7.09 Hz, CH₃), 1.21-1.68 (m, 32H, CH₂), 3.12-3.17 (t, 2H, J = 7.39 Hz, S-CH₂), 7.38-7.48 (m, 2H, CH_{arom}), 7.52-7.89 (m, 2H, CH_{arom}), 7.73-7.82 (m, 2H, CH_{naph}), 8.35-8.75 ppm (m, 2H, CH_{naph}). ¹³C-NMR (125.66 MHz, CDCl₃): δ = 14.1 (-CH₃), 22.7-32.0 (-CH₂-), 33.4 (SCH₂-), 116.1 (S-C_{naph}), 146.3 (O-C_{naph}), 129.6, 131.0, 131.5, 131.9, (CH_{naph}), 132.1, 132.2 (C_{naph}), 115.9, 124.7, 125.5, 126.5 (CH_{arom}), 132.8 (N-C_{arom}), 150.4 (O-C_{arom}), 181.2 (C=O), 144.4 ppm (C=N). MS [+ESI]: m/z = 532.5 [M+H]⁺, Micro analysis: C₃₄H₄₅NO₂S, (M_A= 531.79 g/mol). Calculated: C, 76.79; H, 8.53; N, 2.63; S, 6.03% Found: C, 76.95; H, 8.84; N, 2.66; S, 5.98%.

RESULTS AND DISCUSSION

The aim of this work, the novel 6-(alkylthio)benzo[a]phenazine-5(7H)-ones (compounds **5a-c**)

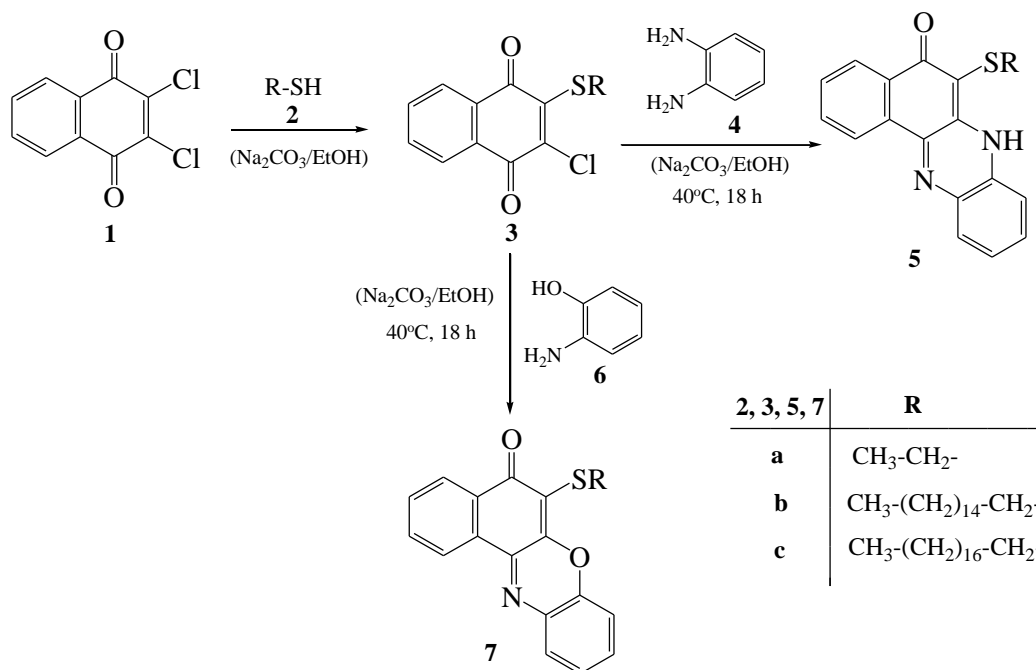
and 6-(alkylthio)-5H-benzo[a]phenoxazine-5-ones (compounds **7b-c**) were synthesized by the condensation reactions of phenyl-1,2-diamine **4** or 2-aminophenol **6** with 2-(alkylthio)-3-chloro-1,4-naphthoquinone compounds (**3a-c**), respectively. As shown in Scheme 1, the condensations between **3a-c** and **4** or **6** were carried out in ethanol in the presence of sodium carbonate (Na₂CO₃) at 40°C about 18 h.

The known compounds 2-(ethylthio)-3-chloro-1,4-naphthoquinone (**3a**), 2-(hexadecylthio)-3-chloro-1,4-naphthoquinone (**3b**) and 2-(octadecylthio)-3-chloro-1,4-naphthoquinone (**3c**) were synthesized according to related literatures [7-9]. These compounds were used for starting materials. All these new compounds were separated and purified by column chromatography and structures were established by micro analysis, FT-IR, ¹H- and ¹³C-NMR, and mass spectra, chemical reactions, or comparison with authentic samples.

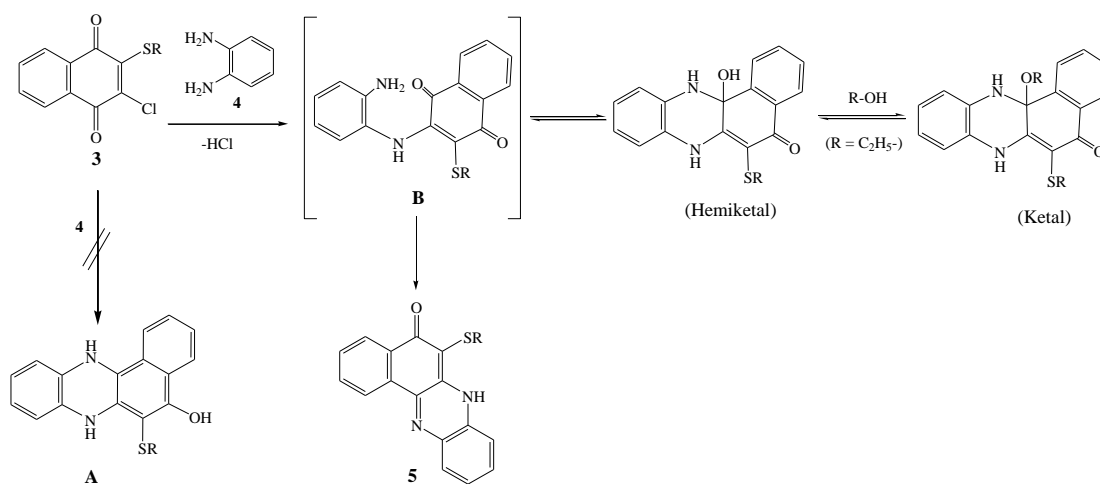
We assume that the reactions of **3a-c** and **4** or **6** in ethanol in the presence of sodium carbonate start with nucleophilic attack of the amino group of **4** or **6** on the halogen atom of **3a-c** with the elimination of hydrogen chloride to give B and D in schemes 2 and 3, respectively. In the formations of B and D, addition of the amino or hydroxyl group to the quinone carbonyl group in equilibrium reaction lead to the formation of the hemiketal, is etherified to the ketal. In addition to this, the open forms (B, D) and a hemiketal/ketal of B and D could not be isolated.

The formation of A and C in from the reactions of **3a-c** with **4** or **6** did not obtain reasonable because amino- and hydroxy-phenazines and phenoxazines were highly unstable [10]. These proposed mechanisms in schemes 2 and 3 were agree well with the mechanism of the synthesis of similar compounds [5].

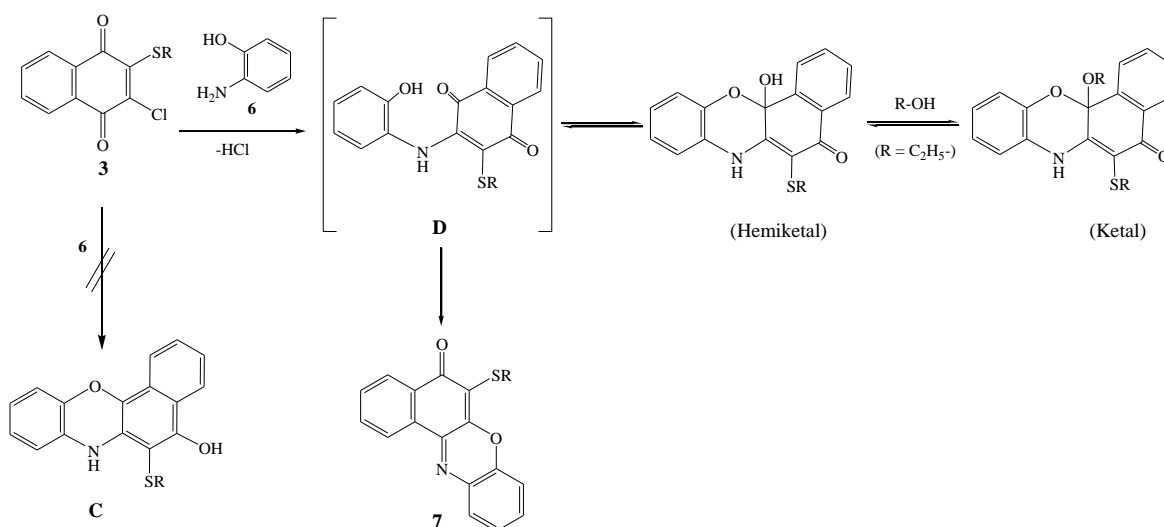
The ¹H spectrum of the products in CDCl₃ displayed distinct signals with appropriate multiplets. ¹H NMR signal of the hydrogen atoms of the adjacent to the nitrogen atom (-NH) in compounds **5a-c** were shifted to a higher field and displayed singlet at 2.87, 2.84 and 3.21 ppm as single broad, respectively. The ¹³C NMR spectra of compounds **5a-c** and **7b-c** gave just one carbonyl signals (C=O) at 178.5, 174.4 167.8, 183.0 and 181.2 ppm, respectively, in the naphthoquinone units of **5a-c** and **7b-c**. The carbonyl signals (C=O) in ¹³C-NMR spectra of **5a-c** and **7b-c** are in close agreement with the spectral characteristic of analogous heterocycles [11-14]. In the ¹³C-NMR spectra of compounds **5a-c** and **7b-c** carbon signals of (C=N) group appeared around at 144 ppm.



Scheme 1. The synthesis of phenazines and phenoxazines derivatives (**5a-c**, **7b-c**)



Scheme 2. Proposed mechanism of the synthesis of phenazine compounds (**5a-c**)



Scheme 3. Proposed mechanism of the synthesis of phenoxazine compounds (**7b-c**)

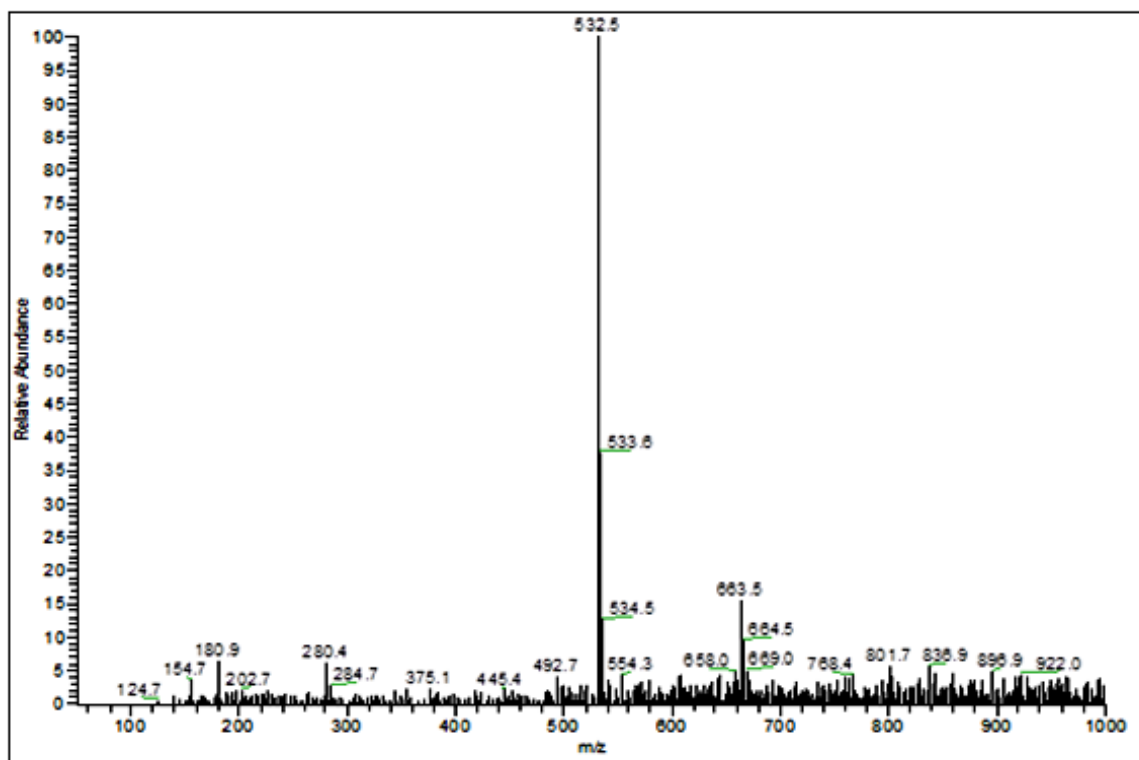


Fig. 1. The MS[+ESI] spectra of compound **7c**

The FT-IR spectra of compound **5a-c**, the characteristic ($-\text{NH}$) band appeared at 3295, 3335 and 3355 cm^{-1} , respectively. In the FT-IR spectrum of **7b-c** the characteristic ($-\text{OH}$) band disappeared, it is proved that intramolecular cyclization reactions had taken place, yielding the compounds **7b-c**. In the FT-IR spectra of compounds **5a-c** and **7b-c** typical strong quinonic carbonyl absorptions were observed at 1588, 1590, 1727, 1663 and 1628 cm^{-1} , respectively. The characteristic imine group ($\text{C}=\text{N}$) band of compounds **5a-c** and **7b-c** appeared at 1600, 1601, 1649, 1595 and 1596 cm^{-1} , respectively.

With the aid of the positive ion mode of electron spray ionization (ESI) mass spectrum of the compounds **5a-c**, the respective molecular ion peaks were observed at m/z (%) 307 (100) $[\text{M}+\text{H}]^+$, 503 (100) $[\text{M}+\text{H}]^+$, 553 (100) $[\text{M}+\text{Na}]^+$, respectively. The major fragment of compound **7c** in the MS [+ESI] spectrum was observed at m/z (%) 532 $[\text{M}+\text{H}]^+$.

CONCLUSION

In continuation of our investigations of quinone [11-16] chemistry, we have studied the reactions of naphthoquinones with phenyl-1,2-diamine **4** and 2-aminophenol **6**. The aim of this study was to the investigation of the cyclization reactions of 2-(alkylthio)-3-chloro-1,4-naphthoquinones **3a-c** with

nitrogen- and oxygen-containing nucleophiles (**4**, **6**) and obtain to highly functionalized heterocyclic new compounds (**5a-c**, **7b-c**). The condensations between **3a-c** and compounds **4** or **6** were carried out in ethanol in the presence of sodium carbonate (Na_2CO_3). These reactions of **3a-c** and **4** or **6** proceeded at 40°C. A probable mechanisms for the formation of all reaction products was presented and detailed spectroscopic data of all compounds were given. All synthesized new compounds **5a-c** and **7b-c** were purified by the column chromatography. Their structures of new synthesized compounds were determined by micro analysis, FT-IR, $^1\text{H-NMR}$, $^{13}\text{C-NMR}$ and MS.

Acknowledgement: The authors would like to express their gratitude to Scientific Research Projects Coordination Unit of Istanbul University for financial support. (Project Number: 43723)

REFERENCES

1. N. L. Agarwal, W. Schafer, *J. Org. Chem.*, **45**, 5144 (1980).
2. A. Butenandt, U. Schiedt, E. Biekert, R. J. T. Cromartie, *Ann. Chem.*, **75**, 590, (1954).
3. W. Schafer, I. Geyer, H. Schlude, *Tetrahedron*, **28**, 3811 (1972).
4. N. L. Agarwal, R. L. Mital, *Z. Naturforsch. B.*, **31**, 106 (1976).

5. N. L. Agarwal, W. Schafer, *J. Org. Chem.*, **45** (11), 2155 (1980).
6. H. Hayakawa, S. Nanya, T. Yamamoto, *J. Heterocyclic Chem.*, 1737 (1986).
7. L. F. Fieser, R. H. Brown, *J. Am. Chem. Soc.*, **71**, 3609 (1949).
8. C. Sayil, C. Ibis, *Russian J. Org. Chem.*, **46**(10), 209 (2010).
9. C. Sayil, C. Ibis, *Bull. Korean Chem. Soc.*, **31**(5), 1233 (2010).
10. W. Schafer, *Prog. Org. Chem.*, **6**, 135 (1964).
11. C. Ibis, N. G. Deniz, *J. Chem. Sci.*, **124**(3), 657 (2012).
12. C. Sayil, S. Kurban, C. Ibis, *Phosphorus Sulfur and Silicon.*, **188**, 1855 (2013).
13. N. G. Deniz, M. Ozyurek, A. N. Tufan, M. R. Apak, *Monatsh. Chem.*, **146**, 2117 (2015)
14. C. Ibis, N. G. Deniz, *Phosphorus Sulfur and Silicon.*, **185**, 2324 (2010).
15. N. G. Deniz, C. Ibis, Z. Gokmen, M Stasevych, V. Novikov, O. Komarovska-Porokhnyavets, M. Ozyurek, K. Guclu, D. Karakas, E. Ulukaya, *Chem. Pharm. Bull.*, **63**(12), 1029 (2015)
16. C. Ibis, M. Yildiz, C. Sayil, *Bull. Korean Chem. Soc.*, 30(10), 2381 (2009).

Synthesis of poly((2-dimethylamino)ethyl methacrylate) via atom transfer radical polymerization and surface characterization by inverse gas chromatography

D. S. Dasdan*

Yildiz Technical University, Faculty of Arts and Sciences, Department of Chemistry, 34220 İstanbul, Turkey

Received August 25, 2016

Poly(2-dimethylamino)ethyl methacrylate) (PDMAEMA) was synthesized via atom transfer radical polymerization. The synthesized PDMAEMA was characterized by FTIR, GPC and DSC. The inverse gas chromatography technique was used to obtain the surface properties of PDMAEMA. The retentions of nonpolar solvents such as n-hexane, n-heptane, n-octane, n-nonane, n-decane and other acidic, basic and amphoteric probes such as tetrahydrofuran, dichloromethane, chloroform, acetone, ethyl acetate and benzene used without further purification on PDMAEMA were measured in the temperature ranges from 303 to 373 K by inverse gas chromatography (IGC). The dispersive component of the surface energy, γ_S^D of studied adsorbent surface was estimated using retention times of different nonpolar organics in the infinite dilution region. Dispersive components of the surface energies, γ_S^D according to Fowkes and Dorris-Gray approaches and the acid, K_A and base, K_D constants for PDMAEMA were calculated.

Keywords: Poly(2-dimethylamino)ethyl methacrylate); Inverse gas chromatography; Surface and adsorption properties; Surface free energies; Lewis acid-base constants

INTRODUCTION

Poly[2-(dimethylamino)ethyl methacrylate] has attracted a significant attention in recent years as a cationic pH and temperature responsive polymer for an increasing number of applications in drug delivery, bioseparation, and microfluidic areas. [1] The inverse gas chromatography(IGC) method which is simple, fast, economical method has been used extensively to study the structure of polymers, the interactions of various liquids and gases with polymers and to provide valuable thermodynamic information for surface characterization of polymeric substances [2-4].

In this study, poly(2-dimethylamino)ethyl methacrylate) (PDMAEMA) which was synthesized via atom transfer radical polymerization using CuBr ligated with N,N,N',N',N''-pentamethyl-diethylenetriamine (PMDETA) as catalyst, and ethyl 2-bromoisobutyrate (EBiB) as initiator under argon atmosphere. The synthesized PDMAEMA was characterized by FTIR, GPC and DSC. The inverse gas chromatography technique was used to obtain the surface properties of PDMAEMA.

EXPERIMENTAL PART

Probes and Instrumentation

The used solvents were high purity grade nonpolar solvents such as n-hexane (Hx), n-heptane (Hp), n-octane (O), n-nonane (N), n-Decane (D) and polar solvents such as dichloromethane (DCM, acidic), chloroform (TCM, acidic), acetone (Ac, amphoteric), ethyl acetate (EA, amphoteric), tetrahydrofuran (THF, basic) and benzene. The all studied solvents and support materials being Chromosorb-W(AW-DMCS-treated, 80/100 mesh) were supplied from Merck AG. Inc. Silane treated glass wool used to plug the ends of the column was obtained from Alltech Associates, Inc.,

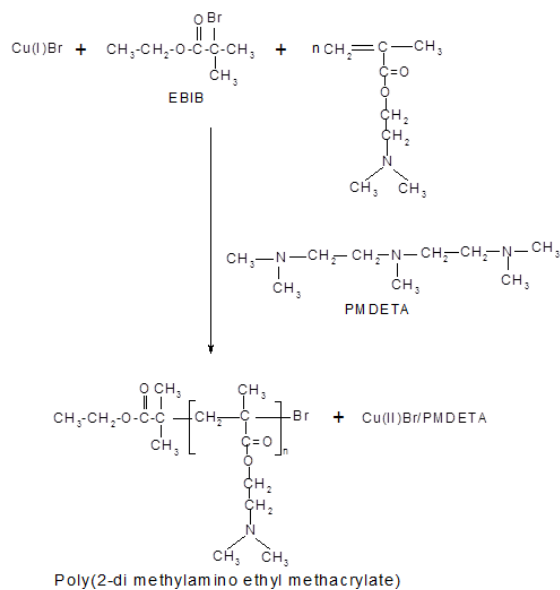
PDMAEMA was used as a stationary phase in the chromatographic column and solvents with a different chemical nature were used as eluents. The retention diagrams of studied solvents on PDMAEMA were plotted at temperatures in K between 303 and 373 by IGC. The sorption properties of the PDMAEMA were determined using a Hewlett-Packard 6890 Series II gas chromatograph, with a thermal conductivity detector (TCD). High purity helium was used as the carrier gas (flow rate in the range 25–28 cm³ min⁻¹). A stainless steel columns (0.5 m long, 3.2 mm o.d.) were packed with PDMAEMA covered on chromosorb. After packing, the columns were conditioned overnight at 373 K. The retention diagrams of studied solvents on PDMAEMA were

* To whom all correspondence should be sent:
E-mail: dolunaykar@yahoo.com

plotted at temperatures in K between 303 and 373 by IGC.

Synthesis of poly((2-dimethylamino)ethyl methacrylate) via atom transfer radical polymerization

Poly(2-dimethylamino)ethyl methacrylate) (PDMAEMA) which was synthesized in Schlenk tube via atom transfer radical polymerization of 2-dimethylamino ethyl methacrylate (7.5 ml) using CuBr (0.039 gr, 0.27 mmol) ligated with N,N,N',N',N''-pentamethyl-diethylenetriamine (0.15 ml, [PMDETA]=0.0466 M, $M_w=173.3$ g/mol, $d=0.83$ gr/cm³; PMDETA) as catalyst, and ethyl 2-bromoisobutyrate (1.32 ml, $M_w=195.06$ g/mol, $d=1.329$ gr/cm; EBiB) as initiator under argon atmosphere in dichloromethane and one day at room temperature. After 24 h, it was observed heterogen phase. Green part of solution was diluted with DCM, heterogen phase was filtered and precipitated in cool n-heptane. Waxy green-blue precipitate was passed on basic alumina for purification. Solution was precipitated in n-hexane and synthesized polymer was characterized by FT-IR, GC and DSC. (Scheme 1)



Scheme 1. Synthetic Route of Poly((2-dimethylamino)ethyl Methacrylate) via Atom Transfer Radical Polymerization

THEORY OF INVERSE GAS CHROMATOGRAPHY

The surface polarity and the acid-base nature of materials can be measured by IGC technique. This technique supplies a basis for determining the potential for chemical interaction between the polymer and solvent. The investigated material is immobilised within a chromatographic column

which is flushed through with inert gas such as helium or nitrogen. The stationary phase characterisation is achieved by utilising the partitioning of the sample between the mobile phase and the stationary phase, indicated by the time taken to elute the sample. The probe-probe interactions in IGC experiments are negligible because of carried out in infinite dilution. The theory and the technique are now quite well described in literature [5-6].

The dispersive component of surface energy, γ_s^D were determined by Dorris-Gray and Fowkes approaches. The adsorption energy for the non-polar solvents increases with the number of carbon atoms in the chain.

According to Dorris and Gray approach, the increment, corresponding to the adsorption energy of a methylene group, $\Delta G_{A[CH_2]}$ is given by [7]

$$\Delta G_{A[CH_2]} = -RT \ln \left(\frac{V_{N,n}}{V_{N,n+1}} \right), \quad (1)$$

where $V_{N,n}$ and $V_{N,n+1}$ are the retention volumes of two n-alkanes having n and n+1 carbon atoms in their chain. This parameter is independent of the chosen state of the adsorbed molecule. Thus at constant temperature, for a series of alkane probes, a plot $RT \ln V_N$ versus the number of carbon atoms should give a straight line from which $\Delta G_{A[CH_2]}$ can be found.

The methylene adsorption energy can also be defined as [7]

$$\Delta G_{A[CH_2]} = 2N_A a[CH_2] \sqrt{\gamma_s^D \gamma_L[CH_2]}, \quad (2)$$

where N_A is Avagadro's number, $a[CH_2]$ is the surface area covered by one methylene group (0.06 nm²) and $\gamma_L[CH_2]$ is the surface free energy of a surface consisting of methylene groups, i.e. polyethylene, given by

$$\gamma_L[CH_2] = 35.6 + 0.058(293 - T), \quad (3)$$

Thus using Eqs.(1)-(3) and the experimentally determined values of the adsorbate net retention volumes, $V_{N,n}$ and $V_{N,n+1}$, the dispersion component of the surface free energy, γ_s^D may be calculated and where the adsorbate net retention volumes, V_N were calculated from the expression:

$$V_N = Q * J * (t_R - t_A) * T / (T_f), \quad (4)$$

In equation (1), t_R is the adsorbate retention time, t_A is the retention time of air, Q is volumetric flow rate measured at column outlet and

at ambient temperature T_f (K), T is the column temperature (K) and J is James-Martin gas compressibility correction factor [8].

According to the Fowkes approach, the dispersive component of surface energy, γ_S^D is calculated following equation [9]:

$$-\Delta G_A = RT \ln(V_n) = 2Na(\gamma_S^D)^{0.5}(\gamma_L^D)^{0.5} + K'' \quad (5)$$

Thus for a series of n-alkane probes, a plot of $RT \ln V_N$ against $a(\gamma_L^D)^{0.5}$ will give a slope of $2N(\gamma_S^D)^{0.5}$. Values of $a(\gamma_L^D)^{0.5}$ and boiling point, T_b ($^{\circ}C$) of apolar solvents are found in the literature [10-11].

The specific component of the free energy is determined from the n-alkane plot of $RT \ln V_N$ against $a(\gamma_L^D)^{0.5}$. The distance between the ordinate values of the polar probe datum point and the n-alkane reference line gives the specific component of the surface free energy, $-\Delta G_A^S$.

An equation may be written for this procedure,

$$-\Delta G_A^S = RT \ln\left(\frac{V_{N,n}}{V_{N,ref}}\right) \quad (6)$$

where $V_{N,n}$ and $V_{N,ref}$ are the retention volume for the polar probe and the retention volume for the n-alkanes' reference line, respectively.

The adsorption of a polar probe onto the adsorbant surface leads to a change in the enthalpy of the system and the entropy of the system. These factors are related to the energy of adsorption by the equation,

$$\Delta G_A^S = \Delta H_A^S - T\Delta S_A^S \quad (7)$$

Here, ΔH_A^S is the adsorption enthalpy by Lewis acid-base interactions, ΔS_A^S is the adsorption entropy Lewis acid-base interactions and T is the column temperature. For each polar probe, ΔH_A^S and ΔS_A^S can be determined from a plot of $-\Delta G_A^S/T$ against $1/T$.

The surface Lewis acidity and basicity constants, K_A and K_D , may be calculated from the equation,

$$-\Delta H_A^S = K_A DN + K_D AN^* \quad (8)$$

Here, DN and AN^* are Gutmann's donor and modified acceptor numbers, respectively. Values of $a(\gamma_L^D)^{0.5}$ and boiling point, T_b ($^{\circ}C$) of non-polar solvents are found in the literature [12,13] and the Gutmann's modified acceptor number, AN^* and

donor number, DN of the polar probes used in this study are found in the literature [14,15].

K_A and K_D are obtained from a plot of $-\Delta H_A^S/AN^*$ versus DN/AN^* with K_A as the slope and K_D as the intercept. Parameters K_A and K_D reflect the ability of the examined surface to act as an electron acceptor and electron donor, respectively [12,13].

RESULTS AND DISCUSSION

Characterization of poly((2-dimethylamino)ethyl methacrylate)

The yield of synthesized PDMAEMA via ATRP was calculated about 50%, $M_n = 3500$ g/mol from GPC, $PDI = 1.1$, very low T_g and structural characterized by FTIR/ATR (Fig.1).

According to FTIR/ATR spectrum of PDMAEMA; $2770-2952$ cm^{-1} aliphatic C-H, 1725 cm^{-1} de ester C=O, 1456 cm^{-1} aliphatic C-H, 1149 and 1270 cm^{-1} C-O-C asymmetric and symmetric, 1059 cm^{-1} C-N, 749 cm^{-1} aliphatic C-H.

Surface properties of poly((2-dimethylamino)ethyl methacrylate)

The net retention volumes, V_N of studied solvents on PDMAEMA were calculated from igc measurements at infinite dilution region using Eq (1). The retention diagrams of studied solvents on PDMAEMA were plotted at temperatures between 303 and 373 K and given Figure 2 (a) for nonpolar and Figure 2(b) for polar solvents.

The slope of the fitted line is equal to $\Delta G_{A[CH_2]}$.

The variation of γ_S^D and $\gamma_L[CH_2]$ with temperature were calculated from Eq.(3) and (4), respectively. The adsorption energy of a methylene group, $\gamma_L[CH_2]$ the surface free energy of a surface consisting of methylene groups, $\Delta G_{A[CH_2]}$ and dispersion component of surface free energy, γ_S^D values calculated by Doris-Gray approach for PDMAEMA determined at studied temperatures and the results were given in Table 1.

The Fowkes equation (Eq. 5, referred to as Schultz and Lavielle approach by some authors) [16] was used to determine the dispersive component of the surface free energy, γ_S^D over a range of studied temperatures and calculated values of $RT \ln V_N$ were plotted against $a(\gamma_L^D)^{0.5}$. An example of the pattern of results obtained was given in Fig. 4 for the isotherm at 303 K.

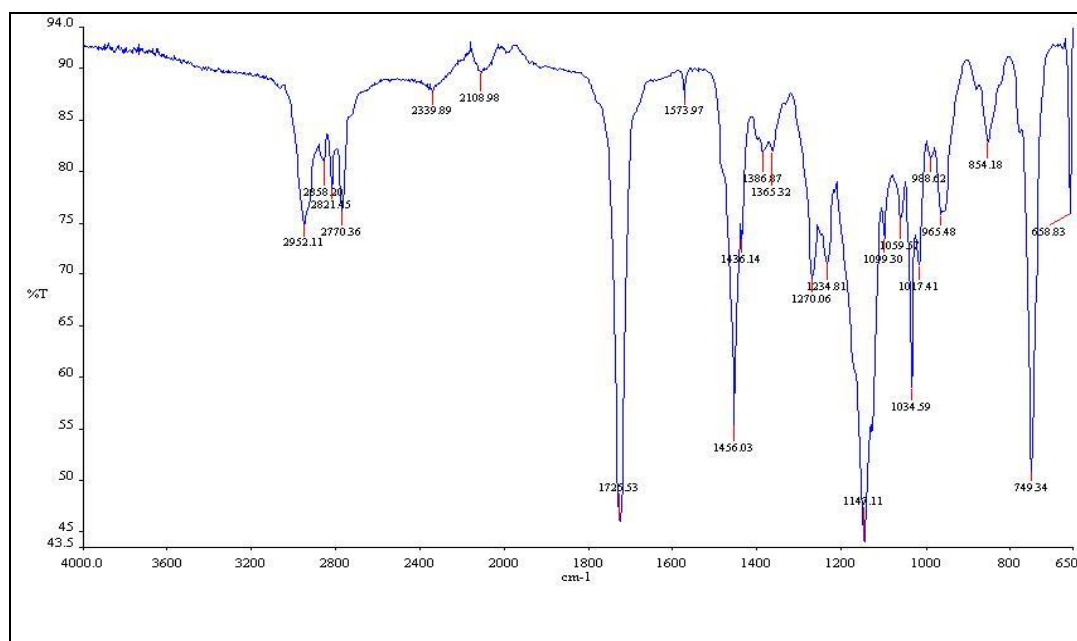


Fig. 1. FTIR/ATR spectrum of PDMAEMA

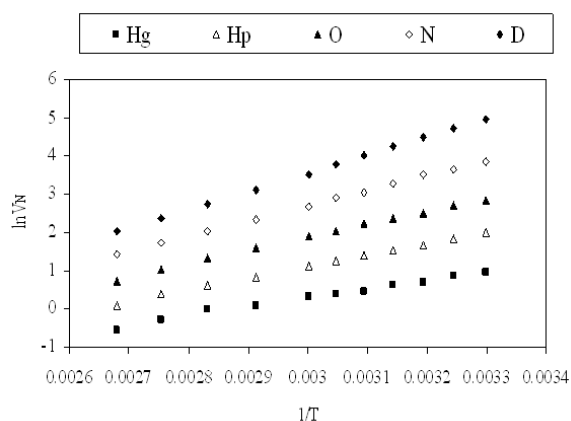


Fig. 2 (a). The retention diagram of non-polar solvents adsorbed onto PDMAEMA

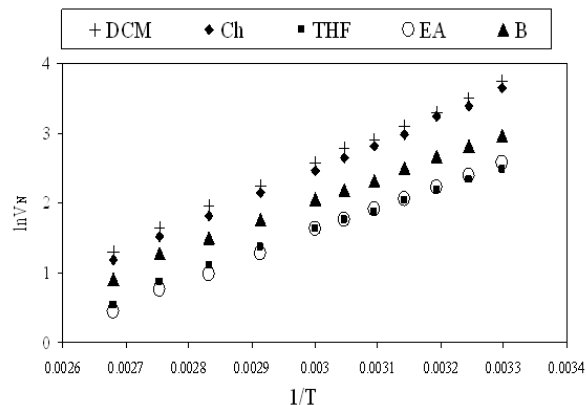


Fig. 2 (b). The retention diagram of polar solvents adsorbed onto PDMAEMA

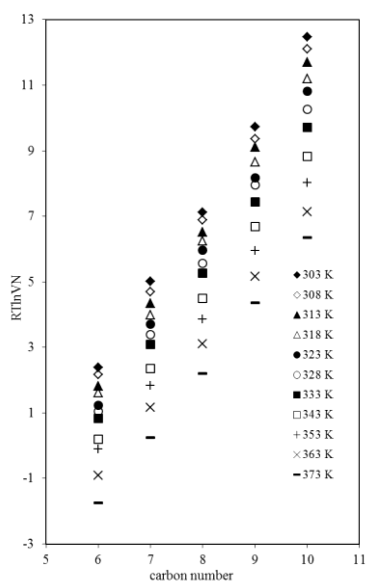


Fig. 3. The plot of $RT \ln V_N$ versus carbon number of non-polar solvents for PDMAEMA

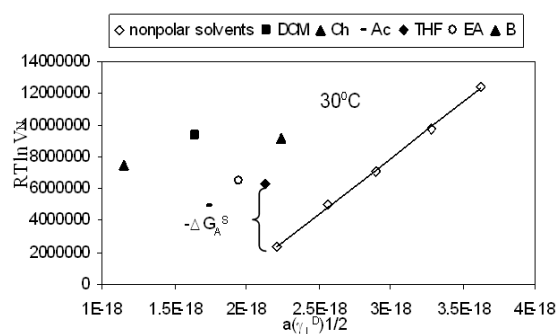


Fig. 4. Variation of the logarithm of the retention volume of non-polar and polar versus solvents $D 0.5 a(\gamma_L) [m^2(mJ/m^2)^{0.5}]$ at 303 K

According to Dorris-Gray approaches, Eq.(2), $\Delta G_{A[CH_2]}$ is independent of the chosen reference state of adsorbed molecule. The $RT \ln V_N$ versus carbon number of non-polar solvents were plotted in Fig.(3) for PDMAEMA. The results of

$\Delta G_{A[CH_2]}$, $\gamma_L[CH_2]$ and γ_S^D of PDMAEMA was given in Table 1.

The linearity was obtained by the non-polar solvents at the studied temperature ranges. The slope ($2N\sqrt{\gamma_S^D}$) of the linear fit, obtained for each non-polar solvent plot, gives the dispersive component of the surface free energy, γ_S^D at that temperature.

The γ_S^D values of PDMAEMA calculated according to Fowkes approach at studied temperature ranges were given in Table 1.

Table 1 report that the variation of γ_S^D as a function of temperature was limited and the γ_S^D values of PDMAEMA decrease significantly between 303 and 373 K.

The values of γ_S^D of PDMAEMA calculated according to Dorris-Gray and Fowkes approaches are very close to each other at the studied temperature ranges. There is no data in the literature to compare these values. The specific component of the surface free energy, ΔG_A^S , is calculated using the difference between the calculated value of $RT \ln V_N$ and that which was derived using the equation of the linear fit of the n-alkane reference line (Eq.7).

ΔH_A^S and ΔS_A^S can be determined from a plot of $-\Delta G_A^S/T$ against $1/T$. (Eq.8)

Table 1. The adsorption energy of a methylene group, $\gamma_L[CH_2]$ the surface free energy of a surface consisting of methylene groups, $\Delta G_{A[CH_2]}$ and dispersion component of surface free energy, γ_S^D values of PDMAEMA calculated by Doris-Gray (D-G) and Fowkes (F) approaches and slope at studied temperatures for PDMAEMA

T(K)	$\gamma_L[CH_2]$ (mJ/m ²)	$\Delta G_{A[CH_2]}$ (10 ⁶ mJ/mol)	γ_S^D (D-G) (mJ/m ²)	Slope (x10 ²⁴)	γ_S^D (F) (mJ/m ²)
303	35.02	2.49	33.87	6.993	33.73
308	34.73	2.45	33.19	6.893	32.78
313	34.44	2.45	33.46	6.894	32.79
318	34.15	2.38	31.88	6.699	30.96
323	33.86	2.36	31.58	6.636	30.38
328	33.57	2.30	30.23	6.468	28.86
333	33.28	2.21	28.08	6.204	26.55
343	32.7	2.16	27.32	6.067	25.39
353	30.96	2.03	25.50	5.721	22.58
363	32.12	2.04	24.73	5.706	22.46
373	31.54	2.01	24.54	5.648	22.01

The values of K_A and K_D were calculated using Eq.(9). The plotting $-\Delta H_A^S/AN^*$ versus DN/AN^* with K_A as the slope and K_D as the intercept. The plot of $-\Delta H_A^S/AN^*$ versus DN/AN^* for PDMAEMA was given at Fig.5.

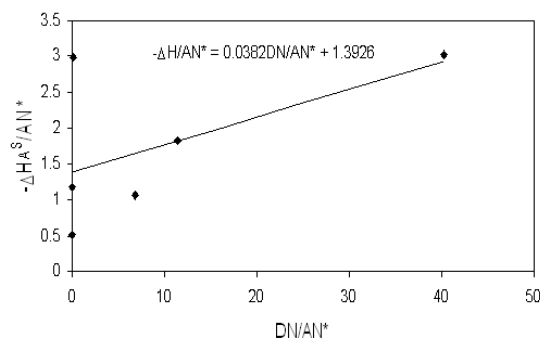


Fig. 5. The plot of $-\Delta H_A^S/AN^*$ versus DN/AN^* for PDMAEMA.

The values of K_A and K_D are found to be 0.04 and 1.4 for PDMAEMA and the values If the ratio of K_D to K_A is greater than 1, solid surface is basic nature and below 1, it implies that the solid surface is acidic nature [17]. According to the K_D/K_A ratio of PDMAEMA, it is found that the surface of PDMAEMA has basic nature.

CONCLUSIONS

Adsorption properties, surface and Lewis acid-base characteristics of PDMAEMA synthesized successfully via atom transfer polymerization have been examined by means of inverse gas chromatography at infinite dilution, in the temperature range from 303 to 373 K. The γ_s^D values of PDMAEMA change ranges from 33.87 to 24.54 mJ/m² (Dorris-Gray approach) and from 33.73 to 22.1 mJ/m² (Fowkes approach) with increasing temperature. The values of K_A and K_D parameters indicated that PDMAEMA surface is basic nature. IGC is a convenient method for the characterization of the surface and adsorption properties and the acid-base characteristics of acrylate derivatives.

Acknowledgements: This research has been supported by Yildiz Technical University Scientific Research Projects Coordination Department. (Proje Numarası: 28-01-02-10)

REFERENCES

1. H. Dong and K. Matyjaszewski, *Macromolecules*, **41**, 6868 (2008)
2. F. Sesigur, D. Sakar Dasdan, O. Yazici, F. Cakar, O. Cankurtaran, F. Karaman, *Journal of Optoelectronics and Rapid Communications*, **10**, 97 (2016).
3. J. E. Guillet, In: *New Developments in Gas Chromatography*; J. H. Purnell, Ed.; Wiley-Interscience: New York, 1973; p 187.
4. J. E. Guillet, J. H. Purnell, *Advances in Analytical Chemistry and Instrumentation, Gas Chromatography*; John Wiley & Sons: New York, 1973.
5. K. E. Fagelman and J. T. Guthrie, *Journal of Chromatography A*, **1095**, 145 (2005).
6. A. Voelkel, *Chemometrics and Intelligent Laboratory Systems*, **72**, 205 (2004).
7. G. M. Dorris and D. G. Gray, *Journal of Colloid and Interface Science*, **77**, 353 (1980)
8. J. R. Conder and C. L. Young, *Physicochemical Measurement by Gas Chromatography*, Wiley-Interscience, New York, NY, USA, 1979.
9. F. L. Riddle Jr. and F. M. Fowkes, *Journal of the American Chemical Society*, **112**, 3259 (1990). D.P. Kamdem, S. K. Bose, and P. Luner, *Langmuir*, **9**, 3039 (1993). 22 di
10. J. M. R. C. A. Santos and J. T. Guthrie, *Materials Science and Engineering R*, **50**, 79 (2005).
11. F.L. Riddle, F.M. Fowkes, *J. Am. Chem. Soc.*, **112**, 3259 (1990).
12. D.P. Kamdem, S.K. Bose, P. Luner, *Langmuir*, **9**, 3039 (1993).
13. Santos JMRCA and Guthrie JT, *Mat. Sci. Eng. R.*, **50**, 79 (2005).
14. J.M.R.C.A. Santos, J.T. Guthrie, *J. Chromatogr. A*, 1070 (2005).
15. J. Schultz, L. Lavielle, C. Martin, *Journal of Adhesion*, **23**, 45–60 (1987).
16. O Yazici, H. Ocak, O. Yasa-Sahin, D. Sakar, O. Cankurtaran, F. Karaman, B. Bilgin- Eran, *Liquid Crystals*, **39**, 1421 (2012).

Immobilization of salophen derivative Schiff base cobalt(II) complex on a copolymer coated platinum electrode and electrocatalytic investigations

D. Cakmak*, S. Yalcinkaya, K. Seymen, C. Demetgül

Department of Chemistry, Faculty of Arts and Sciences, Mustafa Kemal University, 31040, Hatay, Turkey

Received June 26, 2016, Revised September 10, 2016

In this study, o-amino-benzylalcohol (pBA) and o-anisidine (pA) homopolymers and their copolymer (o-amino-benzylalcohol-co-o-anisidine) (Cp) were synthesized on the platinum electrode in 0.5 M H₂SO₄ as a supporting electrolyte medium by electrochemical methods. Then, Co(II) complex of salophen type Schiff base (CoL) was immobilized on these polymer coated electrode surfaces in acetonitrile containing 0.15 M LiClO₄. The prepared modified surfaces were characterized by Cyclic Voltammetry, UV-Vis, SEM-EDAX and ICP-MS techniques. The electrocatalytic activity of modified electrodes was investigated on electrooxidation of Dopamine (DA) as biosensor application. One of the prepared modified electrodes showed good electrocatalytic effect on the oxidation of DA using Square Wave Voltammetry method (SWV). The oxidation peak current of DA increased linearly in the range of 0.2 μM - 2 mM in pH 7 phosphate buffer solution at [CoL] immobilized pA modified Platinum electrode. Limit of Detection (LOD) was calculated as 0.1 μM for DA determination.

Keywords: o-amino-benzyl alcohol, electropolymerization, Schiff Base metal complex, immobilization, electrocatalytic investigation.

INTRODUCTION

Electrode materials that used in electrochemical studies are mainly limited commercial species like carbon, mercury, gold, platinum, so researches are significantly restricted in this area [1].

Electrochemical work areas can be expanded by modifying of electrode surfaces with organic-inorganic compounds in order to improve their properties of selectivity, sensitivity and catalytic activity [2-4]. Conductive polymers have also attracted much attention largely at modification of conventional electrode materials as supporting material [5,6]. Because they have been allowed to immobilization, adsorption and covalent attachment for different species due to its porous structure and functional groups.

Common approach of biosensor applications, with immobilization of enzyme to conducting polymer coated electrode surface have been designed as sensors that have selectivity and catalytic activity [7-9]. In this area, alternative solutions have been gained attention against to enzyme immobilization due to decreased of enzyme activities during immobilization, high-cost, their easily degradation and hard isolation.

Recently, inorganic metal complexes that have active metal centre and functional groups are becoming attractive materials as alternatively in this research area because of their catalytic activity and stability [10,11]. Recently prepared new

electrode materials studies by using directly electropolymerization of metal complexes of inorganic compounds that have various functional groups and to be linked to an electropolymerizable monomer, their characterization and catalytic activity have been attracted much interest research area in scientific literature [12-15].

The previous studies have been shown that, the electrocatalytic properties of modified electrodes containing metal complexes were related with metal species and functional groups of complexes [16].

This study is focused on the preparation of modified electrodes with immobilization of Schiff base metal complex onto new electroactive polymeric supporting materials and also investigation of electrocatalytic activity of these electrodes towards determination of dopamine.

EXPERIMENTAL

Materials and methods

A CHI 604E model electrochemical analyzer was used for SWV and cyclic voltammetry (CV) measurements. All the electrochemical studies were carried out by using of conventional three electrode system. A 1 cm² Pt plate, Pt wire and saturated Ag/AgCl (3M NaCl) were used as working, counter and reference electrodes, respectively.

Schiff base (H₂L) and metal complex (CoL) were synthesized according to the literature [17]. The proposed structures of H₂L and [CoL] are given in figure 1.

* To whom all correspondence should be sent:

E-mail: didem.deleti@gmail.com, dcakmak@mku.edu.tr

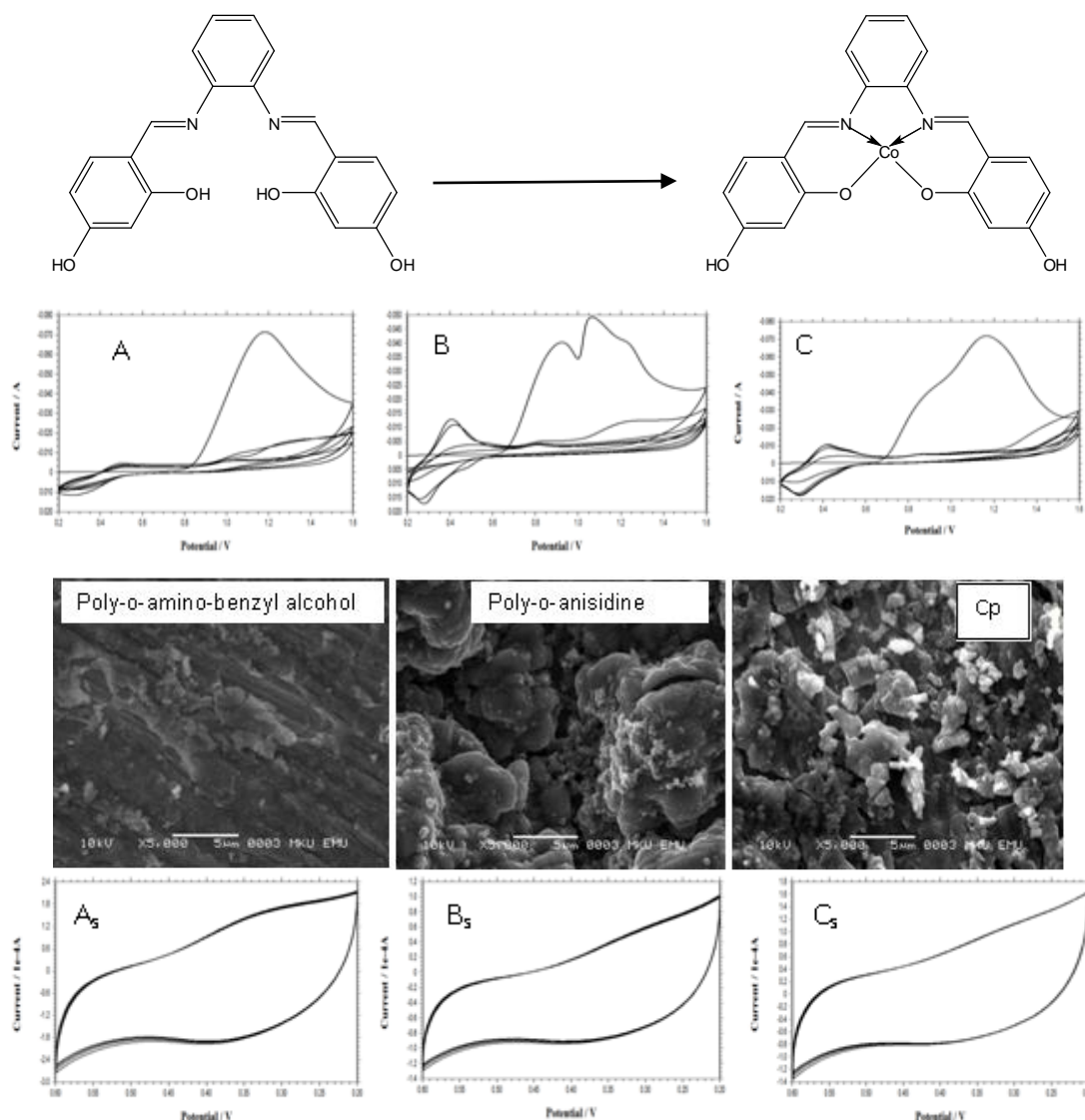


Fig.1. Multicycle voltammograms of o-amino benzyl alcohol (A); o-anisidine (B) and Cp in 0.5 M H₂SO₄ solution as supporting electrolyte at Pt electrode; The SEM images of homopolymer and copolymer coatings on Pt electrode and Successive CVs of poly-o-amino benzyl alcohol (A_s), poly-o-anisidine (B_s) and poly(o-anisidine-co-o-aminobenzyl alcohol) (C_s) films in 0.3 M KCl solution at 0.2-0.6 V potential range.

Electropolymerization procedure was performed by CV with scanning from 0.2 V to 1.6 V at a sweep rate of 100 mV s⁻¹ for 25 cycles in 0.5 M H₂SO₄ solution containing homopolymers. Copolymer (Cp) was also synthesized in 0.5 M H₂SO₄ solution containing 0.05 M o-anisidine and 0.05 M o-amino benzyl alcohol. Immobilization procedure was performed by CV with scanning from -0.2 to 2.0 V at a sweep rate of 50 mV s⁻¹ for 25 cycles in 1 mM [CoL] solution in acetonitrile containing 0.15 M LiClO₄. For electrocatalytic activity studies, Phosphate buffer solution (PBS) pH 7 was used as supporting electrolyte. Solutions of DA (1mM), ascorbic acid (AA, 1mM) and uric acid (UA, 1mM) were prepared daily by dissolving them in water.

RESULTS AND DISCUSSION

A typical multicycle CV voltammograms for electropolymerizations of o-anisidine, o-aminobenzyl alcohol and its copolymer on Pt electrode were given in Fig.1. While one oxidation peak was observed for o-amino benzyl alcohol at 1.2 V, two oxidation peaks were observed for anisidine at 0.9 V and 1.1 V belongs to monomer oxidation. On the other hand, at the voltammogram of copolymer were seen an overlapped oxidation peak arising from two monomer oxidation. Polymer film of pBA was obtained dark blue color, whereas pA was obtained black color. The color of coating has shifted from dark blue to black color, as the ratio of anisidine increases in the copolymer. The SEM images and electrochemical stability

voltammograms (successive CVs) were also given in Fig.1. SEM images of homopolymer and copolymer films were recorded in order to investigate the surface morphology and structure. It can be easily seen from SEM images that the surface morphologies of homopolymers and copolymer were different from each other. Also, these images were shown that the pA coating have more porous structure than the pBA coating. Stability voltammograms have given to get the information about the stability and electroactivity of the polymer and copolymer films obtained on Pt electrode with investigating of electrochemical behavior during successive cycles. The oxidation of the film was observed in the forward scan and the reduction was obtained at the reverse scan. Current values of the polymer film were highly stable and regularly changed between its redox states during these successive cycles. It could be concluded that the polymer film was both stable and extremely electroactive [18].

FT-IR spectra of homopolymer and copolymer films are shown in Fig.2. In the spectra of polymer and copolymer films, the bands are broader than the bands belongs to monomers of pA and pBA as described in the literature [19]. It is clear that after polymerization, due to either increasing molecular

weight or the molecular weight distribution of the polymers, the signals of polymers become broader than their monomers. This result is significant evident for polymer formation in this study. The peaks which were come from $-NH_2$ groups, were observed at 3458 cm^{-1} and 3368 cm^{-1} for o-anisidine monomer and at 3390 cm^{-1} and 3300 cm^{-1} for o-amino benzyl alcohol, whereas these peaks disappeared after polymerization. Disappearance of $-NH_2$ group peak indicates that the polymerization occurs through the $-NH$ group. This situation has confirmed the proposed structures of the homopolymers and copolymer.

Electropolymerization voltammograms of [CoL] on both the bare and the homopolymer- copolymer coated Pt electrode were given in Fig.3. Oxidation peak potential of [CoL] which was observed around 1.7 V at bare Pt, shifted to lower potential values at copolymer coated Pt electrode (Cp-Pt) and peak current decreased with successive cycles during immobilization. Film was very stable during the successive cycles according to stability voltammograms. The SEM micrographs were indicating to significant differences among coating morphologies of Cp and Cp-[CoL]. This difference confirmed the immobilization of metal complex onto the copolymer.

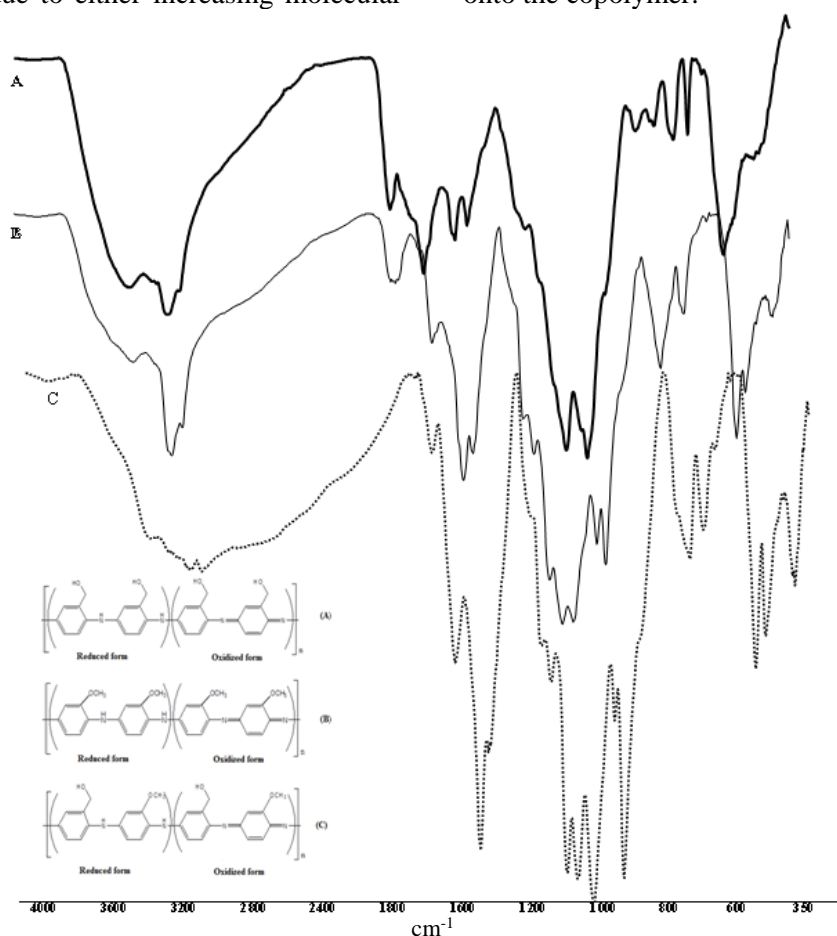


Fig.2. The FT-IR spectra and proposed structures of pBA (A), pA (B) and Cp (C).

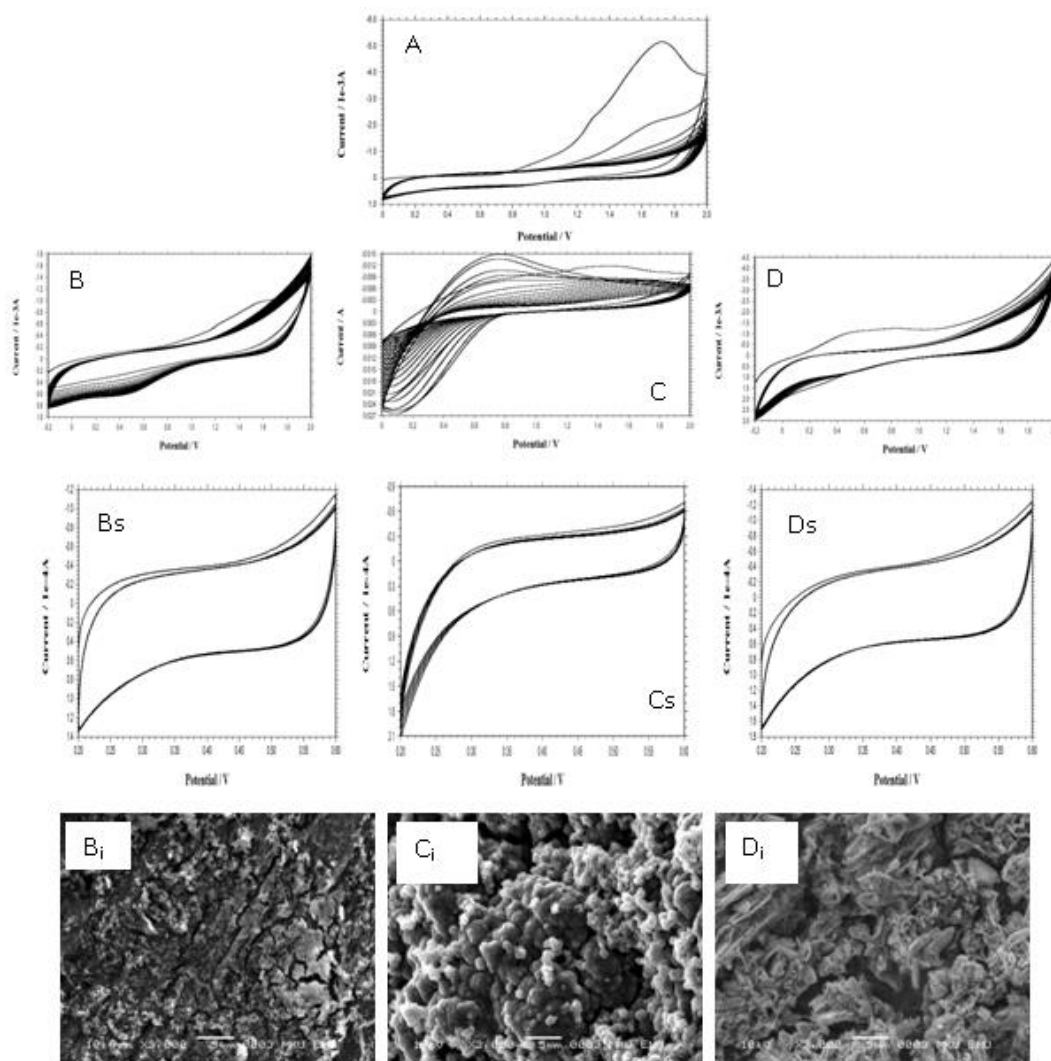


Fig.3. Electropolymerization voltammograms of [CoL] on the bare Pt (A), on the pBA-Pt (B), on the pA-Pt (C) and on the Cp-Pt (D) in acetonitrile containing 0.15 M LiClO₄ with 25 cycles. Successive CVs (Bs, Cs, Ds) and SEM images (Bi, Ci, Di) of pBA-Pt, pA-Pt and Cp-Pt, after immobilization of [CoL], respectively.

In the UV spectrum of the copolymer film after immobilization of [CoL], the band was observed at range of 330–450 nm were attributed to the $n-\pi^*$ transition of the non-bonding electrons present on the nitrogen of the azomethine group of the Schiff base moiety [20]. In addition, the weak bands observed in the 500–700 nm region can be attributed to $d-d$ transitions of the metal ions [21]. Cobalt ion distribution at Cp-[CoL] modified surface was illustrated as red points at spectrum of SEM-EDAX mapping analysis (Fig.4.). According to the ICP-MS analysis, quantities of cobalt ion on modified electrodes were determined as 3.96 ppm, 1.96 ppm and 1.92 ppm for pBA-[CoL]-Pt, pAns-[CoL]-Pt and Cp-[CoL]-Pt, respectively. These results have also give an important evidence about the immobilization of [CoL] onto polymer coating.

Catalytic activity studies for DA were investigated in different supporting electrolyte medium like Britton Robinson buffer solution,

acetic acid/acetate buffer solution and phosphate buffer solution at modified electrodes. As a result of these studies, the best electrocatalytic activity for DA oxidation was observed at pA-[CoL]-Pt electrode in pH 7 PBS. CV and SWVs were recorded in this medium for DA at bare Pt and pA-[CoL]-Pt (Fig.5.). In comparison with the bare platinum electrode, at this modified electrode, anodic peak current belongs to DA oxidation has increased for six times. Also, as can be seen in Fig.5., anodic peak currents belongs to DA have proportionally increased with changing DA concentration from 0,2 μ M to 2 mM. As a result of these studies a linear calibration curve was obtained for DA in the range of 0,2 μ M-2 mM and LOD was calculated as 0,1 μ M.

When electro-oxidation of DA was investigated in the presence of UA and AA, oxidation peak potential of DA was observed at 0.2 V by using of pA-[CoL]-Pt modified electrode and at 0.3 V was

observed by using of bare Pt electrode. The oxidation peak potential of DA appeared on more negative value at modified electrode than bare Pt electrode and peak shape was sharper at modified electrode than bare electrode. In order to investigate the applicability and selectivity of electrocatalytic effect on the DA oxidation, SWVs were recorded

for different concentrations of DA in the presence of 1mM AA and 1 mM UA. Anodic peak currents for DA have proportionally increased with changing DA concentration. Therefore, linear calibration plots were obtained for DA in the presence of UA and AA, in the region between 1.6 μM and 8 μM and LOD was calculated as 0,65 μM .

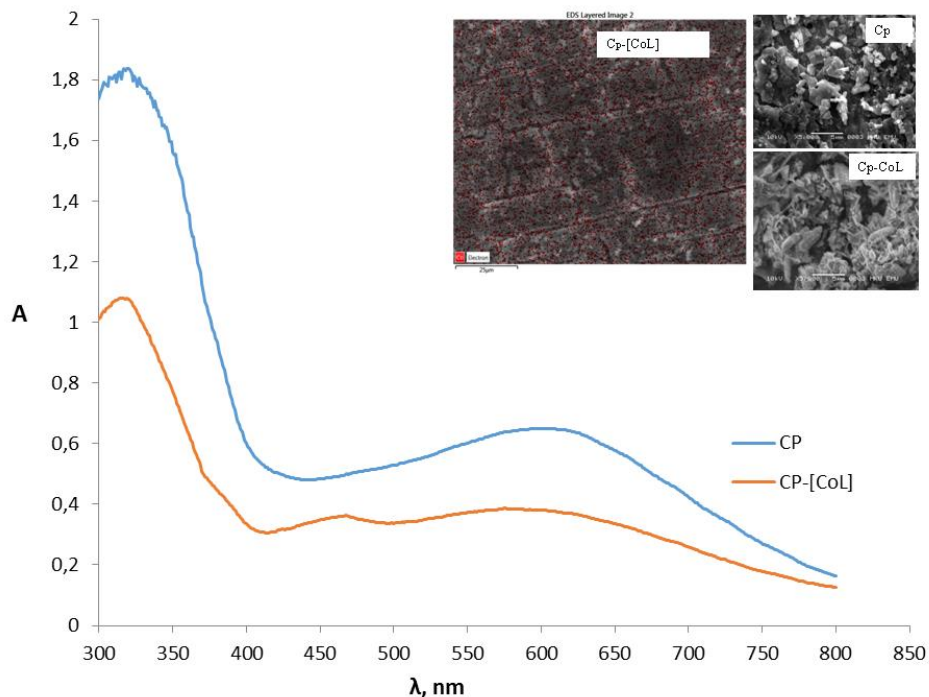


Fig.4. UV-Vis spectra, SEM-EDAX mapping analysis and SEM micrographs for Cp after and before immobilization of [CoL].

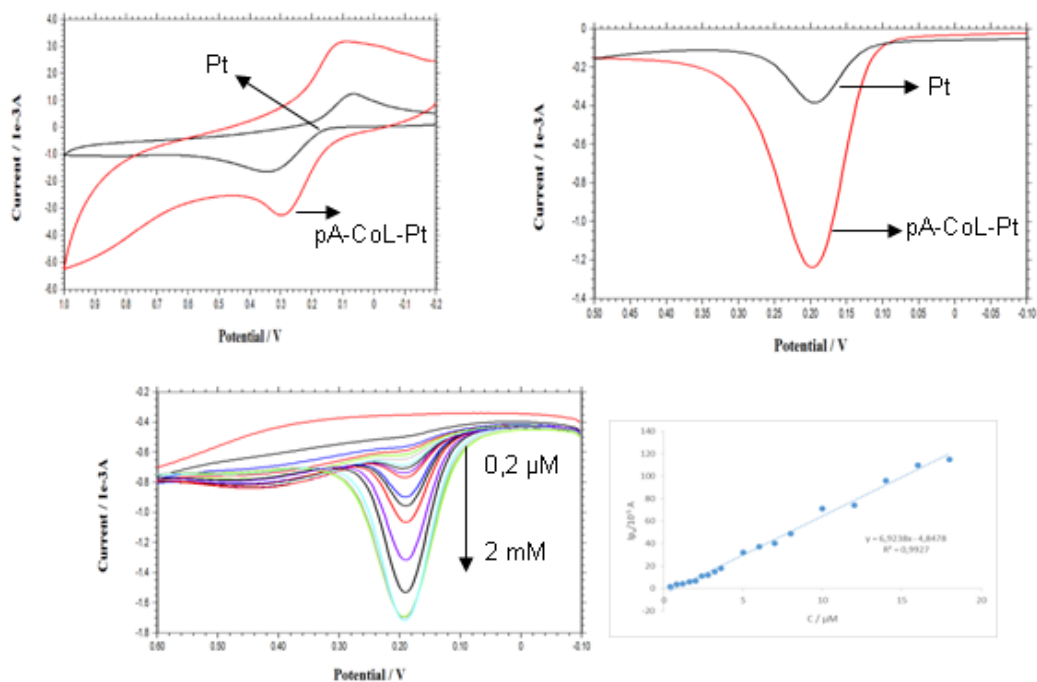


Fig.5. CVs and SWVs of DA at bare Pt and modified electrode, SWVs of various concentrations of DA in pH 7 PBS and calibration plot for DA.

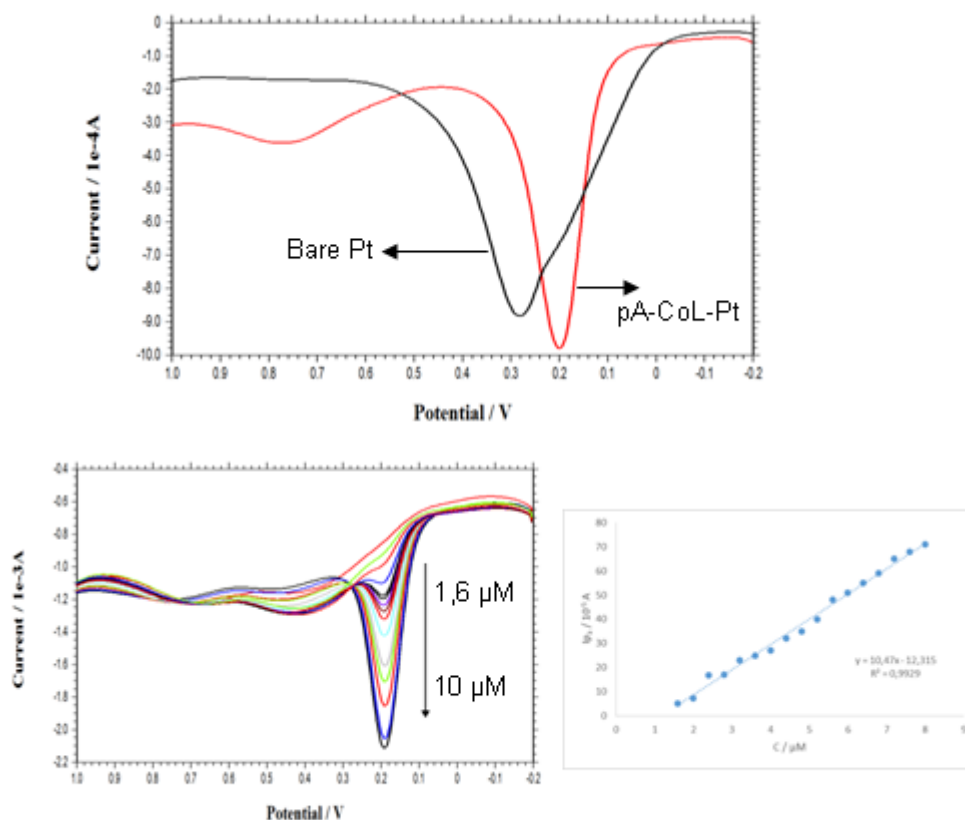


Fig.6. SWVs of DA in the presence of UA and AA at bare Pt and modified electrode in pH 7 PBS; SWVs of DA for various concentrations in pH 7 PBS and calibration plot for DA.

CONCLUSIONS

This study shows that metal complexes have been successfully immobilized onto the electroactive polymeric supporting material by using electrochemical methods. In this way, alternative systems can be developed to enzyme immobilization at biosensor applications. Modified surfaces were characterized by electrochemical, spectroscopic and microscopic techniques. The results of the characterization studies have shown that the films are homogeneous, very stable and extremely electroactive. Modified electrodes exhibited catalytic activity towards the oxidation of DA. Furthermore, they have potential use for other bioanalytical species at further applications.

Acknowledgements: This Project was supported by The Scientific and Technological Research Council of Turkey (Project Number: 114Z691)

REFERENCES

1. A. A. İ.Turan, Z. Üstündağ, A. O. Solak, E. Kılıç, A. Avseven, *Thin Solid Films*, **517**, 2871 (2009).
2. D. Deletioğlu, S. Yalcinkaya, C. Demetgul, M. Timur, S. Serin, *Mat. Chem. and Phys.*, **128**, 500 (2011).
3. D. Uzun, A. B. Gunduzalp, E. Hasdemir, *J. of Electroanal. Chem.*, **747**, 68 (2015).
4. D. Uzun, H. Arslan, A. B. Gündüzalp, E. Hasdemir, *Surf. & Coat. Tech.*, **239**, 108 (2014).
5. J. Zhou, D.O. Wipf, *J. Electrochem. Soc.*, **144** 1202 (1997).
6. S. Yalcinkaya, C. Demetgul, M. Timur, N. Colak, *Carb. Polym.*, **79**, 908 (2010).
7. C. Lete, S. Lupu, B. Lakard, J. Hihn, F. J. Campo, *J. of Electroanal. Chem.*, **744** 53 (2015).
8. L. Cache-Guerente, S. Cosnier, C. Innocent, P. Mailley, *Analyt. Chim. Acta*, **311**, 23 (1995).
9. W. H. Scouten, J. H. T. Luong, R. S. Brown, *Trends in Biotech.*, **13**, 178 (1995).
10. S. Shahrokhian, Z. Kamalzadeh, A. Bezaatpour, D. M. Boghaei, *Sens. and Act. B: Chem.*, **133**, 599 (2008).
11. K. Wang, J. Xu, H. Chen, *Biosens and Bioelect.*, **20**, 1388 (2005).
12. A. Ourari, D. Aggoun, L. Ouahab, *Inorg. Chem. Commun.*, **33**, 118 (2013).
13. M. R. Parra, T. Garcia, E. Lorenzo, F. Pariente, *Sens. and Act. B*, **130**, 730 (2008).
14. C. S. Martin, M. F. S. Teixeira, *Procedia Engineering*, **47**, 1161 (2012).
15. K. Cheung, W. Wong, D. Ma, T. Lai, K. Wong, *Coord. Chem. Reviews*, **251**, 2367 (2007).
16. Z. Zhang, X. Li, C. Wang, C. Zhang, P. Liu, T. Fang, Y. Xiong, W. Xu, *Dalton Trans.*, **41**, 1252 (2012).

17. M. Niu, G. Liu, D. Wang, J. Dou, *Acta Cryst.*, **65**, 1357 (2009).
18. S. Yalçinkaya, T. Tuken, B. Yazici, M. Erbil, *Prog. in Org. Coat.*, **63**, 424 (2008).
19. M. A. Valle, M. A. Gacittua, E. D. Borrego, P. P Zamora, F. R. Diaz, M. B. Camarada, M. P. Antilen, J. P. Soto, *I. J. of Electrochem. Soc.*, **7**, 2552 (2012).
20. M. Karakaplan, C. Demetgül, Serin, S., *J. of Macromolec. Sci. Part A: Pure and Appl. Chem.*, **45**, 406 (2008).
21. C. Çelik, M. Tümer, S. Serin, *Synth.React. Inorg. Met.-Org. Chem.*, **28** 529 (1998).

Greenhouse gases in urban areas

E. Bozkurt*

Marmara University Environmental Engineering Department Kadikoy, Istanbul, 34722, Turkey

Received June 26, 2016, Revised September 10, 2016

The majority of citizens live in urban areas that dominate the economy and energy use. People living in these areas can affect the balance of nature since the gradual increase in the earth's surface temperature is caused predominantly by human activity. Humans cause the emission of gases such as carbon dioxide through exhaust from cars and power plants. If this negative effect continues, climate change due to global warming is inevitable. While CO₂ concentration was around 250-280 parts per million (ppm) in the late 1800s, according to the National Oceanic Atmospheric Administration, it reached 380 ppm in the 2000s and 400 ppm in 2015. If we do not act and if emissions continue to increase, the global mean temperature may increase by over 30C by 2030. In this study, GHG emissions for 2020 are predicted for some countries then arithmetic means and standard deviations for GHG emissions are calculated by Excel. Data on GHG emissions for Europe, Turkey and the U.S. are used for the periods 2004-2013, 1990-2010 and 2000-2011, respectively. Chemical processes to mitigate GHG in the atmosphere are explained. Oxidation and methanol synthesis are useful processes to decrease the amount of GHG. Therefore, energy consumption in urban areas is very important. Reducing energy consumption in cities is possible by increasing the density (increasing the number of people per square meter in the city), the use of public transport such as subways, buses, trams, and light rail, and the use of energy derived from waste.

Keywords: Urban; Global warming; Energy consumption; Air quality

INTRODUCTION

Ecologically important types of urban biotopes are rivers, lakes, marshes, cliffs, sand dunes, forests, scrub, and valleys [1]. People living in urban areas have ecological impacts on the environment because of land used for housing, traffic and industrial areas [2]. Human activities like the burning of fossils fuels and deforestation intensify the greenhouse effect. Increasing concentrations of greenhouse gases cause global warming, ocean acidification, smog pollution, and ozone depletion. The air temperature in the world has increased by about 0.7-0.8°C over the last 100 years. Precautionary measures should have been taken against this increase. Global warming can cause fish migration, increased melting of glacial ice and snow, desertification, rises in sea levels, changes in the amount of precipitation, stronger storms and extreme events.

Global warming and climate change

Greenhouse gases absorb and emit radiation in the atmosphere. These gases are water vapor, carbon dioxide (CO₂), methane (CH₄), nitrous oxide (N₂O), and ozone and their contributions to the greenhouse effect are 36-72%, 9-26%, 4-9%, and 3-7%, respectively [3]. The greenhouse gas (GHG)

effect increases the temperature of the earth because radiation from the planet's atmosphere warms the surface of planet. Greenhouse gases produced by human activity are known as anthropogenic greenhouse gases. Greenhouse gas concentrations have increased since the beginning of the Industrial Revolution [4]. GHGs are covered by the Kyoto Protocol. This international treaty was adopted in 1997 and entered into force in 2005. Turkey became a party to the United Nations Framework Convention on Climate Change Kyoto Protocol in 2009. High global warming potential (GWP) gases are mostly anthropogenic. Gases that have a greater impact on climate change are CO₂, CH₄, N₂O, hydrofluorocarbons (HFCs), perfluorocarbons (PFCs) and sulfur hexafluoride (SF₆). SF₆ has a much longer lifetime and stronger radiative properties than CO₂. However, 72% of totally emitted greenhouse gas is CO₂, 18% is CH₄ and 9% is N₂O. The most important cause is CO₂. This emission is created by industrial, transportation and agricultural activities, producing energy, and burning fuels like oil, natural gas, diesel, petrol, and ethanol [5].

Climate change conferences

The first conference on climate change, the United Nations Framework Convention on Climate Change, was held in 1992 when 195 countries and nearly 150 world leaders met in Paris for the United Nations Climate Change Conference (COP21) from 30 November to 12 December 2015. National

* To whom all correspondence should be sent:
E-mail: esin.bozkurt@marmara.edu.tr

leaders came to an agreement that will enable us to realize the transition towards a clean economy and stop dangerous climate change. By limiting emissions the aim of the Paris Agreement is to keep the temperature increase to below 2°C. Finance flows are planned for low GHG emissions and climate-resilient development. The Agreement will be open for signature from 22 April 2016 to 21 April 2017. The period for implementation or contribution is between 2021 and 2030.

Developing countries need financial aid to adapt to changes being wrought by climate change. They need to replace fossil fueled development with cleaner alternatives. The financial, technology and capacity-building support was agreed in Cancun in 2010. Industrialized countries committed to providing funds rising to \$100 billion a year by 2020 for developing countries for both mitigation and adaptation actions [6]. Low carbon technologies that are energy efficient and renewable energy can play central roles in global efforts. Improving forest management also reduces emissions.

Climate change in turkey

Different regions of Turkey can be affected differently by climate change although its impact is quite heterogeneous across the country. For example, the Southeastern Anatolia region and the Central Anatolia region are both arid areas under threat of desertification. The Aegean and Mediterranean regions do not have enough water resources so these areas will also be affected. The impacts of global warming on agriculture are changes in temperature, sea level, rainfall, heat waves, CO₂, ozone, pests, diseases, and the nutritional quality of foods. The extinction risk to animal and plant species, the migration of animals, adaptation and water resource problems can all be blamed on global warming [7].

Between 1990 and 2012, Turkey's gross domestic product and population increased by 230% and 30%, respectively. Turkey's energy demand increases by 6-7% per year. Turkey's total emissions in 2012 expressed in CO₂ equivalent were 440 million tons. The emission equivalent rates for these sectors are 70.2 percent in energy, 14.3 percent in industrial processes, 8.2 percent in waste and 7.3 percent in agriculture. Turkey's per capita GHG emission was 5.9 tons CO₂ equivalent for 2012. Including industrial emissions, Turkey's ratio for global emissions is 0.7 percent. The Republic of Turkey's intended nationally determined contribution (INDC) has been presented with decisions 1/CP.19 and 1/CP.20. Turkey plans

to reduce GHG by up to 21 percent from the business as usual level by 2030. GHGs in the national inventory include CO₂, CH₄, N₂O, HFCs, PFCs, SF₆, and nitrous trifluoride (NF₃). Turkey's INDC covers seven sectors: energy, industry, transport, building and urban transformation, agriculture, waste and forestry. Hydroelectric and solar powered electricity production will be increased. In addition to these power sources, nuclear power plants are planned. Electricity transmission and distribution losses will be reduced to 15%. The rehabilitation measures will take place within electric power plants. Energy efficiency in industry and the use of waste as an alternative fuel will be increased. Fuel saving and controlling the use of fertilizers are included in plans for agriculture areas. Materials can be recovered and recycled from waste and converting waste to energy with methane production will apply in landfills. Transport will be improved by increasing maritime and rail transport instead of road transport, the use of combined and sustainable transport, promotion of alternative fuels and clean vehicles and the scrapping of old vehicles. Constructing energy efficient buildings and the dissemination of Green Buildings, passive energy, and zero energy buildings are other plans for reducing energy consumption [8].

EXPERIMENTAL

Energy circulation plan in urban areas

Urban areas are the most crowded places in the world. Population growth and land use change in urban areas should be analyzed. Elemental needs of human beings such as infrastructure, shelter, energy, and water should be planned for urban regions. Cities have significant amounts of global energy demand and GHGs. If urban areas organize an energy circulation plan, a sustainable urban future is possible for livable places. Important targets can be reducing waste and fuel consumption and optimizing transportation. Some examples can be given for these items. Building more public rail transit facilities can reduce the number of cars and take their carbon footprints off the roads. With housing development, residents should be able to live in public housing with nearby jobs, schools and public transport. Undesirable and dangerous walkways prevent people from walking so pedestrian paths should be created to encourage walking [9]. When people walk or bike they do not add to air pollution and will be generally healthier. When people need to use a vehicle they should be able to find a convenient bus stop [10].

Buyers of hybrid/electric cars might pay lower purchase tax. Increasing the number of people per square meter in the city is possible with tall buildings. Subways, buses, trams, light rail and other forms of public transport reduce travel by private vehicle. This gives people energy efficient choices. Gray water from showers, bathtubs, laundry and bathroom sinks in the home can be treated and reused.

In Diyarbakir, green spaces are proposed to represent at least 7-8m² per person [11]. The number of roadside trees and green spaces can be improved. Trees can be planted in children’s parks and school playgrounds, on roofs and walls and around apartment complexes [12].

Energy efficient design, building insulation and user behavior can reduce the amount of energy used for heating, cooling, lighting, ventilation, and cooking. These lower energy consumption so air pollution is reduced [13, 14].

Greenhouse gas chemistry

Many trace gases such as CH₄, CO, and HCFCs are removed from the atmosphere by oxidation. OH is the initiator of radical-chain oxidation. CO and methane are sinks for OH [15].

All GHGs but CO₂ and H₂O can be removed by chemical processes. While GHG containing H atoms can be removed by reaction with hydroxyl radicals (OH) in the troposphere, N₂O, PFCs, SF₆, CFCs and halons can be destroyed by solar ultraviolet radiation (UV) at short wavelengths [16].

Capture, disposal or chemical recycling technologies can be used to mitigate GHG. After recycling in a chemical process, CO₂ and methane

can be formed as useful products such as methanol or dimethyl ether. Methanol is a liquid material so it is easily stored and transported. Methanol is an important industrial chemical and potential fuel. Conventional vehicles can use methanol in the same way as gasoline or diesel to power an internal combustion engine. Methanol has an energy density of 17.6kJ/cm, which is about twice that of hydrogen. Methanol synthesis is a method of converting hydrogen to methanol with CO₂ in a thermal reactor at about 220°C under moderate pressure (20-50 bars) [17].

The synthesis of methanol and dimethyl carbonate leading to the utilization of CO₂ can be used in industry. Dry reforming is the most recognized method because it uses CO₂ [18, 19].

Greenhouse gas emission estimation for Europe

Linear regression is an approach for modeling the relationship between a scalar dependent variable y and one or more independent variables. GHG emissions for 29 countries between 2004 and 2013 are shown in Fig. 1 [20]. Data on GHG emissions for Europe are taken from the European Environment Agency. This study investigated GHG emissions. Statistics on GHG emissions between 2004 and 2013 are applied to provide estimates for 29 countries (Table 1).

Linear regression estimation for 29 countries was applied. Arithmetic means, standard deviations, regression formulas, coefficients and predictions for GHG emissions are calculated by Excel (Table 1). Predictions of GHG emissions in 2020 range from three million tonnes to 826 million tonnes while the global GHG emission prediction for 2020 is 3505.56 million tonnes.

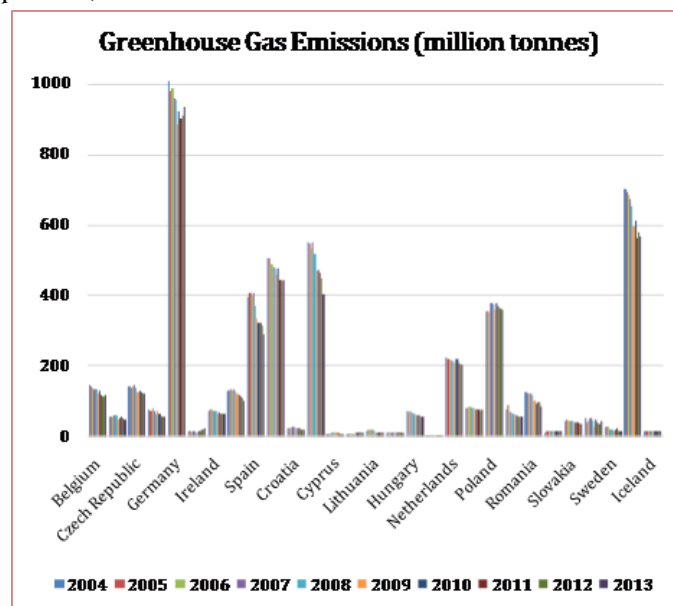


Fig. 1. GHG emissions for 29 countries between 2004 and 2013 [20].

Table 1. Linear regression estimation for 2020.

Country	Arithmetic Mean (million tonnes)	Standard deviation	Regression formula	Prediction of GHG emission in 2020 (million tonnes)
Lithuania	14	3.90	$y = 0.6606x + 5,3151$	16.55
Luxembourg	12	0.65	$y = -0.2048x + 13,001$	9.52
Hungary	64	6.39	$y = -2.1747x + 76,26$	39.29
Malta	3	0.10	$y = 0.0068x + 2,9584$	3.07
Netherlands	213	7.39	$y = -2.2063x + 224,81$	187.30
Austria	79	3.45	$y = -1.0345x + 84,551$	66.96
Poland	365	10.69	$y = 1.0723x + 358,67$	376.90
Portugal	66	10.34	$y = -3.2483x + 83,722$	28.50
Romania	109	14.52	$y = -4.7352x + 134,81$	54.31
Slovenia	14	0.99	$y = 0.0699x + 13,904$	15.09
Slovakia	41	3.31	$y = -1.0111x + 46,999$	29.81
Finland	43	7.10	$y = -0.9827x + 48,207$	31.50
Sweden	21	5.40	$y = -1.5287x + 29,14$	3.15
United Kingdom	634	52.78	$y = -17.622x + 730,86$	431.29
Iceland	16	0.46	$y = 0.0707x + 16,078$	17.28

Table 2. Turkey's sectoral regression estimations.

Country	Arithmetic Mean (million tonnes)	Standard deviation	Regression formula	Prediction of GHG emission in 2020 (million tonnes)
Lithuania	14	3.90	$y = 0.6606x + 5,3151$	16.55
Luxembourg	12	0.65	$y = -0.2048x + 13,001$	9.52
Hungary	64	6.39	$y = -2.1747x + 76,26$	39.29
Malta	3	0.10	$y = 0.0068x + 2,9584$	3.07
Netherlands	213	7.39	$y = -2.2063x + 224,81$	187.30
Austria	79	3.45	$y = -1.0345x + 84,551$	66.96
Poland	365	10.69	$y = 1.0723x + 358,67$	376.90
Portugal	66	10.34	$y = -3.2483x + 83,722$	28.50
Romania	109	14.52	$y = -4.7352x + 134,81$	54.31
Slovenia	14	0.99	$y = 0.0699x + 13,904$	15.09
Slovakia	41	3.31	$y = -1.0111x + 46,999$	29.81
Finland	43	7.10	$y = -0.9827x + 48,207$	31.50
Sweden	21	5.40	$y = -1.5287x + 29,14$	3.15
United Kingdom	634	52.78	$y = -17.622x + 730,86$	431.29
Iceland	16	0.46	$y = 0.0707x + 16,078$	17.28

Table 3. U.S.'s sectoral regression estimations.

Sector	Arithmetic Mean (million tonnes)	Standard deviation	Regression formula	Prediction of GHG emission in 2020 (million tonnes)
Energy	4166.00	132.81	$y = -24.416x + 53156$	3835.68
Transportation	1835.75	65.56	$y = -10.383x + 22669$	1695.34
Industrial processes	332.75	17.38	$y = -3.3182x + 6990.7$	287.94
Agriculture	450.25	12.30	$y = 2.7857x - 5139.3$	487.81
Forestry and land use	28.25	6.38	$y = -0.0325x + 93.396$	27.75
Waste	133.00	3.67	$y = -0.7143x + 1566.2$	123.31
Forestry and land use (Sinks)	-868.50	115.44	$y = -16.286x + 31809$	-1088.72
Total net emissions	6077.50	232.44	$y = -52.364x + 111145$	5369.72

Greenhouse gas emission estimations for sectors in Turkey and the U.S.

Sectoral GHG emissions of Turkey and U.S. are estimated by linear regression for 2020. Sectoral GHG emission data for Turkey and the U.S. are taken respectively from T.C. Turkish Statistical Institute and Inventory of U.S. Greenhouse Gas Emissions and Sinks in Figs. 2, 3. In this study, arithmetic means, standard deviations, regression formulas, coefficients and predictions for GHG emissions are calculated by Excel (Tables 2, 3).

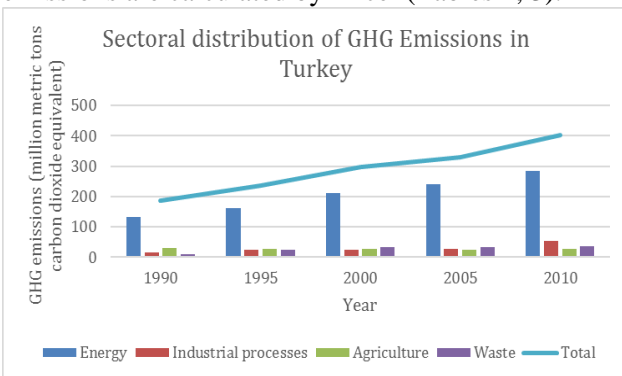


Fig. 2. Sectoral distribution of GHG emissions in Turkey [21].

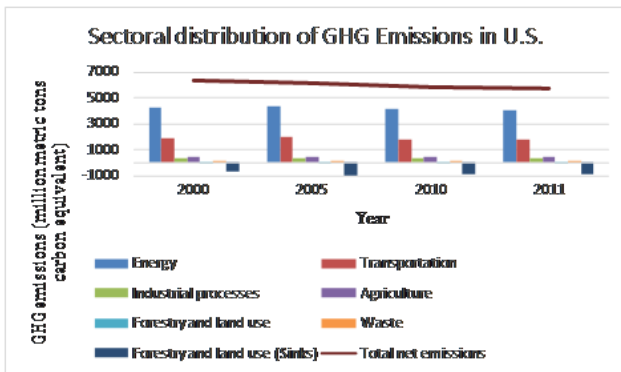


Fig. 3. Sectoral distribution of GHG emissions in the U.S. [22].

Sectoral GHG predictions in Turkey and in the U.S. are shown respectively in Tables 2 and 3. Linear regression estimations for Turkey and the U.S. are respectively 499.88 million tonnes and 5369.72 million tonnes for 2020.

RESULTS AND DISCUSSION

High global warming potential (GWP) gases and their chemical properties are explained in this study. GHG emissions are increasing because of population growth and the increase in living standards. Linear regression estimations for Turkey and the U.S. are respectively 500 million tonnes and 5370 million tonnes for 2020. Prediction of GHG emissions in 2020 range from three million tonnes to 826 million tonnes for Europe. Global GHG emission prediction for 2020 is 3506 million tonnes. Precautionary measures that should be taken against global temperature increase are explained. Chemical processes like oxidation and methanol synthesis reduce the amount of GHG in the atmosphere. Energy circulation items against further temperature rise can be the planting of trees in school gardens and on roofs and walls and around public institutions and religious buildings, the expansion and reformation of green areas in children’s parks, and improving green areas around buildings and on roadsides.

Acknowledgements: This study was sported by Marmara University, Scientific Research Projects Committee (BAPKO) with a project number FEN-D-130416-0144.

REFERENCES

1. <http://www.imo.org.tr/resimler/ekutuphane/pdf/11177.pdf>.
2. M. Bochow, T. Peisker, K. Segl, H. Kaufmann, Modelling of urban biotope types from hyperspectral

- imagery using a fuzzy logic approach, Proceeding of the 2nd Workshop of the EARSeL SIG on Land Use and Land Cover, Bonn, 2006, p. 424.
3. J. M. Wallace, P. V. Hobbs, Atmospheric science: and introductory survey, 2rd ed. Academic Press, London, 2006.
 4. J. C. Zachos, G. R. Dickens, R. E. Zeebe, *Nature*, **451**, 279 (2008).
 5. C. Yang, S. Yeh, S. Zakerinia, K. Ramea, D. McCollum, *Energy Policy*, **77**, 118, 130 (2015).
 6. D. Bodansky, *American Journal of International Law*, **104**(2), 230 (2010).
 7. K. Öztürk, *Gazi Eğitim Fakültesi Dergisi*, **22**, 1 (2002).
 8. http://www4.unfccc.int/submissions/INDC/Published%20Documents/Turkey/1/The_INDC_of_TURKEY_v.15.19.30.pdf.
 9. D. Burden, P. Lagerwey, *Walkable Communities, Incorporated*, Available at: http://www.cityofandersonsc.com/planning/road_diet_article.pdf, 1 (1999).
 10. C. Alexander, S. Ishikawa, M. Silverstein, M. Jacobson, I. Fiksdahl-King, S. Angel, A pattern language: towns, buildings, construction, Oxford University Press, United States of America, 1977.
 11. A. Em, in: Diyarbakir'da çevre ve doğa (Diyarbakir Tarım, Doğa ve Çevre Sempozyumu, Diyarbakir, 2010), K. Haspolat, K. Guven, R. G. Guven (eds), Diyarbakir, 2010, p. 30.
 12. A.H. Han, *International Journal of Urban Sciences*, **11**(2), 168 (2007).
 13. H. Vandevyvere, S. Stremke, *Sustainability*, **4**(6), 1309 (2012).
 14. J. Keirstead, N. Shah, Urban energy systems: an integrated approach, Routledge, Oxford, UK, 2013.
 15. P. J. Crutzen, M. O. Andreae, *Science* **250**, 1669 (1990).
 16. D. Ehhalt, M. Prather, F. Dentener, R. Derwent, E. J. Dlugokencky, E. Holland, P. Midgley, Atmospheric chemistry and greenhouse gases (No. PNNL-SA-39647) Pacific Northwest National Laboratory (PNNL), Richland, WA (US), 2001.
 17. A. Bill, A. Wokaun, B. Eliasson, E. Killer, U. Kogelschatz, *Energy Conversion and Management*, **38**, 415 (1997).
 18. <http://nortech.oulu.fi/eng/eneproconf.html>.
 19. M. Perez-Fortes, J. C. Schoneberger, A. Boulamanti, E. Tzimas, *Applied Energy*, **161**, 718 (2016).
 20. <http://appsso.eurostat.ec.europa.eu/nui/setupDownloads.do>
 21. <http://www.tuik.gov.tr/PreHaberBultenleri.do?id=10829>
 22. <https://www3.epa.gov/climatechange/ghgemissions/sources.html>.

BULGARIAN CHEMICAL COMMUNICATIONS

Instructions about Preparation of Manuscripts

General remarks: Manuscripts are submitted in English by e-mail or by mail (in duplicate). The text must be typed double-spaced, on A4 format paper using Times New Roman font size 12, normal character spacing. The manuscript should not exceed 15 pages (about 3500 words), including photographs, tables, drawings, formulae, etc. Authors are requested to use margins of 3 cm on all sides. For mail submission hard copies, made by a clearly legible duplication process, are requested. Manuscripts should be subdivided into labelled sections, e.g. **Introduction, Experimental, Results and Discussion, etc.**

The title page comprises headline, author's names and affiliations, abstract and key words.

Attention is drawn to the following:

a) **The title** of the manuscript should reflect concisely the purpose and findings of the work. Abbreviations, symbols, chemical formulas, references and footnotes should be avoided. If indispensable, abbreviations and formulas should be given in parentheses immediately after the respective full form.

b) **The author's** first and middle name initials, and family name in full should be given, followed by the address (or addresses) of the contributing laboratory (laboratories). **The affiliation** of the author(s) should be listed in detail (no abbreviations!). The author to whom correspondence and/or inquiries should be sent should be indicated by asterisk (*).

The abstract should be self-explanatory and intelligible without any references to the text and containing not more than 250 words. It should be followed by key words (not more than six).

References should be numbered sequentially in the order, in which they are cited in the text. The numbers in the text should be enclosed in brackets [2], [5, 6], [9–12], etc., set on the text line. References, typed with double spacing, are to be listed in numerical order on a separate sheet. All references are to be given in Latin letters. The names of the authors are given without inversion. Titles of journals must be abbreviated according to Chemical Abstracts and given in italics, the volume is typed in bold, the initial page is given and the year in parentheses. Attention is drawn to the following conventions:

a) The names of all authors of a certain publications should be given. The use of "*et al.*" in

the list of references is not acceptable.

b) Only the initials of the first and middle names should be given.

In the manuscripts, the reference to author(s) of cited works should be made without giving initials, e.g. "Bush and Smith [7] pioneered...". If the reference carries the names of three or more authors it should be quoted as "Bush *et al.* [7]", if Bush is the first author, or as "Bush and co-workers [7]", if Bush is the senior author.

Footnotes should be reduced to a minimum. Each footnote should be typed double-spaced at the bottom of the page, on which its subject is first mentioned.

Tables are numbered with Arabic numerals on the left-hand top. Each table should be referred to in the text. Column headings should be as short as possible but they must define units unambiguously. The units are to be separated from the preceding symbols by a comma or brackets.

Note: The following format should be used when figures, equations, *etc.* are referred to the text (followed by the respective numbers): Fig., Eqns., Table, Scheme.

Schemes and figures. Each manuscript (hard copy) should contain or be accompanied by the respective illustrative material as well as by the respective figure captions in a separate file (sheet). As far as presentation of units is concerned, SI units are to be used. However, some non-SI units are also acceptable, such as °C, ml, l, etc.

The author(s) name(s), the title of the manuscript, the number of drawings, photographs, diagrams, etc., should be written in black pencil on the back of the illustrative material (hard copies) in accordance with the list enclosed. Avoid using more than 6 (12 for reviews, respectively) figures in the manuscript. Since most of the illustrative materials are to be presented as 8-cm wide pictures, attention should be paid that all axis titles, numerals, legend(s) and texts are legible.

The authors are asked to submit **the final text** (after the manuscript has been accepted for publication) in electronic form either by e-mail or mail on a 3.5" diskette (CD) using a PC Word-processor. The main text, list of references, tables and figure captions should be saved in separate files (as *.rtf or *.doc) with clearly identifiable file names. It is essential that the name and version of

the word-processing program and the format of the text files is clearly indicated. It is recommended that the pictures are presented in *.tif, *.jpg, *.cdr or *.bmp format, the equations are written using "Equation Editor" and chemical reaction schemes are written using ISIS Draw or ChemDraw programme.

The authors are required to submit the final text with a list of three individuals and their e-mail addresses that can be considered by the Editors as potential reviewers. Please, note that the reviewers should be outside the authors' own institution or organization. The Editorial Board of the journal is not obliged to accept these proposals.

EXAMPLES FOR PRESENTATION OF REFERENCES

REFERENCES

1. D. S. Newsome, *Catal. Rev.–Sci. Eng.*, **21**, 275 (1980).
2. C.-H. Lin, C.-Y. Hsu, *J. Chem. Soc. Chem. Commun.*, 1479 (1992).
3. R. G. Parr, W. Yang, *Density Functional Theory of Atoms and Molecules*, Oxford Univ. Press, New York, 1989.
4. V. Ponec, G. C. Bond, *Catalysis by Metals and Alloys* (Stud. Surf. Sci. Catal., vol. 95), Elsevier, Amsterdam, 1995.
5. G. Kadinov, S. Todorova, A. Palazov, in: *New Frontiers in Catalysis* (Proc. 10th Int. Congr. Catal., Budapest, 1992), L. Guzzi, F. Solymosi, P. Tetenyi (eds.), Akademiai Kiado, Budapest, 1993, Part C, p. 2817.
6. G. L. C. Maire, F. Garin, in: *Catalysis. Science and Technology*, J. R. Anderson, M. Boudart (eds), vol. 6, Springer-Verlag, Berlin, 1984, p. 161.
7. D. Pocknell, *GB Patent 2 207 355* (1949).
8. G. Angelov, PhD Thesis, UCTM, Sofia, 2001.
9. JCPDS International Center for Diffraction Data, Power Diffraction File, Swarthmore, PA, 1991.
10. *CA* **127**, 184 762q (1998).
11. P. Hou, H. Wise, *J. Catal.*, in press.
12. M. Sinev, private communication.
13. <http://www.chemweb.com/alchem/articles/1051611477211.html>.

CONTENTS

<i>Preface</i>	4
<i>T. Tekpetek, Y.Y. Gurkan</i> , Investigation of possible degradation reactions of amoxicillin molecule.....	5
<i>Y. Yeşiloğlu, S. Gülen</i> , Total phenolic and flavonoid contents and antioxidant activity of extracts from <i>Vitis vinifera</i> L.....	9
<i>S. Altuntaş, H. Hapoğlu</i> , Control of adiabatic continuous stirred tank reactor at an unstable operating point.....	14
<i>N. Çolak, A. B. Gündüzalp, S. Mamaş, D. Akkaya, K. Kaya</i> , Synthesis, spectroscopic studies and electrochemical properties of Schiff bases derived from 5-chloro-2-hydroxybenzaldehyde with methyl 2-amino-6-methyl-4,5,6,7-tetrahydrobenzo[b]thiophene-3-carboxylate.....	20
<i>M. Ates, N. Uludag</i> , Synthesis and application of conducting polymers and their nanocomposites as a corrosion protection performances.....	27
<i>U. Yıldız, B. Çoban</i> , A comparative DNA binding study for heteroleptic platinum(II) complexes of pip and hpip.....	33
<i>M. Ates</i> , Symmetric device performances of carbon based nanostructures for supercapacitors	39
<i>S. Kurban, N. Gulsah Deniz, C. Sayil</i> , Synthesis and cyclization reactions of novel benzo[a]phenazine- and phenoxazine-5-ones derivatives.....	43
<i>D. S. Dasdan</i> , Synthesis of poly((2-dimethylamino)ethyl methacrylate) via atom transfer radical polymerization and surface characterization by Inverse gas chromatography.....	49
<i>D. Cakmak, S. Yalcınkaya, K. Seymen, C. Demetgül</i> , Immobilization of salophen derivative Schiff base cobalt(II) complex on a copolymer coated platinum electrode and electro-catalytic investigations.....	55
<i>E. Bozkurt</i> , Greenhouse gases in urban areas.....	62
Instructions to the authors.....	68